

UNIVERSITÀ DEGLI STUDI DI BRESCIA



DOTTORATO DI RICERCA IN INGEGNERIA MECCANICA E INDUSTRIALE

Settore scientifico disciplinare: CHIM/07

Ciclo XXXV

# **Chitosan from food waste: a sustainable source for environment, water quality and agriculture**

Dottoranda: MARINA MADDALONI

Supervisor: Prof. IVANO ALESSANDRI  
Co-supervisors: Dr.ssa Irene Vassalini  
Dr.ssa Sara Cortesi

“Anima così leggera  
Che non mi ferma niente  
Non mi serve il vento per andare oltre  
Superarmi ancora e ancora

...

Quanti sogni servono a sentir di meritare?  
Quanti sogni servono a volare, volare?”

# Table of contents

---

List of abbreviation.....	vi
Abstract.....	vii
Sommario.....	ix
Chapter 1.....	1
1 Introduction.....	1
Chapter 2.....	9
2. Chitosan from shrimp's shells.....	9
2.1 Introduction: an overview of chitosan structure, sources, and applications.....	10
2.2 Chitosan extraction procedure.....	13
2.2.1 Chemicals and Materials.....	13
2.2.2 Extraction of chitosan from shrimp shells.....	13
2.3 Calculation of DD by potentiometric titration.....	15
2.3.1 Materials and Methods.....	15
2.3.2 Results and Discussion.....	15
2.4 Calculation of DD by FT-IR spectroscopy.....	18
2.4.1 Materials and Methods.....	18
2.4.2 Results and Discussion.....	19
Chapter 3.....	23
3. Food-waste enables carboxylated gold nanoparticles to completely abat Cr(VI) in drinking water.....	23
3.1 Introduction.....	24
3.2 Experimental.....	29
3.2.1 Chemicals and Materials.....	29
3.2.2 Synthesis of Citrate-capped AuNPs (Cit.-AuNPs).....	29
3.2.3 Functionalization of AuNPs: 3 mercaptopropionic acid-Cit. AuNPs,11 mercaptoundecanoic acid -Cit.-AuNPs systems.....	30
3.2.4 Extraction of chitosan from shrimp's shells.....	30
3.2.5 Dissolution of chitosan.....	31
3.2.6 Functionalization of AuNPs with chitosan.....	31
3.2.7 Spectroscopic evaluation of Cr(VI) removal capabilities of the different systems.....	31
3.2.8 Preparation of AuNPs-based electrodes.....	32
3.2.9 Electrochemical determination of Cr(VI).....	32
3.3 Results and Discussion.....	33
3.4 Conclusions.....	43
Chapter 4.....	44

<b>4. From water for water: different functionalized chitosan bubbles hydrogel for sustainable dyes removal.....</b>	<b>44</b>
<b>4.1 Introduction.....</b>	<b>46</b>
4.1.1 Hydrogels: structure and properties.....	46
4.1.2 Ionotropic gelation .....	49
4.1.3 Chitosan bubbles for sustainable dye removal from water.....	51
4.1.4 Brief introduction of general chemical physical properties of PEDOT:PSS .....	56
4.1.5 Brief introduction of chemical-physical properties of TiO <sub>2</sub> .....	57
4.1.6 Brief introduction of chemical-physical properties of AgNPs and AuNPs .....	58
<b>4.2 Experimental .....</b>	<b>60</b>
4.2.1 Chemicals and Materials .....	60
4.2.2 Synthesis of CH hydrogel bubbles .....	60
4.2.3 Synthesis of CH@PEDOT:PSS hydrogel bubbles.....	60
4.2.4 Synthesis of CH@TiO <sub>2</sub> hydrogel bubbles.....	60
4.2.5 Synthesis of AuNPs.....	61
4.2.6 Synthesis of AgNPs .....	61
4.2.7 Synthesis of CH@AuNPs and CH@AgNPs hydrogel bubbles .....	61
4.2.8 Dyes adsorption tests.....	62
4.2.9 Dye photodegradation tests under solar illumination .....	63
<b>4.3 Results and discussions.....</b>	<b>64</b>
4.3.1 MB and MO dye adsorption.....	64
4.3.2 MB and MO dye photodegradation.....	69
4.3.3 In-depth study on the adsorption capacity of CH@PEDOT bubbles.....	75
<b>4.4 Synthesis and characterization of chitosan hydrogels in form of films.....</b>	<b>84</b>
4.4.1 Materials and Methods .....	84
4.4.2 Results and discussions .....	88
<b>4.5 A preliminary study on chitosan bubbles containing CsPbBr<sub>3</sub> perovskite, used for MB removal .....</b>	<b>98</b>
4.5.1 Experimental: synthesis of CsPbBr <sub>3</sub> and CH@PVK bubbles .....	99
4.5.2 Results .....	100
<b>4.5 Conclusions .....</b>	<b>105</b>
<b>Chapter 5 .....</b>	<b>107</b>
<b>5. Preliminary study of chitosan nanoparticles-induced resistance against <i>Tobacco Necrosis Virus</i> in <i>Phaseolus Vulgaris</i>.....</b>	<b>107</b>
<b>5.1 Introduction.....</b>	<b>108</b>
5.1.1 Tobacco Necrosis Virus (TNV).....	111
<b>5.2 Experimental .....</b>	<b>113</b>
5.2.1 Chemicals and Materials.....	113

5.2.2	Synthesis of chitosan nanoparticles (CsNPs) .....	113
5.2.3	Atomic force microscopy (AFM) characterization.....	113
5.2.4	CsNPs Phytotoxicity test.....	114
5.2.5	Preparation of TNV inoculum .....	114
5.2.6	Tobacco necrosis virus (TNV)- Administration.....	114
5.3	Results and discussions.....	115
5.4	Conclusions .....	121
Chapter 6	.....	122
6.	Concluding Remarks .....	122
References	.....	125

## List of abbreviation

---

Abbreviation	Explanation	Abbreviation	Explanation
<b>IARC</b>	<b>International Agency for Research on Cancer</b>	<b>3MPA</b>	<b>3-MercaptoPropionic Acid</b>
<b>WHO</b>	<b>World Health Organization</b>	<b>11MUA</b>	<b>11-MercaptoUndecanoic Acid</b>
<b>US EPA</b>	<b>United States Environmental Protection Agency</b>	<b>Cit.AuNPs</b>	<b>Citrated capped gold Nano Particles</b>
<b>DD</b>	<b>Degree of Deacetylation</b>	<b>BW</b>	<b>Bottled Water</b>
<b>DA</b>	<b>Degree of Acetylation</b>	<b>MB</b>	<b>Methylene Blue</b>
<b>AuNPs</b>	<b>Gold Nano Particles</b>	<b>MO</b>	<b>Methyl Orange</b>
<b>AgNPs</b>	<b>Silver Nano Particles</b>	<b>CH</b>	<b>Chitosan hydrogel</b>
<b>TiO<sub>2</sub> NPs</b>	<b>Titania Nano Particles</b>	<b>CH@</b>	<b>Chitosan bubbles</b>
<b>CsNPs</b>	<b>Chitosan Nano Particles</b>	<b>PEDOT:PSS</b>	<b>Poly 3,4-ethylenedioxythiophene/polystyrene</b>
<b>MW</b>	<b>Molecular Weight</b>	<b>PVK</b>	<b>CsPbBr<sub>3</sub> Perovskites</b>
<b>ATR</b>	<b>Attenuated Total Reflection</b>	<b>TNV</b>	<b>Tobacco Necrosis Virus</b>
<b>FT-IR</b>	<b>Fourier Transform-Infrared Spectroscopy</b>	<b>ROS</b>	<b>Reactive Oxygen Species</b>
<b>PB</b>	<b>Probe Band</b>	<b>SAR</b>	<b>Systemic Acquired Resistance</b>
<b>RB</b>	<b>Reference Band</b>	<b>PRR</b>	<b>Pathogenesis Related Reaction</b>
<b>AA</b>	<b>Ascorbic Acid</b>	<b>HR</b>	<b>Hypersensitivity Reaction</b>
<b>CA</b>	<b>Citric Acid</b>	<b>LLD</b>	<b>Low Limit Detection</b>

## Abstract

---

The eco-sustainable use of molecules derived from food and agricultural waste represents one of the most interesting challenges of the last few years.

In fact, a direct consequence of the increasing world population is the non-stop increment of food waste, which has a major impact not only on economy and society, but also on environment, as it severely contributes to greenhouse gas emissions. Nowadays, indeed, only 1% of the food waste is recycled for industrial uses. At the same time, the supply of clean water to the growing population and the need to seek a viable alternative to the use of copper-based agricultural pesticides for crop protection, are becoming urgent issues.

In this work, we exploit the possibility to merge these aspects developing all-in one systems, based on materials derived from food waste, which are able to capture, degrade, and remove environmental pollutants in water and to work as resistance inductors for plants protections against crop viruses.

In particular, we exploited the possibility to extract chitosan from shrimp's shells waste and we characterized the Degree of Deacetylation (DD) of the obtained material through FT-IR spectroscopy and potentiometric titration, in order to compare it with the same biopolymer commercially available.

We demonstrated that the extracted chitosan can be combined with other organic molecules from food waste (e.g., ascorbic and citric acid) and empower different types of gold nanoparticles in removal of hexavalent chromium species from Milli-Q and real water.

Moreover, the efficiency of chitosan in polluted water cleaning through adsorption and photodegradation in real sun irradiation conditions, was demonstrated also when the biopolymer is formulated as hydrogels bubbles and combined with active components such as photocatalytic nanoparticles (AgNPs, AuNPs and TiO<sub>2</sub> NPs) or polymer blends (PEDOT:PSS), for the removal of organic dyes such as Methylene Blue or Methyl Orange.

The good mechanical properties of chitosan-based hydrogel in form of films and the antimicrobial activity of gels against target bacteria and fungi, were proven with explorative tests.

Finally, the effectiveness of chitosan nanoparticles as resistance inducers against *Tobacco Necrosis Virus* has been demonstrated.

In summary, this work demonstrates that food waste can be recovered and reused to obtain valued added-materials for environmental remediation and crop protection. In particular, the use of chitosan as material-based template, whose functional properties can be rationally controlled and designed, is a promising strategy that allows us to combine its effectiveness with interesting antimicrobial properties which allows its use in real systems.

## Sommario

---

L'uso eco-sostenibile di molecole derivanti da rifiuti agricoli e/o alimentari rappresenta una delle sfide più interessanti degli ultimi anni.

Infatti, una conseguenza diretta dell'aumento della popolazione mondiale è proprio l'incremento continuo degli scarti alimentari, che ha un forte impatto non solo dal punto di vista economico e sociale, ma anche ambientale, in quanto contribuisce fortemente alle emissioni di gas serra. Ad oggi, solo l'1% dei rifiuti alimentari viene riciclato per usi industriali.

D'altro canto, la domanda sempre più alta di acqua potabile da fornire alla popolazione in crescita, e la necessità di cercare una valida alternativa all'uso di pesticidi agricoli a base di rame per la protezione delle colture, stanno diventando questioni urgenti.

In questo lavoro di tesi, sfruttiamo la possibilità di unire questi aspetti, sviluppando sistemi "tutto-in-uno", basati su materiali derivati da rifiuti alimentari, che sono in grado di catturare, degradare, e rimuovere gli inquinanti ambientali in acqua, e di lavorare come induttori di resistenza per la protezione delle piante contro i virus delle colture.

In particolare, è stata sfruttata la possibilità di estrarre chitosano da gusci di gamberetti, il cui grado di deacetilazione (DD) è stato caratterizzato mediante spettroscopia FT-IR e titolazione potenziometrica, al fine di confrontarlo con due campioni commercialmente disponibili.

In questa tesi, è stato quindi dimostrato che il chitosano estratto può essere combinato con altre molecole organiche derivanti da rifiuti alimentari (ad esempio, acido ascorbico e citrico) ed è in grado di potenziare diversi tipi di nanoparticelle d'oro nella rimozione di specie di cromo esavalente da acqua Milli-Q e acqua reale.

Inoltre, è stata dimostrata l'efficienza del chitosano nella bonifica di acqua inquinata da coloranti organici come il blu di metilene e il metil arancio, mediante adsorbimento e fotodegradazione in condizioni simulate di irraggiamento solare, quando il biopolimero è formulato come hydrogel in forma di bubbles, ed è combinato con componenti attivi come nanoparticelle fotocatalitiche (AgNPs, AuNPs e TiO<sub>2</sub> NPs) o miscele polimeriche (PEDOT:PSS).

Le proprietà meccaniche degli hydrogel a base di chitosano in forma di film e l'attività antimicrobica dei gel contro batteri e funghi target, sono state dimostrate con test esplorativi.

Infine, è stata provata l'efficacia delle nanoparticelle del chitosano come induttori di resistenza contro il virus della necrosi del tabacco (TNV).

In sintesi, questo lavoro dimostra che i rifiuti alimentari possono essere recuperati e riutilizzati per ottenere materiali ad alto valore aggiunto per la bonifica ambientale e la protezione delle colture. In particolare, l'uso di materiali basati sul chitosano, le cui proprietà funzionali possono essere razionalmente controllate e progettate, è una strategia promettente che ci permette di combinare la sua efficacia con interessanti proprietà antimicrobiche del polimero, che ne consentono l'uso in sistemi reali.

# Chapter 1

---

## 1 Introduction

Among the consequences of the increasing local and global population there is the exponential increment of food waste. In the last few years, the **Food and Agriculture Organization (FAO)** estimated that 1/3 of the agriculture products is discarded<sup>1</sup>, and according to the *UNEP Food Waste Index 2021* the waste of valuable resources occurs at all stages of the Food Supply Chain (FSC) with about 61% of waste coming from households, 13% from retail and 26% from food service<sup>2</sup>.

Despite the waste of food resources is an ethical and moral issue, it has also enormous economic and environmental repercussions. In fact, only in Europe, it is measured that 88 tonnes of food waste cost to the European economic budget about 143 billion euros/year and involve the emission into the atmosphere of 170 000 000 tonnes/years of CO<sub>2</sub>, linked to products disposal at the end of their life<sup>3</sup>.

For these reasons, exploring new directions for minimizing food waste is a paramount goal for scientists and policymakers.

In the 2008 the *US Environmental Protection Agency (US-EPA)* developed a hierarchy showing different strategies for the prevention, use and re-use of food waste (**Figure 1.1**)<sup>4</sup>. At present, the reduction at source and the re-use of inedible food as animal feed seem to be the most practiced choices, while the industrial use represents only the 1% of the residue reduction<sup>5</sup>.

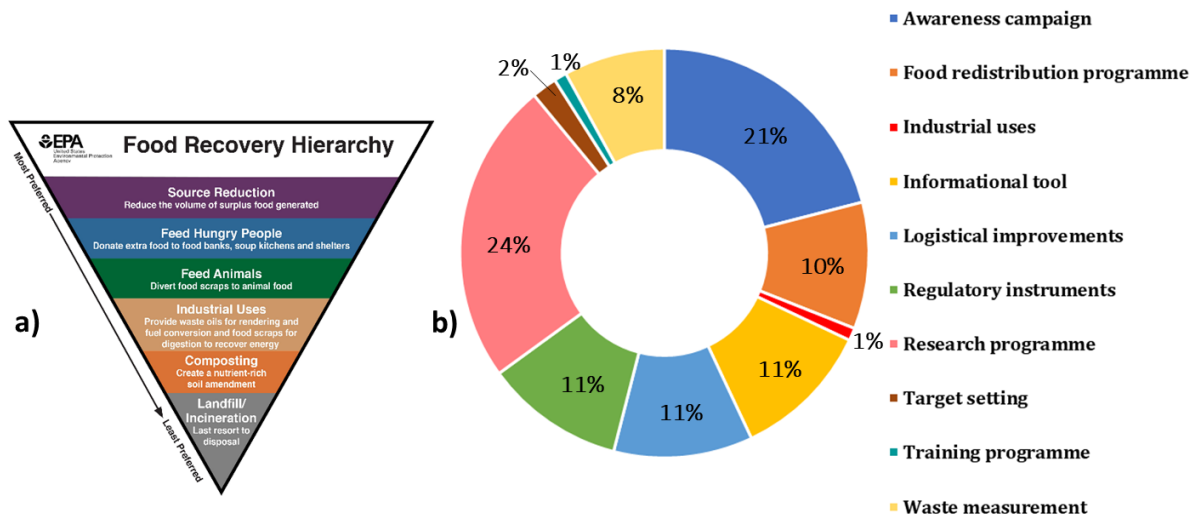


**Figure 1.1:** a) US EPA Food recovery Hierarchy<sup>4</sup> b) Type of strategies for food waste prevention<sup>5</sup>.

However, in the last few years, scientific interest seems to move precisely in the direction of using food waste as basis for the development of innovative technological solutions.

In particular, we can look at food wastage as a source of many high-value molecules, which can find applications in different fields,

In this optics, the whole FSC, including all residues originated from retails, agriculture, household and all food utilization/production processes, can be considered as an appealing source of low-cost and low-environmental impact chemicals.

For example, molecules such as biopolymers (e.g., chitin, chitosan, starch, alginate pectin) phenols, carboxylic acids (e.g., malic, citric, ascorbic), amines or flavonoids can be easily recovered from fruit, vegetable, or animal waste<sup>6</sup>. And even the milk produced in excess could be a valuable source of amyloid proteins and casein<sup>7</sup>.

As visible in **Table 1.1**, in the last few years, different efforts have been concentrated on the extraction of high value-molecules from a wide variety of food waste leading to their use in different sectors, mainly re-use in food industry or pharmaceuticals, but also production of fertilizers, packaging, and biofuels.

**Table 1.1:** Examples of molecules extracted from food waste and their use.

<b>Waste Source</b>	<b>High-value molecules</b>	<b>Current main use</b>
Orange and apple peel	Pectin	Gelling agent
Green plants	Cellulose	Paper, cellophane, biofuels...
Citrus peel	Citric acid	Flavouring and preservative agent, reductant agent, medical, cosmetics...
Coffee waste	Pectinase enzyme	Wine production
Citrus peel	Ascorbic acid	Medical field, environmental field
Cashew waste	Succinic acid	Pharmaceutical ingredient
<b>Crustaceans 'shells</b>	<b>Chitin and Chitosan</b>	<b>Environmental remediation, pharmaceutical field</b>
Potato peels	Polyphenols	Antioxidants
Pineapple waste	Vanillic acid	Flavouring agent
Sea algae	Alginate	gelling agent
	Agarose	Biology field
Corn	Starch	Food field

According to the most recent report of the *Fishing and Aquaculture* department of FAO<sup>8</sup>, one of the markets globally more productive is the aquaculture one, with a production of 122.6 million tonnes of goods only in the 2020. A great slice of these tonnes, about 23%, is represented by the production of crustaceans, in particular shrimps and prawns. Throughout the world, and in all ages, in fact, shrimps have been the most exchanged aquatic products and even today are intensively produced in Asia and Latin America and imported especially in Europe. Unfortunately, crustaceans are made for more than 50 percent of their original weight by heads and shells that are not edible and lead to the production of a huge amount of wastes<sup>9,10</sup>. However, when we look at food waste as a resource, we can consider that crustaceans' shells are made of calcium carbonate (20-50%), proteins (20-40%) and chitin (15-40%). Interestingly, chitin can be converted into chitosan<sup>10</sup> through simple chemical treatments. This

means that we can exploit the abundance of this raw materials for a great number of applications.

In particular, environmental remediation and monitoring, which actually are critical areas in sustainable development, can have considerable advantages<sup>11</sup>, but also other fields of application are to be considered.

For example, Goci et al. demonstrated as chitosan-based polymer nanocomposite can be used for remediation of mercury, copper and cobalt, or as adsorbents for oil spills and dyes<sup>12</sup>. The use of chitosan, in fact, allows to obtain high porous material with interesting properties of biodegradability and biocompatibility, that can be functionalized with high added value molecules and easily recycled.

Moreover, in medical and biopharmaceutical fields, chitosan has attracted growing interest as agent for treatment and prevention of infections, especially for the possibility to apply it as delivery carrier of drugs and pharmaceutical compounds. The opportunity to use chitosan - based systems in drug delivery field, is strictly related not only to its capacity to retains drugs

molecules when it is in form of hydrogel, but also to the presence on chitosan backbone of carboxyl and amino groups that can interact with glycoproteins in mucus during viral infection, thus, guarantying drug bioavailability and high retention and release time<sup>13</sup>.

Also in the agricultural field, chitosan is arousing a considerable interest for its capacity to induce defence action in plants (that will be better discussed in the next sections) or to promote their growth<sup>14</sup>.

A deepen overview of the use of this exceptional biopolymer in different field and application is reported in **Table 1.2**.

**Table 1.2:** Main area of application of chitosan.

Field of application	Use	References
Environmental remediation	<ul style="list-style-type: none"> <li>• Removal of dyes;</li> <li>• Removal of emerging pollutants;</li> <li>• Treatment of oily compounds</li> <li>• Abatement of heavy metal ions.</li> </ul>	15-18
Agriculture protection	<ul style="list-style-type: none"> <li>• Stimulation of plant growth;</li> <li>• Induction of plant defence mechanisms</li> <li>• Coating seeds to repair them from freezing.</li> </ul>	19,20
Biomedical and biopharmaceutical	<ul style="list-style-type: none"> <li>• Prevention of infections;</li> <li>• Drug delivery systems;</li> <li>• Wound care healing;</li> <li>• Bacteriostatic and amicrobic systems.</li> </ul>	21-24
Food and drink	<ul style="list-style-type: none"> <li>• Food packaging</li> </ul>	25
Cosmetic	<ul style="list-style-type: none"> <li>• Oral care;</li> <li>• Contact lens;</li> <li>• Hair care;</li> <li>• Skin toning.</li> </ul>	26

In this study, we will focus especially on environmental monitoring and remediation, by exploiting the presence of many functional groups in the biopolymer, which can interact with a large number of pollutant molecules, thus facilitating their capture and removal.

In particular, the branch of environmental monitoring and remediation on which we will focus in this thesis is the one related to water quality. The use of chitosan-based materials in water quality monitoring gives us the chance to obtain systems that exploit the antibacterial activity of chitosan without the risk of degradation due to viruses and bacteria attacks, inevitably present in wastewater. The nature of this antimicrobial activity will be discussed in **Chapter 2** and **Chapter 4**.

Water quality monitoring is a very tricky challenge due to the complexity of real water samples and the variety and low concentrations of the pollutants contained in them.

**Table 1.3** shows examples of the most common water pollutants and their limiting concentration imposed by the **World Health Organization (WHO)**<sup>27</sup>.

**Table 1.3:** Most common pollutants limits in wastewater imposed by WHO<sup>27</sup>.

<b>Water contaminant</b>	<b>WHO limit</b>
Cr	0.05 mg/L
Pb	0.05 mg/L
Hg	0.01 mg/L
Cd	0.005 mg/L
Cu	0.05 mg/L
Phosphate	1 mg/L
PCB	2 ppm
Sulphate	500 mg/L
Nitrate	10 mg/L
Emerging pollutants	not defined

According to their forms or the sources of pollution, water pollutants can be of different types: microbiological, if they are caused by microorganism (virus, bacteria, protozoa...), or anthropomorphic if they are originated by human activities and produced by households, agriculture, or industrial practices (emerging pollutants, pesticides, chemical species from industrial waste...). Nowadays, traditional treatments for water remediations include filtration, ion exchange, chemical reduction followed by precipitation and electrolysis<sup>28-30</sup>, but all these

technologies have a great number of disadvantages such as high cost, large quantity of chemicals required, sometimes the sensitivity is not too high, and they can lead to the production of dangerous waste by-products. Moreover, water is treated in centralized plants prior the distribution, but during the distribution water quality may degrade due to the re-growth of bacteria or contaminants leaching.

For this reason, it would be appropriate to have clean-up and monitoring systems to be implemented locally.

In this regard, in the last few years, nanomaterials and nano-sensors have attracted growing interest from the scientific community<sup>31</sup>.

The main objective of this thesis was to combine the two hot topics described above, obtaining nanomaterials starting from molecules from food waste.

In particular, we chose to focus our research on the use of **chitosan**, extracted from shrimp's shells, in order to obtain nano-systems useful in the environmental protection field, from the agriculture sector (with focus on protection of plant from pests), to water remediation, with the aim of waste recovery and circular economy.

In **Chapter 2** the extraction procedure of chitosan from shrimp's shells was described. The characterization of the **Degree of Deacetylation (DD%)** of the obtained sample and of two batches of commercial chitosan, used as references, was performed through potentiometric titration and **FT-IR** spectroscopy. In this case the two techniques were used in order to demonstrate that it is possible the characterization of DD by the use of a fast and simple technique, as acid-base titration, and a more precise but simple characterization as **FT-IR** spectroscopy, when the standard technique, <sup>1</sup>H-NMR, is not available.

In **Chapter 3** the preparation of different chitosan-based functionalized gold nanoparticles (AuNPs) for removal of Cr(VI) in water is reported. In this case we exploit the ability of chitosan to dissolve in different acidic media (CH<sub>3</sub>COOH, and citric and ascorbic acid mixture) to obtain chitosan-functionalized AuNPs capable to completely abate Cr(VI). Moreover, a deepen study of the role of each element involved in Cr(VI) abatement (AuNPs, chitosan, chitosan's solvents, AuNPs' capping agents) was carried out with cyclic voltammetry experiments.

In **Chapter 4** we report the preparation of chitosan hydrogels in form of bubbles. Moreover, we demonstrate that bubbles of pure chitosan and bubbles of chitosan functionalized with high added value units such as AuNPs, AgNPs, TiO<sub>2</sub> NPs or PEDOT:PSS, are capable to adsorb and

photodegrade organic dyes as MO and MB. The antimicrobial activity of chitosan hydrogels was confirmed from specific tests with *Pseudomonas Syringae pv. Phaseolicola* and *Alternaria Tenuissima*. In addition, to test the mechanical properties of the obtained hydrogel, they were also formulated in form of films. Furthermore, a brief introductory study on the possibility to stabilize Lead Halide Perovskite in water by introducing them in chitosan bubbles, and on the use of obtained systems for water remediation, is reported.

In **Chapter 5** the possibility to obtain Chitosan nanoparticles (CsNPs) was explored. The obtained NPs were used as resistance inductors of *Tobacco Necrosis Virus* inoculated of *Phaseolus vulgaris* leaves.

Finally, in **Chapter 6**, conclusions and future perspectives of current work are reported.

# Chapter 2

---

## 2. Chitosan from shrimp's shells

In this chapter, the procedure for the production of chitosan from shrimp's shells is described. A brief introduction of the biopolymer, its structure and its current and possible future applications is given. The following paragraphs explain all single steps for the extraction of chitin from real food waste and its conversion into chitosan and puts the spotlights on the differences between the extracted biopolymer, and two commercial references: chitosan produced by Bio-basic®, and chitosan produced by Sigma Aldrich ®. All the different chitosan samples were characterized through potentiometric titration, and **Fourier Transform IR spectroscopy (FT-IR)** All the tests used to characterize the extracted material and to evaluate the **Degree of Deacetylation (DD)**, were performed in triplicate.

## 2.1 Introduction: an overview of chitosan structure, sources, and applications.

Chitosan is a non-toxic, biocompatible, and natural polymer derived from the deacetylation of chitin, the second most abundant biopolymer after cellulose. Its structure is made by randomly distributed N-acetyl-d-glucosamine and D-glucosamine (**Figure 2.1**)<sup>32</sup>.

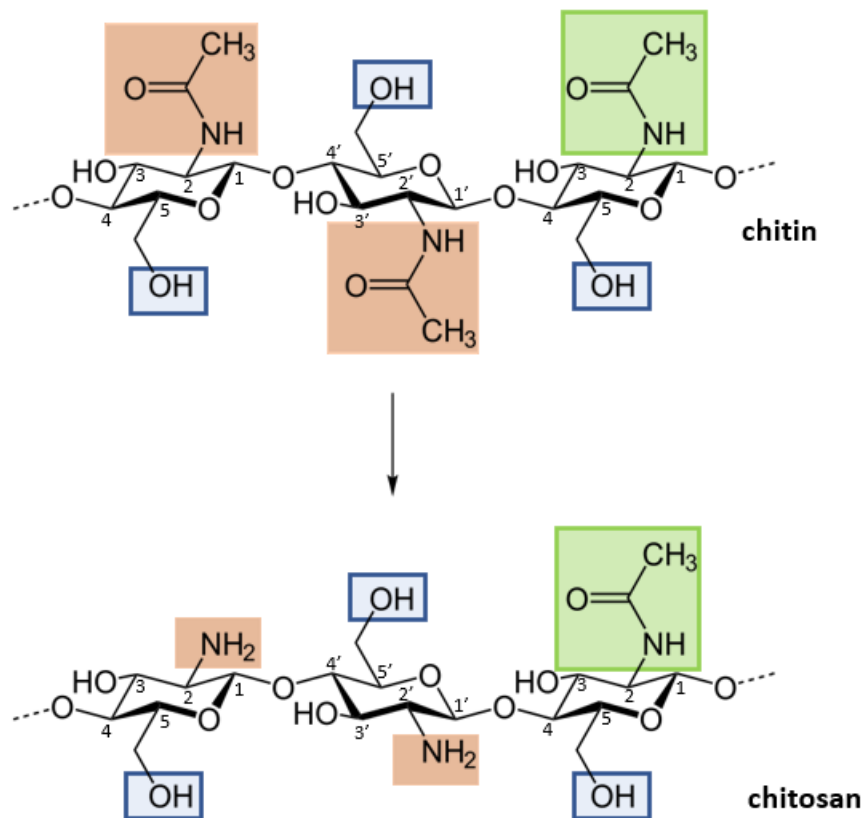


**Figure 2.1:** Schematic representation of deacetylation of chitin to chitosan

Chitin, and therefore chitosan, can be found and extracted from molluscs, fungi cell walls<sup>33,34</sup>, exoskeleton of arthropods and insects' cuticles<sup>35</sup> (**Figure 2.2**).

Today, commercial samples of chitosan are mostly produced starting from crustaceans 'shells, as a result of the plentiful availability of raw materials<sup>8</sup>. However, recently, also extraction from fungi cell walls is arousing great interest due to increasing demand of vegan market <sup>36</sup>.

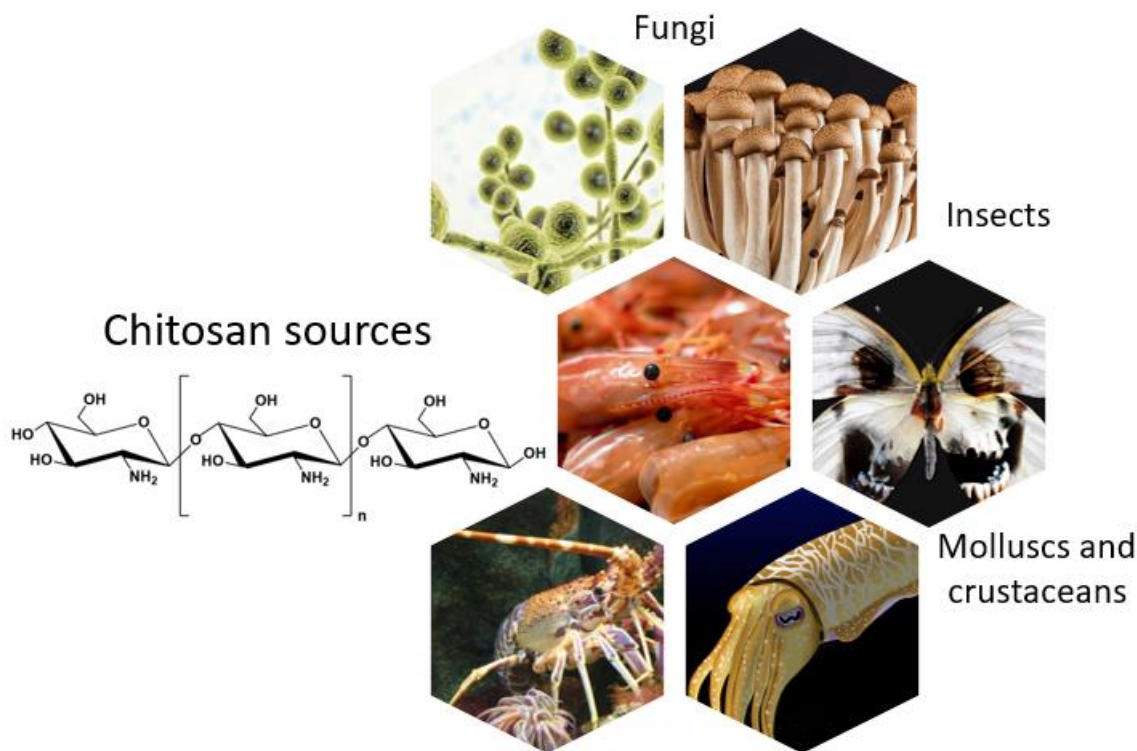


**Figure 2.2:** Examples of chitosan sources.

As we see in **Figure 2.1**, the precursor, chitin, is a biopolymer characterized by N-acetyl-D-glucosamine units bonded together by  $\beta$ -1,4 bonds, in which the main reactive functional groups are the  $-\text{CH}_2\text{OH}$  in position 5 and 5', the  $-\text{OH}$  groups in position 3 and 3', and the  $-\text{NH}_2\text{COCH}_3$  in position 2 and 2'. When deacetylation occurs to obtain chitosan, a variable percentage  $> 60\%$  of the acetyl groups  $-\text{NHCOCH}_3$  react, and primary amino groups are released ( $-\text{NH}_2$  in position 2 and 2' on chitosan in **Figure 2.1**). The result is a chitosan in which the randomly alternation of N-acetyl-D-glucosamine and D-glucosamine units, leads to a biopolymer that in addition to functional groups present in chitin and described above, presents also primary amino groups.

These groups can be properly modified, giving a biopolymer with interesting characteristics and behaviours.

For example, the presence of  $-\text{NH}_2$  groups along the polymeric chain, makes chitosan insoluble in water but soluble in aqueous acid media due to the protonation of amino group ( $\text{pK}_a = \sim 6.5$ )<sup>36</sup>.

Precisely because of its ability to act as a polyelectrolyte cation in acidic solutions, chitosan is characterized by an interesting antibacterial activity, that, together with its biocompatibility and oxygen permeability, make it particularly suitable for applications that exploit its

antimicrobial ability<sup>37</sup>; moreover, the peculiarity of chitosan to be insoluble in water, makes it ideal for preparation of hydrogels<sup>38</sup> (**Table 1.2** in **Chapter 1**).

In particular, for the antibacterial activity, the most accredited hypothesis is that the presence of free amino groups on the glucosamine units that are positively charged at pH < 6.5, could represent the key factor for the interaction with the microbial biological membranes that are negatively charged. This interaction would appear to be the main reason for inducing blockage of vital bacterial activity<sup>39</sup>.

At the same time, this ability to penetrate through biological membranes makes the compound exploitable for the stimulation of organisms at the immune level and gives it also antiviral and antifungal activity<sup>40</sup>.

The bioactivity of chitosan, as well as the other properties that have been described above, are strongly dependent on two parameters: the **Molecular Weight (MW)** and the **Degree of Deacetylation (DD)**.

If the **Degree of Acetylation (DA)** is defined as the percentage of mole fraction of N-acetyl glucosamine units, the percentage of D-glucosamine units obtained after a reaction of deacetylation of chitin, can be defined as **Degree of Deacetylation**:

$$\mathbf{DD} (\%) = 100 - \mathbf{DA}$$

Generally, the biopolymer is defined chitosan, and not chitin, if its **DD** is higher than 50%, and most chitosan commercially available have a percentage of **DD** between 70% and 90%<sup>41-43</sup>.

This parameter is very critical, since it can influence the **MW**, solubility and biological effect<sup>44</sup>. The higher is the value of **DD**, in fact, the higher is the concentration of the -NH<sub>2</sub> groups in the polymer chains and then, the positive charge obtained from the acidification. This results in greater solubility in water and higher antibacterial activity<sup>45</sup>.

For these reasons, the evaluation of **DD** is strongly important when chitosan is extracted from a source as food waste, and in this chapter will be carefully evaluated through **FT-IR** spectroscopy, and potentiometric titration.

## 2.2 Chitosan extraction procedure

The extraction method has been developed by Maddaloni et al. and published in *Environmental Nanotechnology, Monitoring & Management* 18 (2022) 100686<sup>46</sup>.

### 2.2.1 Chemicals and Materials

All chemicals were used as received, without any further purification.

Hydrochloric acid, 37% w/w, sodium hydroxide (commercial grade) and acetic acid (99 %) were acquired from Sigma-Aldrich.

Chitosan was extracted from local shop shrimp's shells as reported in 2.2.2 and compared with two reference materials, commercial chitosan purchased from Sigma Aldrich (high MW, declared DD > 75%) and commercial chitosan purchased from Bio-basic (analytical grade, high MW, DD > 80%).

In all experiments ultrapure Milli-Q water was used, obtained from a Milli-Q Integral 5 system.

### 2.2.2 Extraction of chitosan from shrimp shells

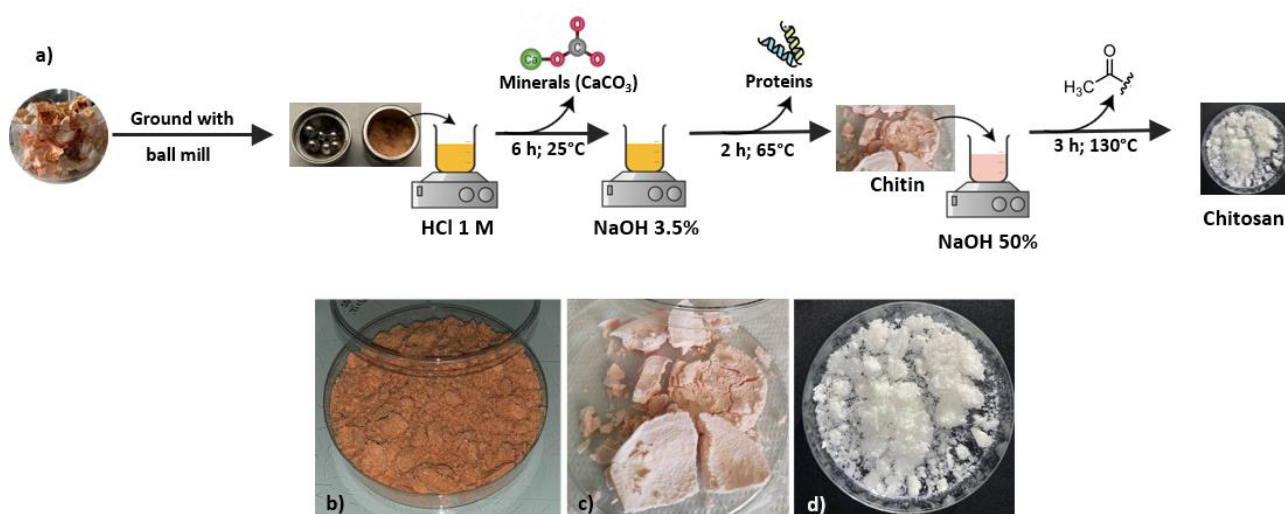


**Figure 2.3:** **a)** Schematic representation of chitosan extraction. **b)** Sample after step of demineralization. **c)** Chitin obtained from deproteinization step. **d)** Chitosan obtained after the deacetylation of chitin.

For direct chitosan extraction from food waste, 20 g of raw materials (crustaceans shells and heads) were washed, dried (150 °C, 30 min.), and finely ground by means of a ball milling (*Retsch MM400*). This step is fundamental to increase the surface area of the starting material, increase its reactivity and facilitate the following steps of chemical conversion. The obtained powder was processed with 150 mL of HCl 1 M for 6 h at room temperature under magnetic stirring to eliminate minerals (CaCO<sub>3</sub>). In fact, in this way, CaCO<sub>3</sub> is converted into H<sub>2</sub>CO<sub>3</sub>, which

is soluble in water (leading to the dissolution of CO<sub>2</sub> in H<sub>2</sub>O). The **demineralized sample (Figure 2.3-b)** was recovered, washed with water until pH = 7 was reached, and then allowed to dry.

Subsequently, **deproteinization** of the demineralized sample was achieved by adding 100 mL of NaOH (3.5 %, at 65 °C for 2 h). The recovered chitin (**Figure 2.3-c**) was washed with water until pH = 7 was reached and it was dried.

Finally, chitosan (**Figure 2.3-d**) was obtained by **deacetylation** of chitin, by treating it with 50 mL of NaOH 50% at 130 °C for, at least, 3 h.

In the end, the recovered sample was washed with water until pH = 7 was reached and it was dried.

**Table 2.3:** Percentage of recovery of chitosan from raw material after treatment.

<b>Raw material (g)</b>	<b>Sample after demineralization (g)</b>	<b>Chitin (g)</b>	<b>Yield<sub>CHITIN</sub> (%)</b>	<b>Chitosan (g)</b>	<b>Yield<sub>CHITOSAN</sub> (%)</b>
<b>20</b>	14.4	3	15%	2.5	12.5%

The **Table 2.3** reports the percentage yield for the recovery of chitin and chitosan from shrimp's shells. The obtained results are in line with the contents of biopolymers declared in the chapter 1 and reported in literature<sup>10</sup>.

## 2.3 Calculation of DD by potentiometric titration

The calculation of **DD** through potentiometric titration is the simplest and low-cost method used in this thesis. It is based on easily accessible apparatus and reagents.

The choice to use different characterization techniques to determine the same parameter for each available batch of chitosan is due to the fact that, although NMR seems to be the most accurate method for the determination of **DD**<sup>47</sup>, it is also expensive, requires deuterated solvents, specialized staff and long time for sample preparation. Moreover, not all laboratories have access to such equipment.

For these reasons, it is a primary issue to find a routine technique that can be used to determine a degree of deacetylation, with results that are comparable to that obtained with <sup>1</sup>H-NMR.

The potentiometric titration is an acid-base titration, based on the protonation of the -NH<sub>2</sub> groups in the polymer chain by a strong acid (HCl), and its subsequent titration with a strong base (NaOH).

### 2.3.1 Materials and Methods

The adopted protocol for sample preparation was the same for all available chitosan (extracted, Bio-basic and Sigma Aldrich). All experiments were carried out in triplicate.

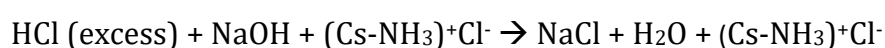
0.2 g of dried chitosan was dissolved in 20 mL of HCl 0.1 M and 25 mL of Milli-Q water. After 30 minutes of continuous stirring on heating plate to promote the dissolution, an additional 25 mL aliquot of Milli-Q water was added and stirring continued for another 30 minutes.

When the biopolymer was completely dissolved, the solution was titrated adding NaOH 0.1 M and the variation of pH were measured with the use of a pH- meter (SI Analytics, Lab 845).

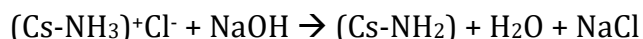
### 2.3.2 Results and Discussion

When the biopolymer completely dissolved in HCl is titrated with NaOH, a curve of measured pH vs added NaOH volume is obtained (**Figure 2.4**). This curve presents two inflection points, one at V<sub>1</sub> and one at V<sub>2</sub>.

At Volume V<sub>1</sub>, the excess of HCl that is not directly involved into chitosan protonation, reacts with the added NaOH, and it is neutralized:



When a volume  $V_2$  of NaOH is added during the titration, also the positively charges on chitosan are neutralized:



The difference between the two inflection points ( $V_2-V_1$ ) corresponds to the amount of HCl consumed from  $-\text{NH}_2$  groups of chitosan and allows us to determine the **DD (%)**.

The degree of deacetylation of chitosan was calculated using the following formula:

$$\text{DD (\%)} = 2.03 * \frac{V_2 - V_1}{m + 0.0042 * (V_2 - V_1)} \quad (1)$$

where:

- $m$  is the weighed mass of chitosan;
- $V_1$  and  $V_2$  are the volume of the NaOH added at the two deflection points;
- 2.03 is a coefficient obtained from the **MW** of monomeric unit of chitin;
- 0.0042 is a coefficient obtained from the difference between **MW** of chitin and chitosan.

For each sample, three titrations were performed and in **Figure 2.4** one titration curve either for extracted chitosan and chitosan produced by Bio-basic is reported as example. The graphs of the first derivative of pH as function of volume of NaOH added during the titration, allow us to better determine the value of  $V_1$  and  $V_2$  necessary for the calculation of **DD (Formula (1))**. The final value of **DD (%)** was obtained based on the average value of three tests (**Table 2.4**).

The curve obtained with chitosan by Sigma Aldrich is not reported since it was not possible the completely dissolution of biopolymer in HCl 0.1 M. This suggests that the degree of deacetylation of the purchased batch was lower than that commercially declared.

Further information will be collected with the other techniques, that do not require chitosan dissolution in water.

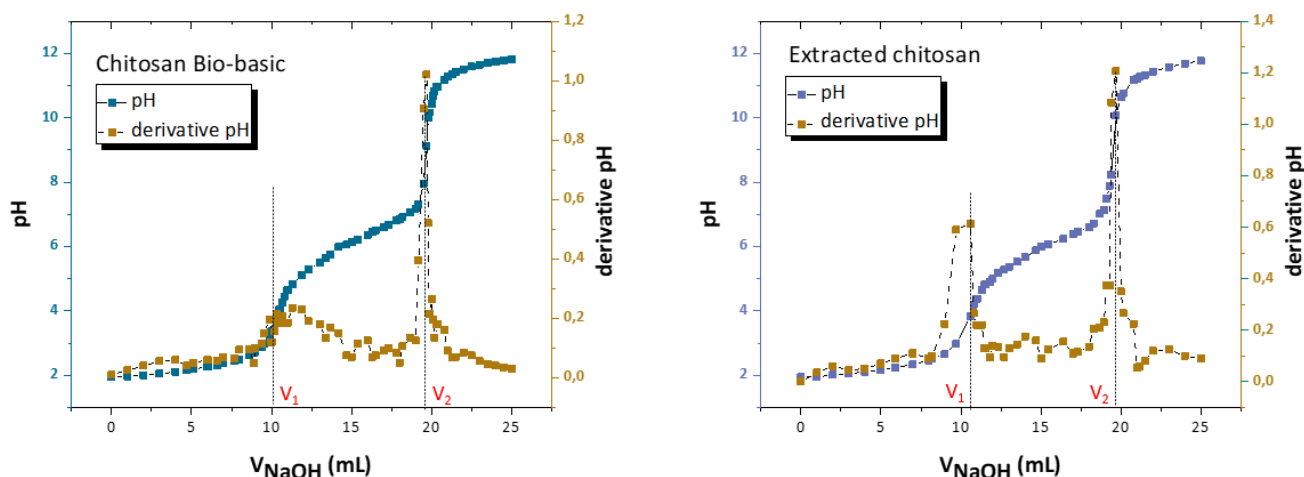


**Figure 2.4:** Example of titration curve obtained for extracted chitosan and for commercial chitosan purchased by Bio-basic.

**Table 2.4:** Average value of **DD(%)** calculated for the extracted chitosan and chitosan purchased by Bio-basic from potentiometric titration.

<i>Sample</i>	<i>Calculated DD (%)</i>
<i>Extracted chitosan</i>	76,34±0,15
<i>Chitosan Bio-basic</i>	78,29±0,60

For the chitosan Bio-basic the degree of deacetylation is in line with that commercially declared. The value of **DD (%)** calculated for extracted chitosan confirms that the biopolymer extracted in our lab from food waste has a degree of deacetylation comparable to the commercial reference.

The relatively high value of standard deviation is the result of the limits of this method for the determination of **DD**. The adding of a base such as NaOH during the titration, in fact, makes difficult the mixing of solution at high values of pH, due to the precipitation of biopolymer that is insoluble in alkaline environment. This behaviour can cause an error that reflects on the standard deviation.

Given these considerations, despite the disadvantage of a quite long sample preparation time, the potentiometric titration seems a good routine method that can provide a first acceptable estimation of the chitosan degree of deacetylation.

## 2.4 Calculation of DD by FT-IR spectroscopy

The **Fourier Transform IR (FT-IR)** spectroscopy is a valid alternative to calculate the degree of deacetylation of chitosan.

Unlike the technique just described, and the more complex and expensive  $^1\text{H-NMR}$ , the **FT-IR** technique has the advantage that it doesn't require a long and challenging sample preparation and it has no need of dissolving the biopolymer in any solvent<sup>47</sup>.

Moreover, IR- spectroscopy presents the advantage to be a high sensitivity and non-destructive technique.

### 2.4.1 Materials and Methods

Infrared spectra were recorded directly on the powders using a Nicolet™ iN10 Infrared Microscope.

The spectra were acquired in transmission mode putting the sample on a barium fluoride specimen holder.

A Slide-On MicroTip Ge ATR crystal was used to collect attenuated total reflectance (**ATR**) spectra (average angle =  $27^\circ$ ). A little amount of chitosan powder has been placed on specimen holder and pressed to ensure a uniform contact between the sample and the **ATR** tip.

For each chitosan (extracted, Bio-basic and Sigma) three measures were collected in three different points of the sample. In all cases, a total of 64 scans were accumulated at the wavenumber region from  $400$  to  $4000\text{ cm}^{-1}$  with a resolution of  $4\text{ cm}^{-1}$ , and the resulting spectra were visualized using OMNIC™ software.

## 2.4.2 Results and Discussion

In **Figure 2.5** a characteristic **FT-IR** spectrum obtained for chitosan is reported, with some assignment bars for the most relevant bands.

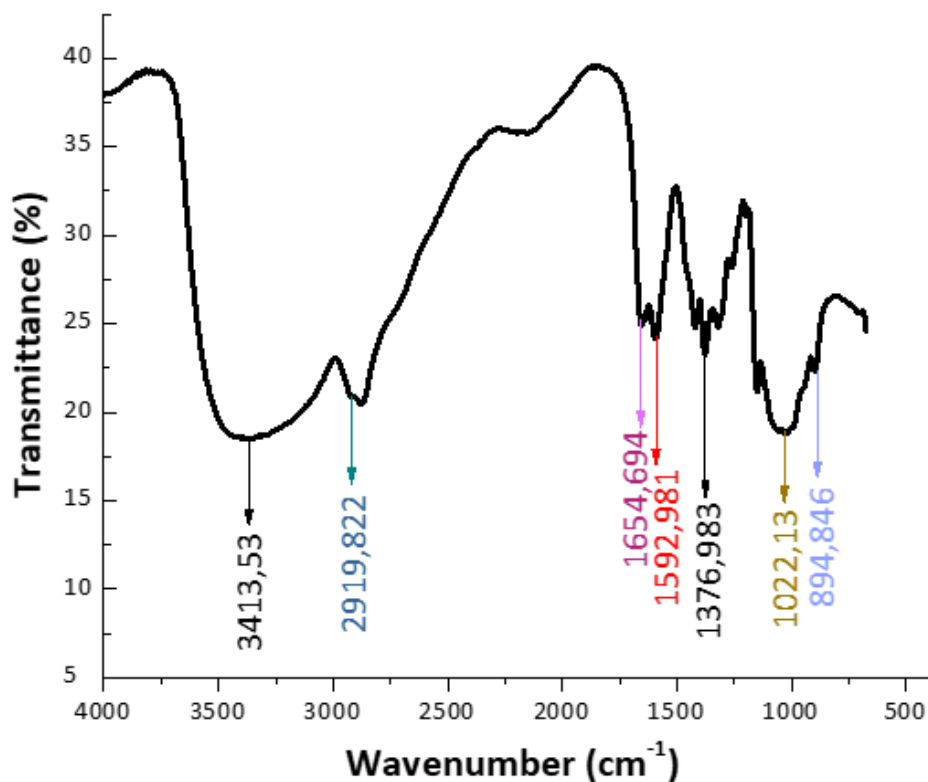


**Figure 2.5:** FT-IR spectrum acquired on extracted chitosan powder, with assignment of the peaks related to the main functional groups of the molecule.

A typical chitosan **FT-IR** spectrum shows a well-known band at 3413 cm<sup>-1</sup>, characteristics of the O-H stretching of the hydroxyl group and the N-H stretching of the primary amine of chitosan<sup>48</sup>.

At 2919 and 2892 cm<sup>-1</sup> it is possible to locate two typical bands of a polysaccharide structure. In fact, they are attributable to symmetric and asymmetric C-H stretching, respectively, and are common to molecules such as glucans, carrageenans and xylan<sup>49</sup>.

A clear sign of the fact that the chitosan is not completely deacetylated, is the presence of the bands at 1654 cm<sup>-1</sup> and 1376 cm<sup>-1</sup> attributable to C=O stretching of acetyl group and C-N stretching of amide II, respectively.

The adsorption band at 1592 cm<sup>-1</sup> corresponds to N-H bending of amine I, while that at 1022 cm<sup>-1</sup> gives us information about the pyran structure of the biopolymer<sup>50,51</sup>.

At a first visual comparison between the three types of chitosan, whose spectra are compared in **Figure 2.6**, it is evident as the band at 1655 cm<sup>-1</sup>, indicating the content of N-acetyl groups, is much higher in chitosan purchased by Sigma than in the commercial Bio-basic reference and the in-lab extracted sample, which have very similar spectra.

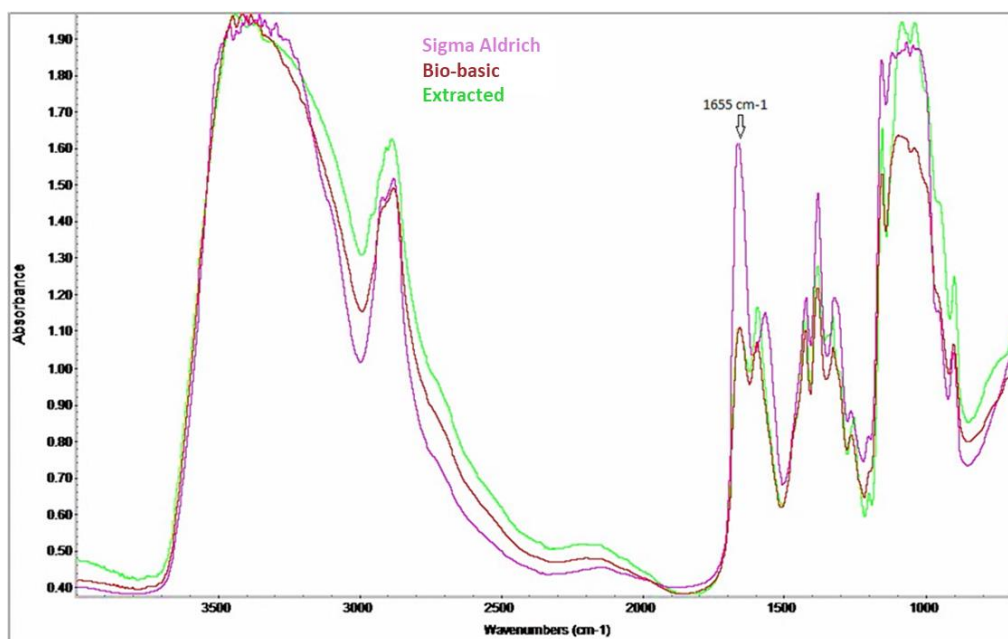


**Figure 2.6:** Comparison between the three FT-IR spectra of the Bio-Basic, Sigma Aldrich and extracted chitosan.

This first analysis seems to confirm what we saw in **paragraph 2.4**, but an accurate calculation of DD is necessary.

The **DD (%)** is generally determined by choosing a characteristic band (also called **Probe Band, PB**) and a reference band (**RB**), that is associated to a functional group presents both in acetylated and in deacetylated monomeric units.

However, choosing the appropriate **PB** and **RB** is not trivial and there are many factors to take into accounts: the intensity of the bands, the environment in which the measure is done, the type of available instrument...

In a number of publications<sup>47</sup>, the **DD** is determined through the following formula:

$$DD\% = 100 - \left[ \left( \frac{A_{1655}}{A_{3450}} \right) * \frac{100}{1.33} \right] \quad (2)$$

where:

$A_{1655}$  = absorbance of the N-acetyl group 1655 cm<sup>-1</sup> (**PB**).

$A_{3450}$  = absorbance of the O-H stretching at 3450 cm<sup>-1</sup> (**RB**).

$1.33 = A_{1655}/A_{3450}$  for a fully acetylated polymer.

This formula is the mostly widely used because, generally, shows the higher agreement with NMR spectroscopy results<sup>47</sup>, but it also introduces the absorbance at  $3450\text{ cm}^{-1}$  as **RB**, that considers all the stretching due to O-H bonds, even that caused by humidity.

Commonly, to avoid the influence of the humidity that can introduce inaccuracies in the evaluation of DD, the sample is prepared in KBr pellets and stabilized under humidity-controlled atmosphere before the acquisition<sup>52</sup>.

In the present case, we decided to make the measure independent to the contribution of humidity by substituting the Formula (2) with the following<sup>47</sup>:

$$\mathbf{DD\%} = 100 - \left[ \left( \frac{A_{1320}}{A_{1420}} - 0.3822 \right) * \frac{1}{0.03133} \right] \quad (3)$$

where:

$A_{1320}$  = absorbance characteristic of N-acetyl glucosamine;

$A_{1420}$  = reference band, characteristic of chemical hydrolysis of acetyl groups

0.3822 and 0.03133 are two constants resulting from the linear correlation between the ratio  $A_{1320}/A_{1420}$  and experimental DA ( $A_{1320}/A_{1420} = 0.3822 + 0.03133*DA$ ).

In the **Table 2.5** were reported the results obtained for the three samples.

**Table 2.5:** Experimental results for the calculation of DD% of the three types of chitosan.

	Sample	A <sub>1320</sub>	A <sub>1420</sub>	DD %	DD <sub>AVERAGE_FTIR</sub> (%)	DD <sub>AVERAGE_TITRATION</sub> (%)
<b>Extracted</b>	# 1	0.1902	0.1897	80.19	80.35 ± 0.37	76.34±0.15
	# 2	0.5260	0.5360	80.87		
	# 3	0.4650	0.4660	80.3		
<b>Bio-Basic</b>	# 1	0.1902	0.1904	80.31	80.70 ± 0.47	78.29±0.60
	# 2	0.1748	0.1764	80.57		
	# 3	0.3111	0.3206	81.22		
<b>Sigma-Aldrich</b>	# 1	0.0409	0.0397	79.27	78.93 ± 0.38	-
	# 2	0.1300	0.1250	79.00		
	# 3	0.1320	0.1251	78.52		

As we see from the **Table 2.5** the results obtained with **FT-IR** spectroscopy are in good agreement with results obtained with pH-metric titration. Both techniques underline as the extracted chitosan presents a good deacetylation degree, quite similar to chitosan Biobasic, whose DD is in line with the parameter commercially declared, while the chitosan by Sigma Aldrich is the biopolymer with the lowest DD among the three samples analysed. Probably the different characteristics respect to the other chitosan, and the difficulties to dissolve it, are related not only to DD but also to MW.

## Chapter 3

---

### 3. Food-waste enables carboxylated gold nanoparticles to completely abate Cr(VI) in drinking water

The contents and results of this chapter has been published on *Environmental Nanotechnology, Monitoring & Management* 18 (2022) 100686<sup>53</sup>.

In these paragraphs, the effectiveness of the synergic combination of high added value molecules extracted from food waste, with carboxylated gold nano-particles (AuNPs) is demonstrated in hexavalent chromium removal from real and MilliQ water.

To be specific, we demonstrated that when chitosan extracted from shrimp's shells is dissolved in 1:3 mixture of ascorbic and citric acids, can improve the efficiency of citrated-capped AuNPs (Cit-AuNPs) in Cr(VI) removal, from 18.4 to > 99% when the solution of pollutant is obtained with Milli-Q water, and 80.6 % when is obtained with drinking water.

Moreover, it has been shown that when 3-mercaptopropionic or 11-mercaptoundecanoic acids are used instead of citrate as capping-agent for AuNPs, the efficiency reaches 100% both in drinking and MilliQ water. In particular, the use of 11-mercaptoundecanoic acid seems to be the best solution as AuNPs capping-agent, both in terms of stability and efficiency.

The study of the rule of each different component of our systems in abatement of hexavalent chromium, was carried out by **UV-vis spectroscopy** and **cyclic voltammetry**.

### 3.1 Introduction

The increasing worldwide industrialization has brought, in addition to evident advantages, also some negative aspects that deserve a special attention.

The growing industrial activity, in fact, deeply affects the water quality, producing high quantity of wastewater.

The produced wastewater must be treated before to achieve the environment, in order to reduce the concentration of all water pollutants that may be present, so that they will be not hazardous.

For this reason, sensing and removal of environmental contaminants such as organic molecules (e.g. dyes and emergent pollutants) and heavy metal ions (e.g. arsenate/arsenite, bivalent mercury, hexavalent chromium...) is become a primary goal in scientific field<sup>54</sup>.

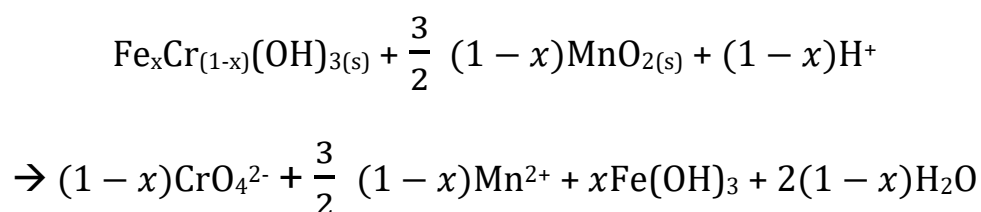
One of the most hazardous and pervasive water pollutants, affecting highly industrialized area, is hexavalent chromium (Cr(VI))<sup>55</sup>.

Chromium is a natural metal that represents the 21<sup>th</sup> most abundant compound on earth crust-shaped<sup>56</sup>. Its most common oxidation states are +2, +6 and +3, that is also the most chemically stable.

The states +5 and +4 are also possible for this metal but are less stable and therefore more rarely found.

In nature, hexavalent chromium is present in different environmental components such as soil, air and water, but in this case its concentration is very low<sup>57</sup>.

In particular, Cr(VI), is generally released in aquifer materials via oxidation of Cr(III) presents in minerals as  $\text{Fe}_x\text{Cr}_{(1-x)}(\text{OH})_3$  that reacts with the co-existing manganese (IV) minerals<sup>58</sup>:



where  $0 < x < 1$  and represents the molar fraction of Cr in  $\text{Fe}_x\text{Cr}_{(1-x)}(\text{OH})_3$ .

However, Cr(VI) has also most alarming anthropological sources, which increase its concentration in the environment and, therefore, its level of hazard. Its compounds, indeed, are widely used in fertilizers, tanning, cement or metallurgic industries<sup>59-61</sup>.

The danger is due to the highly carcinogenic and mutagenic nature of Cr(VI), whose extreme toxicity is linked above all to its tendency to bio-accumulation. For this reason, in the 2012, Cr(VI) has been classified as pollutant belonging to group I of human carcinogen agent by **IARC** (**I**nternation **A**gency for **R**esearch on **C**ancer).

In fact, many severe medical diseases such as chromosome aberrations, dermatitis, and cancer (particularly of gastrointestinal apparatus) are correlated to the oxidative power of this metal that leads to the premature spoilage of biological molecules (DNA, proteins, lipids)<sup>62</sup>.

Different analysis of **US EPA** (**U**nited **S**tates **E**nvironmental **P**rotection **A**gency) revealed that Cr(VI) is largely present in drinking water<sup>58,63</sup>, so to reduce risks for humans and for environment, the **World Health Organization (WHO)** has imposed a concentration of 0.05 mg/L as the upper limit of total Cr in drinking water<sup>64</sup>.

Hence, the availability of a simple and low-cost method for detection and removal of Cr(VI) is an urgent issue.

Nowadays, several methodologies are used for the efficient removal of hexavalent chromium and other metal ions from waters, including chemical precipitation<sup>29</sup>, liquid-liquid extraction<sup>30</sup>, reduction with Fe(0) and Fe(II)<sup>28,65</sup> or ion exchange<sup>66,67</sup>. The main disadvantage of these technologies is the use of too expensive and pollutant solvents that make the whole process less sustainable, both environmentally and economically.

For the detection, instead, **inductively coupled plasma optical emission spectroscopy (ICP-OES)** and emission/adsorption spectroscopies are still the main used methodologies, even if they require a too long and expensive sample preparation and don't permit a rapid response.

These is the reasons why developing new strategies both for Cr(VI) detection and removal is an important aim.

In this regard, organic molecules extracted from food waste could be a valid resource for producing high performing adsorbents for different water pollutants<sup>68</sup>.

For example, in the laboratory in which this thesis was developed, efficient eggshell based - membrane functionalized with ascorbic and citric acid, has been devised as example of sustainable combination of nanotechnology and food waste for Cr(VI) abatement<sup>69</sup>.

In this thesis we deepen this aspect, by combining differently-functionalized AuNPs with chitosan from shrimp's shells, for developing systems capable to interact with Cr(VI) in solution and totally abate it.

The possibility to enable AuNPs towards new boosted reduction/adsorption capability of Cr(VI) is an exciting new frontier in environmental remediation field.

Gold nanoparticles are a typical example of plasmonic nano-particles, largely used in a wide range of fields such as biological, catalysis, surface enhanced Raman spectroscopy (**SERS**) and optical sensing.

In the field of environmental remediation, they were used also for capture and detection of heavy metal cations like  $Pb^{2+}$  and  $Hg^{2+70}$ , and in recent years have been used into laser-induced breakdown spectroscopy, which makes it possible to detect several heavy metals by means of hand-held instruments.

In particular, in the case of Cr(VI), AuNPs allowed the revelation of hexavalent chromium species with a limit of detection of  $9 \mu\text{g/L}^{71}$ .

Another field of interest is electrochemistry, in which gold nanoparticles have been used as active electrodes for the detection of hexavalent chromium in water by the use of cyclic voltammetry<sup>71</sup>.

Finally, it has been demonstrated that, in presence of electron donors such as oxalic or formic acids, AuNPs are capable to assist photo-reduction of hexavalent chromium to trivalent chromium<sup>72,73</sup>.

Given all these applications, it is worth deepening the interaction between Cr(VI) and AuNPs.

AuNPs are generally synthesized through "colloidal synthesis" that involves the reduction of gold (III) chloride trihydrate with a reduction agent, that usually works also as anionic capping agent, with the aim to stabilize AuNPs and prevent their aggregation. Citrate is a typical capping agent, commonly used during the reaction; it is therefore expected that, due to the nature of the synthesis, the NPs are negatively charged.

On the other hand, Cr(VI) can be found in water solution in the form of anionic chromate ( $\text{CrO}_4^{2-}$ ,  $\text{HCrO}_4^-$ ,  $\text{Cr}_2\text{O}_7^{2-}$ ) whose concentrations strongly depend on pH.

This suggests that the interaction between AuNPs and Cr(VI), both negatively charged, is not enhanced on the basis of the simple electrostatic interaction.

However, it has been demonstrated that agents as citrate, are capable to efficiently sequester Cr(III)<sup>74</sup>, and this suggests that the abatement of Cr(VI) could be done by exploiting *in situ* reduction of Cr(VI) to Cr(III) following by the seizure of trivalent chromium by capping agent. Among the possible reducing agents, organic acids extracted from fruit peel can be appealing choice, as they could further contribute to recycle food waste through a circular economy approach.

In fact, it has been recently demonstrated that rational combination of citric and ascorbic acids allows a more efficient sequential reduction/scavenging of hexavalent chromium<sup>69</sup>.

For these reasons, on the basis of these previous results, in this study we borrow the same strategy, by exploiting the presence of chitosan as key element to enhance the capacity of the studied systems to abate hexavalent chromium, in an environment-friendly and sustainable way.

The adsorption skills of chitosan are already well-known and used for wastewater treatment<sup>17,18</sup>, in this thesis we use chitosan as concentrator exploiting its adsorption capability and its solubility in aqueous acidic solutions.

Generally, chitosan (Cs) is dissolved in acetic acid (CH<sub>3</sub>COOH) aqueous solution, but in this work, we explored the possibility to dissolve the biopolymer in a mixture of ascorbic (AA) and citric acid (CA), so that to be able to take advantage from the capacity of this mixture to reduce/scavenge Cr(VI) species.

Simultaneously, we tried to identify the best combination of chitosan/chitosan's solvent/AuNPs's capping-agent for the creation of a functional system, varying not only chitosan's solvent but also the capping agents for AuNPs.

**Table 2.1:** Combination of Active Medium and AuNPs Capping Agent explored in the study, where 3MPA is 3-mercaptopropionic acid and 11MUA is 11-mercaptoundecanoic acid, used as alternative to sodium citrate (Citrate) as capping agents. It is interesting to note that all chosen capping agents are carboxylic acids or salts of them.

Active medium	Cs in	Cs	Cs in	Cs	Cs in	Cs
	CH <sub>3</sub> COOH	in AA+CA	CH <sub>3</sub> COOH	in AA + CA	CH <sub>3</sub> COOH	in AA + CA
AuNPs capping agent	Citrate	Citrate	3MPA	3MPA	11MUA	11MUA

The role of each component reported in **Table 2.1**, and the factors involved in the interaction with Cr(VI) in the resulting systems, were studied through cyclic voltammetry. To purpose this scope electrodes with nude AuNPs were electrochemically prepared, the area of which has subsequently been properly functionalized.

It is worth noting that for the construction of our systems, not only chitosan can be recovered from food waste (crustacean's exoskeletons) but also the acids used as solvents can be successfully extracted from vegetable scraps (broccoli leaves and stems, citrus peels, etc.).

In this way, it is possible to develop low-cost systems for sensing and remediation of hexavalent chromium in real water matrices based on the reuse of products from agricultural and food waste, profiting from the absorption capabilities of chitosan, used as a concentrator, and the capacity of waste-extracted organic acids, used as chitosan's solvents, to interact with hexavalent chromium.

## 3.2 Experimental

### 3.2.1 Chemicals and Materials

All chemicals were used as received, without any further purification.

Hydrochloric acid, 37% w/w, TRIS base (molecular weight: 121.14 g/mol), sodium hydroxide (commercial grade), gold (III) chloride trihydrate ( $\text{HAuCl}_4 \geq 99.9\%$  trace metal basis), trisodium citrate dehydrate (99.0%), acetic acid (99%), diphenylcarbazide (DPC), sulfuric acid ( $\text{H}_2\text{SO}_4$ , 97%), citric acid, L-ascorbic acid (99%), 3-mercaptopropionic acid (>99%), 11-mercaptopundecanoic acid (95%), acetone ( $\geq 99.5\%$ ), Indium tin oxide coated glass slide, square (ITO, surface resistivity 8–12  $\Omega/\text{sq}$ ) and ethanol (99.8% v/v) were acquired from Sigma-Aldrich.  $\text{K}_2\text{Cr}_2\text{O}_7$  was purchased from Carlo Erba.

Chitosan was extracted from local shop shrimp's shells as reported in paragraph 2.2.2.

TRIS-HCl was obtained from TRIS base and HCl.

In all experiments ultrapure Milli-Q water was used, obtained from a Milli-Q Integral 5 system. All glassware used for Cit.-AuNPs synthesis were washed with fresh prepared aqua regia ( $\text{HNO}_3$  (conc.): HCl(conc.) 1:3).

### 3.2.2 Synthesis of Citrate-capped AuNPs (Cit.-AuNPs)

Cit.-AuNPs were synthesized following the classical Turkevich procedure<sup>75</sup>. 20 mL of  $\text{HAuCl}_4$  1 mM was placed on a heating plate under magnetic stirring. When the solution was boiling, 3 mL of  $\text{Na}_3\text{C}_6\text{H}_5\text{O}_7$  38.8 mM were added: the solution turned from colorless to dark red. After 5 min. under vigorous stirring, the solution was recovered and put in a water bath down to room temperature.

To remove the excess of citrate, the obtained AuNPs were centrifuged at 12500 rpm for 15 min and re-suspended in Milli-Q water.

The TEM image recorded for Cit.AuNPs and the UV-vis spectrum, were reported in **Figure 3.1**

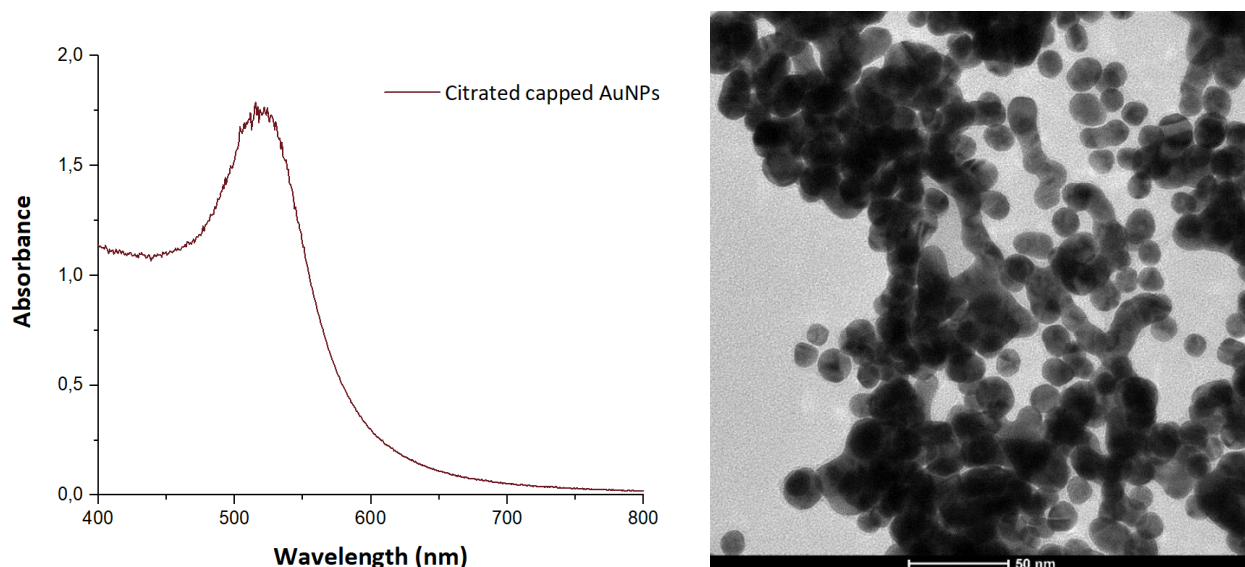


**Figure 3.1:** UV-vis spectra and TEM images of Cit.AuNPs obtained with colloidal synthesis. The TEM image was kindly providing from Rocco Di Girolamo, University of the study of Naples.

### 3.2.3 Functionalization of AuNPs: 3 mercaptopropionic acid-Cit. AuNPs, 11 mercaptoundecanoic acid -Cit.-AuNPs systems

To prepare thiolate-AuNPs, starting from Cit.- AuNPs, 1 mM solutions of 3 mercaptopropionic acid (3MPA) and 11 mercaptoundecanoic acid (11MUA) were prepared in ethanol. Then, 2 mL of prepared solution were added to 5 mL of Cit.-AuNPs. The obtained solutions were left overnight, and then centrifuged and re-suspended in milliQ water to remove the excess of capping agents.

### 3.2.4 Extraction of chitosan from shrimp's shells

Chitosan was extracted from local shop shrimp's shells as reported in **paragraph 2.2.2**.

### 3.2.5 Dissolution of chitosan

Chitosan in general is soluble in acidic media, usually  $\text{CH}_3\text{COOH}$  solutions. In this study, we performed chitosan dissolution using as solvents  $\text{CH}_3\text{COOH}$  5% solution and an acidic mixture of ascorbic acid (AA) 0.025 M + citric acid (CA) 0.075 M. In both cases, the final concentration of chitosan is 0.1 g/L.

### 3.2.6 Functionalization of AuNPs with chitosan

A 2 mL solution containing 40  $\mu\text{L}$  of TRIS-HCl buffer solution (1 M, pH = 7.41) and 200  $\mu\text{L}$  (1 g/L) was prepared in order to obtain a solution with final concentration of TRIS-HCl 20 mM and 0.1 g/L of chitosan. TRIS-HCl buffer was used in order to avoid chitosan precipitation in alkaline environment. 98  $\mu\text{L}$  of this solution were added to 900  $\mu\text{L}$  of AuNPs (Cit. or thiolate nanoparticles). The obtained solution was mixed for 20 min at room temperature and then used for further experiments. Other experiments were conducted on the same functionalized NPs after the removal of exceeding chitosan, by means of centrifugation and resuspension in MilliQ water.

### 3.2.7 Spectroscopic evaluation of Cr(VI) removal capabilities of the different systems

2  $\mu\text{L}$  di Cr(VI) 4,12 mM solution (obtained from  $\text{K}_2\text{Cr}_2\text{O}_7$  dissolution in MilliQ) were added to 998  $\mu\text{L}$  of solution of differently functionalized AuNPs and they were mixed for about 30 min. Then, the solution was centrifuged at 9500 rpm for 15 min. in order to separate AuNPs, and the supernatant was recovered and analysed. To quantify the chromium remained in the supernatant, the protocol devised by USEPA (Method 7196A) was used <sup>76</sup>. Briefly, 20  $\mu\text{L}$  of DPC 0.020 M solution in acetone and 4  $\mu\text{L}$  of  $\text{H}_2\text{SO}_4$  10% v were added to 1 mL of supernatant. The mixture was left to react 5–10 min.

DPC, reduces Cr(VI) to Cr(III), and forms with it a complex,  $[\text{CrDPCO}]^+$ , characterized by an intense fuchsia colour, that allows to detect chromium by means of a UV-vis-NIR spectrophotometer (QE 65,000 Ocean Optics), evaluating the absorbance at 540 nm <sup>76</sup>.

### 3.2.8 Preparation of AuNPs-based electrodes

For electrodepositing AuNPs on Indium Tin Oxide (ITO) coated glasses (surface resistivity 8–12  $\Omega$ /sq) we used a three-electrodes configuration, using Pt wire as counter electrode, SCE (Saturated Calomel Electrode) as reference electrode and ITO coated glasses as working electrodes.

As electrolyte, a solution made of HAuCl<sub>4</sub> 1 mM, H<sub>2</sub>SO<sub>4</sub> 10 mM, and Na<sub>2</sub>SO<sub>4</sub> 10 mM was used. Measurements were performed with Voltalab (VoltaLab 80 Universal Electrochemical Laboratory, 230 V, 47.5–63 Hz and 115 V). Five cycles of potential (cyclic voltammetry) were applied to the electrode from + 1.50 V to - 0.6 V at a scanning rate of 100 mV/s.

The reaction responsible of AuNPs production and deposition is the following:



The obtained AuNPs-ITO electrodes were, then, functionalized through immersion for 1 h in the following solutions:

- Ascorbic acid + citric acid 1 mM (25% ascorbic acid + 75% citric acid);
- Citrate 1 mM; • Chitosan (CH) 0.1 g/L dissolved in CH<sub>3</sub>COOH 5%;
- CH<sub>3</sub>COOH 1 mM;
- Chitosan (CH) 0.1 g/L dissolved in ascorbic acid 0.025 M + citric acid 0.075 M;
- 11-mercaptoundecanoic acid 1 mM; • 3-mercaptopropionic acid 1 mM.

### 3.2.9 Electrochemical determination of Cr(VI)

Cr(VI) was detected by means of cyclovoltammetry, using a three-electrodes configuration, with a Pt wire as counter electrode, SCE as reference electrode and (differently functionalized) AuNPs- ITO coated glasses as working electrodes, immersed in an electrolytic solution containing Cr(VI) 6.86 mg/L, HCl 0.01 M and NaCl 0.01 M.

Measurements were performed with Voltalab (VoltaLab 80 Universal Electrochemical Laboratory, 230 V, 47.5–63 Hz and 115 V).

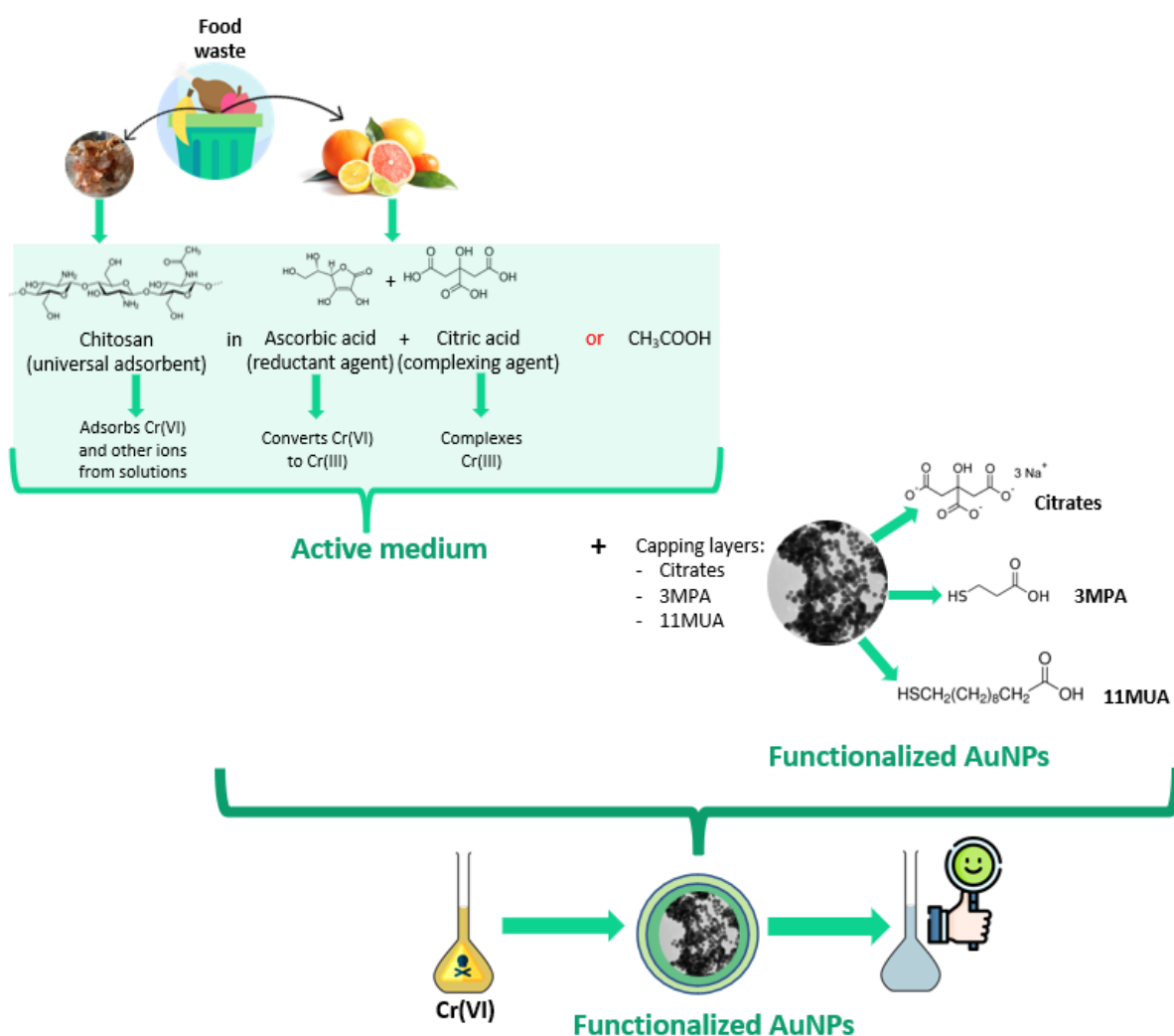
Potential was scanned between 0.6 V and -0.4 V, with a scanning rate of 100 mV/s.

The presence of Cr(VI) was determined by following its reduction reaction:



### 3.3 Results and Discussion

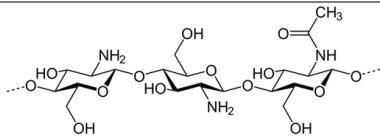
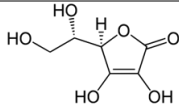
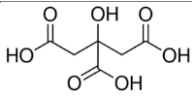
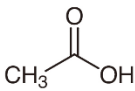
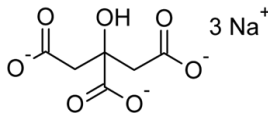
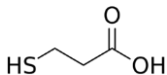
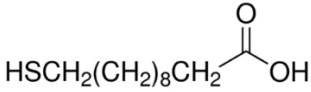
As illustrated in **paragraph 3.1** the aim of this work is to study the combination of different functionalized AuNPs with chitosan obtained from crustaceans' waste and dissolved in a mixture of citric and ascorbic acids, in order to obtain a fully sustainable hybrid system capable to abate hexavalent chromium oxyanions in MilliQ and real water.



**Figure 3.2:** Experimental layout implemented for the abatement of hexavalent chromium from water. Chitosan extracted from food waste was dissolved in acetic acid or in a mixture of citric and ascorbic acid, also extracted from food waste. The so-obtained “active medium” was combined with different type of functionalized gold nanoparticles (Cit.AuNPs, 3MPA-AuNPs and 11MUA-AuNPs) in order to reduce Cr(VI) in water.

The structure and specifics of materials used to develop our nanotechnology are summarized in **Table 3.1**, while a general scheme of the experimental template is reported in **Figure 3.2**.

**Table 3.1:** List of each single element used to develop the studied nano-systems and their structure.

Molecule	Role	Structure	Short name
<b>Chitosan</b>	Adsorber		CH
<b>Ascorbic acid</b>	Reductant agent		AA
<b>Citric acid</b>	Complexing agent		CA
<b>Acetic Acid</b>	Solvent		CH <sub>3</sub> COOH
<b>Sodium citrate</b>			Citrate
<b>3-mercaptopropionic acid</b>	Capping agent		3MPA
<b>11-mercaptoundecanoic acid</b>			11MUA

Initially, UV-vis spectroscopy was used to obtain the data that are systematically compared, in order to investigate the different roles of each component of our systems (chitosan, acid mixture, capping agents).

**In Figure 3.3a** the results of the first set of experiments were reported.

In this first step, the efficiency of hexavalent chromium removal spiked in Milli-Q water was investigated only for the three different capped AuNPs: Citrated-AuNPs (Cit.AuNPs), 11-mercaptoundecanoic acid-AuNPs (11MUA-AuNPs) and 3 mercaptopropionic acid-AuNPs (3MPA-AuNPs).

In **paragraph 3.2.2** Turkevich's procedure for the synthesis of Cit.AuNPs has already been described. As we explained, the anions citrate work both as reductant agents for Au<sup>3+</sup> and capping agents to stabilize AuNPs and prevent their aggregation.

However, the resulting interaction between citrate and AuNPs is labile, and they can be easily replaced by other molecules as 3MPA and 11MUA, characterized by binding -SH groups.

It is important to note that all the selected capping agents are characterized by carboxylic groups which are probably engaged in Cr(VI) species removal. Indeed, all three types of tested nanoparticles enable a small, but significant, abatement of hexavalent chromium, that is not evident in a reference batch of uncapped AuNPs (U-AuNPs), obtained through laser ablation synthesis.

In particular, from the comparison between Cit.AuNPs and 3MPA-AuNPs it is evident that the efficiency in Cr(VI) removal is almost the same (-18.4% and -19.3%, respectively), whereas it is subtly reduced when 11MUA is used as a capping agent.

The two carboxylic acids differ in the length of the alkyl chain, which is longer in 11MUA than in 3MPA, and probably precisely the increasing length might be at the origin of the differences in hexavalent chromium abatement.

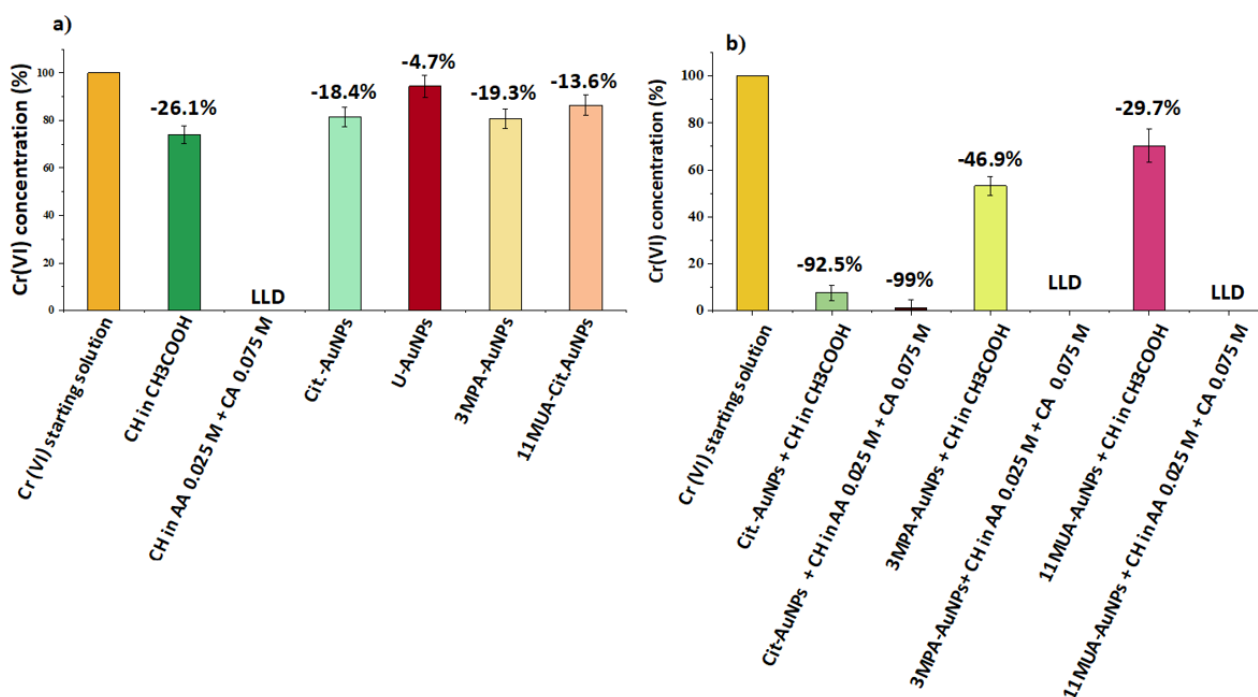


**Figure 3.3:** Abatement of Cr(VI) in a) Au NPs capped with citrates (Cit-Au NPs), 3-mercaptopropionic acid (3MPA-Au NPs) and 11-mercaptoundecanoic acid (11MUA-AuNPs); b) the same type of Au NPs utilized in 4.3a suspended in chitosan/acid active media, obtained by dissolving chitosan either in acetic acid 5% solution or 0.025/0.075 ascorbic (AA)/citric (CA) acid solution. Data acquired from the USEPA diphenylcarbazide-colorimetric analysis. LLD: Below the Lower Limit of Detection.

In the second set of experiments, whose results are reported in **Figure 3.3b**, we tried to increase the efficiency of the systems in Cr(VI) removal, by adding chitosan extracted from shrimps' shells. In addition, the effects of different solvents used for chitosan were evaluated.

In **paragraph 3.1** we described the characteristic of chitosan to be soluble in aqueous acidic media, and we have already mentioned that it is conventionally solubilized in acetic acid 5%. However, in this work, in order to exploit the synergic combination of citric and ascorbic acid,

we investigate the possibility to use a mixture of them as a solvent for chitosan dissolution. In this regard, we used a 1:3 ascorbic acid: citric acid molar mixture (AA/CA). In particular, the choice of the ratio 0.025M/0.075 AA/CA was based on the optimized results of our previous work<sup>77-79</sup>.

Examining the results in **Figure 3.3b**, it is instantly clear that, independently of the type of solvent, when chitosan is added to our systems, the removal of Cr(VI) increases for each type of nanoparticles. However, it is also possible to note that, this behaviour is more pronounced when the mixture AA/CA is used as chitosan solvent and Cr(VI) is almost completely removed. The key role of the mixture ascorbic/citric acid in abatement of hexavalent chromium is also demonstrated with experiments in which chitosan dissolved in AA/CA mixture is used without any type of AuNPs. In fact, in this case, we observe that when chitosan is dissolved in CH<sub>3</sub>COOH 5%, the content of Cr(VI) in the solution is reduced by 26%, while when the AA/CA mixture was used, the abatement of Cr(VI) was complete (the limit of detection of the USEPA DFC colorimetric assay utilized for these experiments was 5 ug/L).

Based on the obtained results, it is possible to corroborate that the presence of the acidic active medium AA/CA is fundamental to ensure the complete reduction of hexavalent chromium. At the same time, it is clear that the activity of the active medium is not affected by the presence of capped AuNPs.

However, when real drinking water is used instead of Milli-Q, it must be considered that it contains various ions that can compete with Cr species in the interaction with chelating/adsorption sites. These interactions could represent interferences that change the decontamination process.

To verify if and how it happens, we spiked hexavalent chromium in real bottled water whose chemical composition is defined in **Table 3.2**.

**Table 3.2:** Chemical composition of bottled water. Chemical-physical constants: Water temperature at the source: 10.8°C · pH at the source: 7.60 · specific electrical conductivity at 20°C: 91 µS/cm · fixed residue at 180°C: 60 mg/L · Hardness °f 5.9 · free CO<sub>2</sub> at the source: 6.0 mg/L

<b>Substances dissolved in one litre of water expressed in ions</b>			
Ca <sup>2+</sup>	11.2 mg/L	SO <sub>4</sub> <sup>2-</sup>	5.6 mg/L
Mg <sup>2+</sup>	3.5 mg/L	NO <sub>3</sub> <sup>-</sup>	3.8 mg/L
Na <sup>+</sup>	2.0 mg/L	Cl <sup>-</sup>	2.0 mg/L
K <sup>+</sup>	0.70 mg/L	F <sup>-</sup>	< 0.1 mg/L
HCO <sub>3</sub> <sup>-</sup>	50 mg/L	SiO <sub>2</sub>	7.1 mg/L

As expected, in real bottled water (BW) there is a reduction of the efficiency of Cr(VI) abatement when Cit-AuNPs are dispersed into chitosan dissolved in CH<sub>3</sub>COOH (from -92.5% in MilliQ water to -61.3% in BW). A similar performance is observed also when the biopolymer is dissolved in the AA/CA mixture, where the abatement of Cr(VI) switches from -99 % in MilliQ water to -80.6% in BW (**Figure 3.4**).

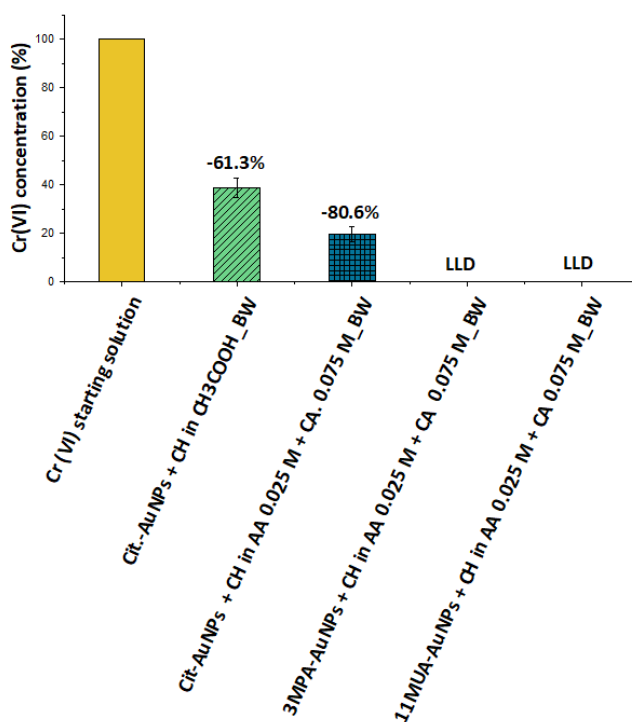


**Figure 3.4:** Efficiency of abatement of Cr(VI) for hybrid capped Au-NPs/chitosan systems in real-world solutions, obtained using bottled instead of MilliQ water.

On the other hand, thiolated capping agents (3MPA and 11 MUA) allowed the complete abatement of Cr(VI) in bottled as much as in MilliQ water.

These experimental data suggest that some of the ionic species normally present in real BW, especially divalent cations as Ca<sup>2+</sup> or Mg<sup>2+</sup>, can effectively compete with Cr(III) species in citrate complexation. In fact, in the pH range of our interest, citrates are known to be effective chelating agents for divalent positive ions. However, when thiolated capping agents as 3MPA and 11MUA replace citrate, no loss of performance occurs, and the systems maintain high removal efficiency also in natural BW.

With the aim of understanding thoroughly the interaction between the different components of our nano-apparatus (chitosan, chitosan's solvents, capping agents and AuNPs) and hexavalent chromium, cyclic voltammetry experiments were used to analyse the different systems during

Cr(VI) detection. Electrochemical techniques enable the detection of chromium, as well as speciation of Cr(III) and Cr(VI).

To do this, AuNPs were electrochemically synthesized and deposited on ITO coated glasses as described in **paragraph 3.2.8**.

After that, the electrodes were immersed in solutions containing the different species described in **3.2.8** section. In this way, we can assume that all the starting AuNPs were the same type, eliminating the potential effects of different synthesis protocols.

**Figure 3.5** reports a typical cyclic voltammetry curve (CV) of AuNPs electrodeposited on ITO, where the peak at 0.606 V indicates the formation of metallic Au. SEM analysis and the red colour that appeared on the ITO glass (**Figure 3.6a, b and c**) also confirm the formation of gold nanoparticles.

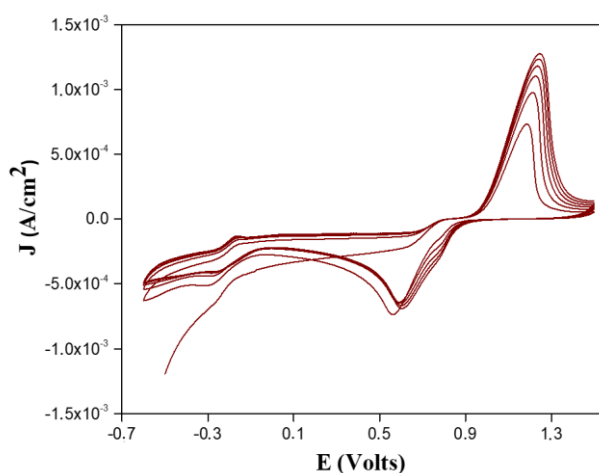


**Figure 3.5:** CV of AuNPs electrodeposited on ITO.

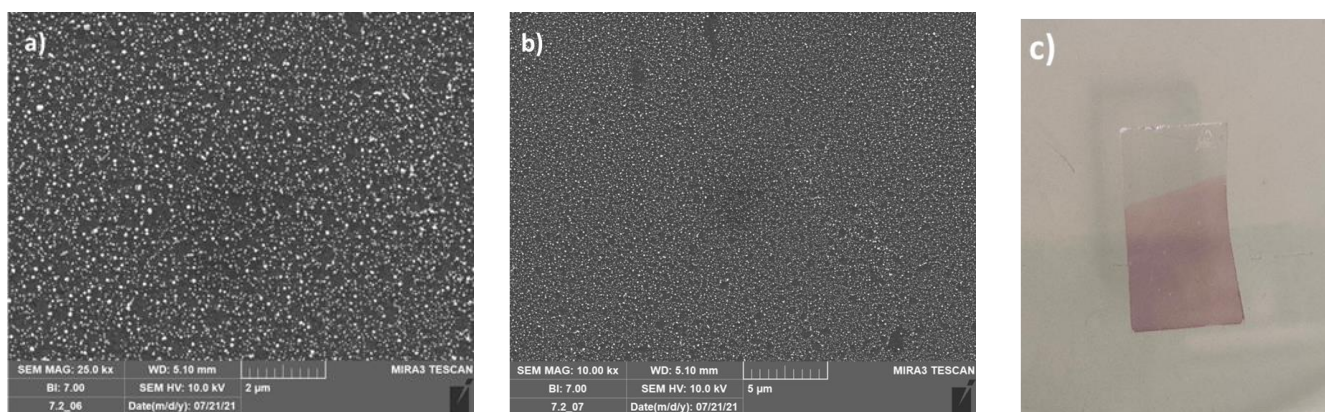


**Figure 3.6:** a) SEM image of AuNPs on ITO electrode functionalized with citric acid + ascorbic acid 1 mM; b) SEM image of AuNPs-ITO working electrode; c) AuNPs electrodeposited on ITO glass.

Afterwards, the obtained AuNPs electrodes were functionalized by immersing them in different solutions:

- Citrate solution (1 mM);
- 3MPA solution;
- 11MUA solution (1 mM);
- CH<sub>3</sub>COOH (1 mM);
- CA+AA (25:75) solution (1 mM);
- Chitosan 0.1 g/L dissolved in CH<sub>3</sub>COOH 5%;
- Chitosan 0.1 g/L dissolved in AA 0.025M + CA 0.075M.

All the obtained systems were tested during the electrochemical detection of Cr(VI).

In **Figure 3.7** and **Table 3.3** the obtained data are summarized.

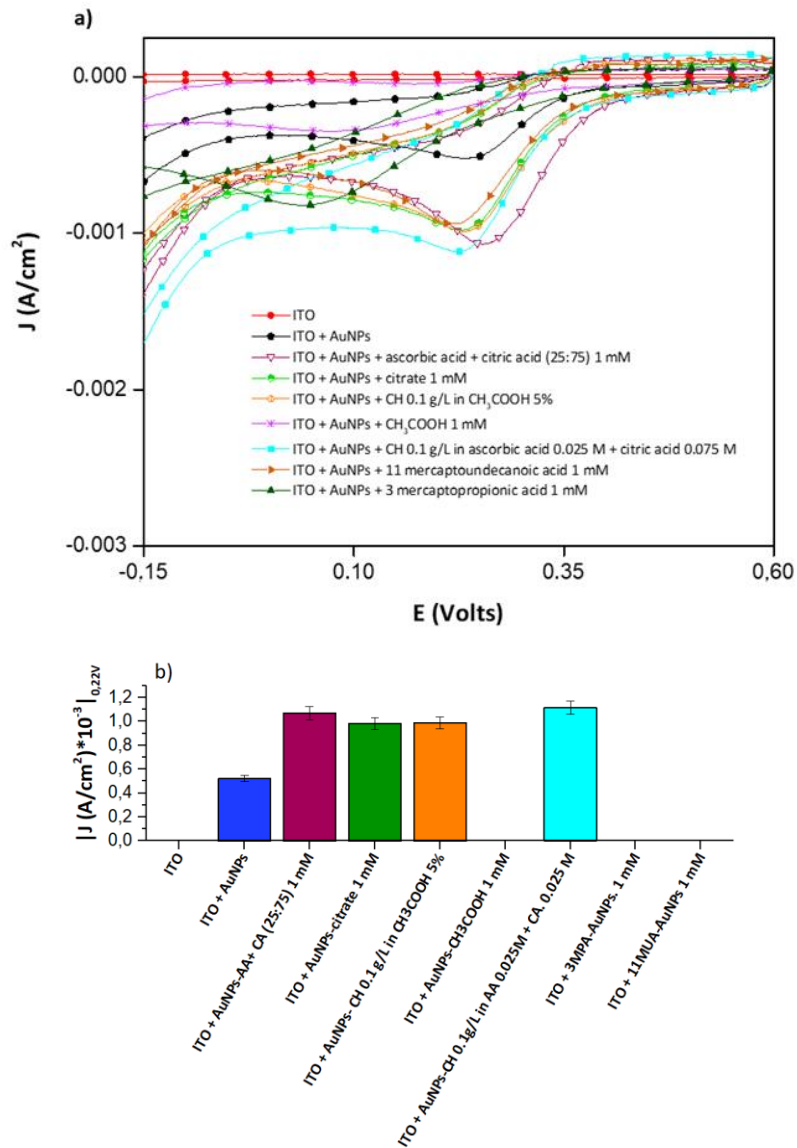


**Figure 3.7:** Electrochemical detection results: a) cyclic voltammograms for different chemical components (AuNPs, capping agent, chitosan, and acids used for chitosan dissolution); b) bar graph of the absolute value of the intensity of the peak in the CV curves for each analysed system.

**Table 3.3:** Electrochemical results obtained with differently functionalized ITO-AuNPs electrodes immersed in an electrolytic solution containing Cr(VI) 6.86 mg/L, HCl 0.01 M and NaCl 0.01 M (prepared with MilliQ water). Data highlighted in orange refers to the 3-MPA sample, which is not stable under the measurement conditions.

Working electrode	$J \cdot 10^{-3}$ (A/cm <sup>2</sup> )	E (Volts)
ITO	0	0
ITO + AuNPs	-0.520	0.237
ITO + AuNPs + ascorbic acid + citric acid (25:75) 1 mM	-1.07	0.254
ITO + AuNPs + citrate 1 mM	-0.980	0.229
ITO + AuNPs + CH 0.1 g/L in CH <sub>3</sub> COOH 5%	-0.989	0.232
ITO + AuNPs + CH <sub>3</sub> COOH 1 mM	-0.348	0.076
ITO + AuNPs + CH 0.1 g/L in ascorbic acid 0.025 M + citric acid 0.075 M	-1.117	0.226
ITO + AuNPs + 11 mercaptoundecanoic acid 1 mM	-0.939	0.218
ITO + AuNPs + 3 mercaptopropionic acid 1 mM	-0.822	0.042

The detection capability of the various systems can be deduced from the reduction peak at 0.2-0.3V, referring to the reduction of hexavalent chromium. For instance, a peak characterized by a higher absolute value is representative of an increase interaction with Cr(VI) in solution, enabling an easier detection; while a higher electrochemical potential indicates the possibility of Cr(VI) reduction in milder conditions, which is advantageous for sustainable remediation.

As indicated from the results in **Figure 3.7**, ITO alone electrode, is not effective in the detection of hexavalent chromium, while when ITO glass is functionalized with AuNPs, electrocatalytic reduction of Cr(VI) occurs. It is interesting that when AuNPs-ITO electrode is functionalized with chitosan dissolved in AA + CA mixture, the highest value of  $|J|$  (that indicates the activity) is obtained, in line with what we see with the UV-vis spectroscopy data.

Moreover, electrochemical measurements performed with systems containing AuNPs and AA +AC mixture, in the absence of chitosan, allow us to verify that the two acids contribute both to Cr(VI) reduction (they shift the reduction potential to a higher value in comparison to that of simple AuNPs) and Cr sequestration (high current density).

Even when ITO + AuNPs electrode is functionalized with CH 0.1 g/L dissolved in CH<sub>3</sub>COOH, it is evident a positive effect that in this case is due to a sequestration action (in fact, the potential is constant while there is a higher current density). Moreover, in this instance, we can surely exclude any positive effect from CH<sub>3</sub>COOH since the electrode ITO+AuNPs functionalized with CH<sub>3</sub>COOH 5% alone, shows worst performance than the starting one

ITO+AuNPs, with a lower reduction potential and a lower density. When the starting electrode ITO+AuNPs is functionalized with 3MPA, we can see a shift of the pick at 0.042 V that suggests an oxidative action from this type of thiol, opening a critical issue related to the stability of 3MPA-AuNPs. In fact, simple resuspension cycles are sufficient to disintegrate and dissolve this type of NPs (**Figure 3.8**), and just this short shelf-life is the reason why, even though UV-vis spectroscopy data underline a good Cr(VI) abatement when suspended in chitosan-AA/CA solutions, they cannot be recommended for practical purposes .



**Figure 3.8:** Gold nanoparticles functionalized with 3-mercaptopropionic acid dissolved after resuspension.

On the opposite, positive effects on the AuNPs electrode activity are recorded in the case of functionalization with citrate and 11MUA. These data support the hypothesis that capping agents are not significantly contributing to Cr(VI) reduction, but they limit their effect to enhancing the surface adsorption of chromium ions.

### 3.4 Conclusions

In summary, we demonstrated that hybrid systems consisting of carboxylated-AuNPs suspended in chitosan acidic solution can be used for the efficient removal of Cr(VI) in both Milli-Q and drinking water. We performed a systematic comparison of the affinity towards Cr(VI) among AuNPs capped with different types of carboxylated molecules: citrates, 3-mercaptopropionic and 11-mercaptoundecanoic acids. CV and UV-Vis experiments demonstrated that the carboxylated capping agents are active in promoting the adsorption of chromium species, whereas they do not influence their reduction to Cr(III). The introduction of chitosan extracted from food waste strongly enhances the adsorption capabilities of these Au NPs. In this respect, chitosan confirms its role of universal scavenger, already demonstrated in previous works on environmental remediation. In particular, its cationic nature enables the efficient attraction of the oxyanionic Cr(VI) species. However, a complete removal of Cr(VI) species can be obtained only by using a mixture of ascorbic and citric acids, which are added to chitosan to assist its dissolution. Ascorbic acid reduces Cr(VI) to Cr(III) and citrates form complexes with Cr(III), enabling the complete removal of hexavalent species. This active medium allows the Au NP suspensions to remain stable and sustain the total abatement of Cr(VI) even in the presence of other ionic species that are normally present in natural, drinking water. In particular, both 3-mercaptopropionic and 11-mercaptoundecanoic acids allow the full abatement of Cr(VI) in drinking water. However, the low stability of Au NPs capped with 3-mercaptopropionic under multiple resuspension cycles makes 11-mercaptoundecanoic acid the best choice in terms of efficiency and stability for this type of applications. Overall, this study demonstrated that molecules extracted from food waste (chitosan, ascorbic and citric acid) can be synergistically combined in order to enhance the functional properties of nanoparticles that are commonly utilized for a variety of applications. This approach feeds the research in the field of sustainable chemistry<sup>54,80,81</sup>, paving the way to a circular design of new classes of materials for environmental remediation.

# Chapter 4

---

## 4. From water for water: different functionalized chitosan bubbles hydrogel for sustainable dyes removal

The content of this chapter is under submission to a peer-reviewed scientific journal, and the main results were presented into a poster-session at “9<sup>th</sup> IUPAC International Conference on Green Chemistry” in Athene.

In these paragraphs, we deepen some aspects of water remediation and exploit the possibility to develop all-in-one systems, based on hydrogel synthesized from food waste, which are capable to capture, degrade and remove environmental pollutants such as organic industrial dyes, from water.

In particular, a brief introduction of hydrogel, their use and ionotropic gelation synthesis method is given.

Moreover, we demonstrate that chitosan hydrogels in form of bubbles are capable to remove both Methylene Blue (MB) and Methyl Orange (MO) from water, two industrial dyes oppositely charged (positive and negative, respectively).

The possibility to use chitosan bubbles allowed us to combine its great adsorption capability with the well-known antibacterial properties.

In addition, the use of hydrogel in form of bubbles makes it possible to enhance the adsorption capability towards specific classes of pollutants and to exploit photocatalytic properties, by adding into chitosan bubbles specific functional units, such as PEDOT:PSS, AuNPs, AgNPs and TiO<sub>2</sub> NPs at different concentrations.

The adsorption test showed that by incorporating PEDOT:PSS into chitosan bubbles, the adsorption capability of the system significantly increases up to reach a removal > 90% for MB and > 80% for MO within two hours. On the other hand, the binary system composed of chitosan and TiO<sub>2</sub> Degussa P25 shows interesting photocatalytic properties both for MB and MO.

Adsorption capability and photocatalytic efficiency under direct sunlight irradiation were investigated by **UV-vis spectroscopy**.

The influence of the additional functional units TiO<sub>2</sub>, AuNPs, and AgNPs on the mechanical properties of the chitosan hydrogels was evaluated by preparing them also in form of films. At the same time the antibacterial and antifungal activity was proved with appropriate tests with *Pseudomonas Syringae pv. Phaseolicola* and *Alternaria Tenuissima*, respectively.

## 4.1 Introduction

### 4.1.1 Hydrogels: structure and properties

Hydrogels are 3D polymeric networks that do not dissolve but swell in water. Their main characteristic, in fact, is to have a "soft" and hydrophilic nature that allows them the uptake of water in such a way as to remain hydrated but, at the same time, solid <sup>82</sup>.

The functional groups that are responsible for such hydrophilicity are, in general,  $-\text{CONH}_2$ ,  $-\text{NH}_2$ ,  $\text{SO}_3\text{H}$ ,  $-\text{OH}$ ,  $-\text{COOH}$  and  $-\text{CONH}$ .

Moreover, their ability to remain in the solid state and swell when immersed in water, is given by the fact that the polymer chains that constitute the hydrogel, are crosslinked.

In particular, the role of crosslinker is keeping together the polymer chains in the hydrogel. When the crosslinker is not present, in fact, the polymer chains that are hydrophilic, are thermodynamically compatible with water, and therefore, they can dissolve in it.

In the presence of the crosslinker, however, what happens is that the crosslinking junctions, which form between the polymer chains, counterbalance solubility thanks to the retractive force of the induced elasticity.

In particular, when these forces are equal, the hydrogel swelling capacity reaches a state of equilibrium<sup>83</sup>.

Quesada-Perez et al.<sup>84</sup> describe hydrogel swelling process as a more or less complex procedure that involves more steps:

- In the 1st step, the functional groups responsible of polymeric molecule hydrophilicity, establish interactions with  $\text{H}_2\text{O}$  molecules that, in this case, is called " primary bond water".
- In the middle step, even the hydrophobic functional groups of the polymer start to interact with water that in this case is called "secondary bound water". The set made by primary and secondary water, constitutes the total water involved in the process.
- In the third and last step, some additional water is adsorbed, giving rise to hydrogel swelling. The water adsorbed when the retroactive forces of elasticity are equal to hydrophilicity at the equilibrium state, is called "free water" or "bulk water". It depends on the specific interactions between  $\text{H}_2\text{O}$  and polymeric chains and temperature<sup>85</sup>.

As we see from **Figure 4.1**, in the 3D network of such material, the portion formed by the junctions of different polymer chains through crosslinking points is called "mesh". It is precisely

the capacity of this mesh to seize the liquids, generally water, which is responsible for the solidity of the hydrogels.

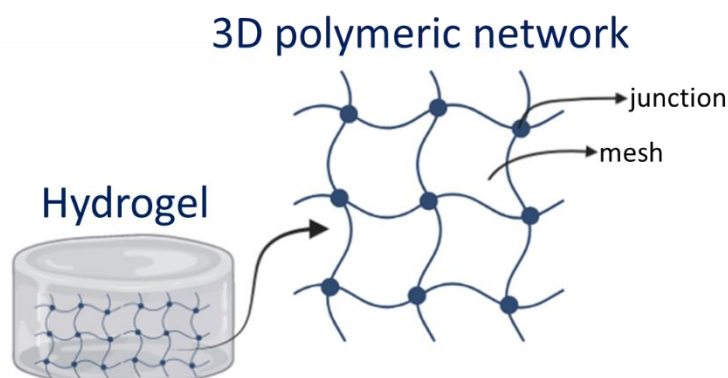


**Figure 4.1:** Schematic representation of the 3D polymeric network of hydrogel materials.

Hydrogels can be classified in different ways, for examples, on the basis of their pore size, swelling properties or structure (crystalline, amorphous or semicrystalline).

In **Figure 4.2**, an overall scheme of the different possible classifications of hydrogel is reported<sup>86</sup>. A detailed analysis of all illustrated categories is beyond the scope of this thesis; however, we will focus on the categories of greatest interest for our purposes.

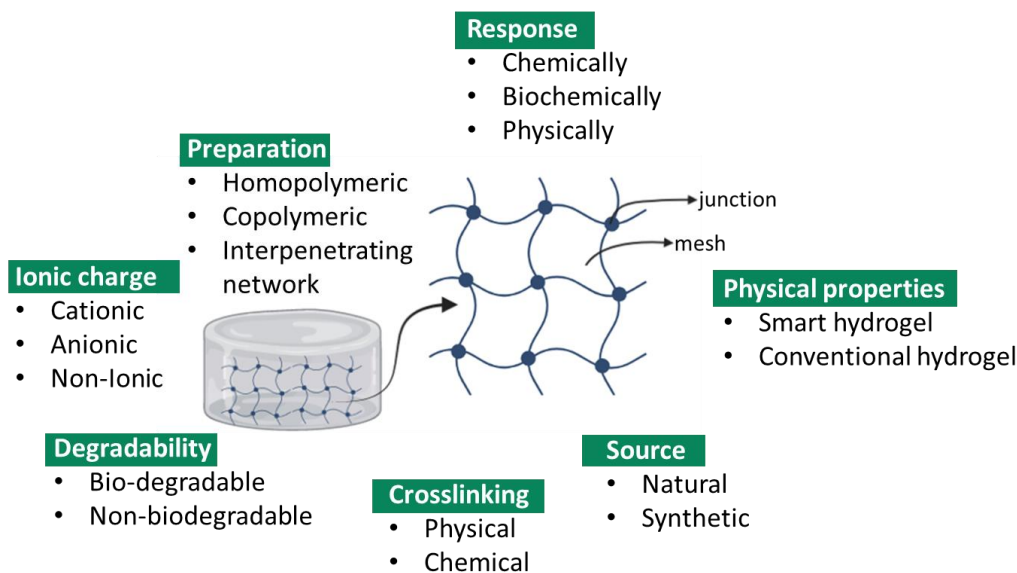


**Figure 4.2:** General hydrogel classification.

On the basis of inter-chain interactions, hydrogels can be divided into physical and chemical hydrogel.

The physical hydrogels are crosslinked through physical interactions such as van der Waals forces, electronic or hydrophobic interactions and hydrogen bonds. These interactions can be easily destructed and recreated in a reversible way<sup>87</sup>, and it is for this reason that in the last few years, these gels are receiving an increasing interest<sup>88-90</sup>.

However, despite physical hydrogels can well adsorb water, they could be characterized by the presence of small free chains that constitute defects of the network<sup>91,92</sup>.

For this reason, sometimes, chemical crosslinkers that establish chemical bonds between polymeric chains, are preferred to guarantee a more stable structure and a more efficient swelling. In this case, the hydrogels are called precisely "chemical hydrogels"<sup>93</sup>.

Then, some hydrogels, whether physical or chemical, can originate from natural sources rather than synthetic, therefore they are called "natural hydrogels".

Natural hydrogels include hyaluronic acid, collagen, alginate, silk fibroin, **chitosan** and all those hydrogels that can be prepared from decellularized tissues. A great advantage in the use of such materials, lies in the characteristics imparted by the source, such as low or no toxicity, biocompatibility and biodegradability, as well as the possibility of using them in injectable gels<sup>94</sup>.

These characteristics, make them full-fledged biomaterials that, now as in the past, attract increasingly attentions in biomedical and environmental fields<sup>95-97</sup>.

In this thesis, natural chitosan-based hydrogels obtained with physical crosslinking, will be considered.

Hydrogel formation is one of the most interesting applications of chitosan<sup>98-100</sup>. Among the advantages in using this biopolymer for the synthesis of hydrogels there are: its low cost (especially if extracted from food waste), the biodegradability that can be modulated by controlling the degree of deacetylation (DD) and biocompatibility<sup>101</sup>.

For all characteristics mentioned above, chitosan hydrogels are widely used in a great number of fields.

In the field of wound dressing<sup>102</sup>, these hydrogels arouse deep interest, especially for their antibacterial activity and due to their capacity to have a stimulatory action on leukocytes<sup>103</sup>.

In the pharmaceutical field, instead, chitosan hydrogels can be considered good candidates for drug delivery thanks to the modulable degradability and short duration in physiological conditions<sup>104-106</sup>.

Moreover, in the last few years, the behaviour of these chitosan-based soft biomaterials is becoming increasingly studied in the field of environmental remediation, especially due to the presence of reactive functional groups, as hydroxyl group (-OH) and primary amine groups (-NH<sub>2</sub>) on the chitosan backbone.

In this thesis, we took advantage of these properties, focusing on the application of hydrogel bubbles made of pure chitosan on water remediation.

Moreover, to enhance the capacity of water storage of this natural gel, that is commonly lower than synthetic ones<sup>107</sup> the bubbles of pure chitosan have been added with active components such as polymeric blends or photocatalytic nanoparticles (Au, Ag and TiO<sub>2</sub> NPs).

In particular, the bubbles used in this work are physical hydrogel prepared according to ionotropic gelation method.

#### **4.1.2 Ionotropic gelation**

Ionotropic gelation is a process in which a Polyelectrolyte (PE) is crosslinked thanks to the contact between macromolecules, or small molecules, of opposite charge. This contact creates a liquid-gel separation and it is possible to distinguish a rich-polymer area (gel) surrounded by a poor-polymer area (liquid)<sup>108</sup>.

This procedure is generally used for the synthesis of hydrogel beads starting from biopolymer as chitosan, pectin, cellulose, alginate etc., that in the last years are becoming increasingly successful in scientific research field<sup>109</sup>.

In the case of chitosan (CS), ionotropic gelation exploits the cationic behaviour of the polymer that at acidic pH (pH < 6, e.g., when it is dissolved in CH<sub>3</sub>COOH (pKa about 6.3-7.2)) comes in the form of cation, due to the protonation of amino groups, thus forming a polyelectrolyte in the form CS-NH<sub>3</sub><sup>+</sup>.

Instead, the gelling agent is, generally, a solution of a counterion of PE that, by combining with it, induces gelation by cross-linking and forms the hydrogel<sup>108</sup>.

In this thesis, NaOH has been used as gelling agent, by exploiting the presence of ions OH<sup>-</sup>, that interact with the cationic polysaccharide and induce the formation of stable connection zones between polymer chains, through the instauration of hydrogen bonds.

In this way a physical hydrogel is formed and within its mesh water or other molecules are physically trapped. At the same time, they can be free to migrate by diffusion depending on their size and the size of the pores of the gel.

The method that is generally employed for the synthesis is based on the diffusion of the counter-ion (in this case OH<sup>-</sup>) within polyelectrolyte droplets introduced into the gelling agent solution.

The use of ionotropic gelation techniques presents different advantages: first of all, the absence of sophisticated instruments and expensive or highly toxic reagents makes this procedure simple, low cost and fast, without long time preparation<sup>110-112</sup>. Moreover, the use of a physical crosslinker makes possible the creation of a reversible hydrogel, that could be used in biomedical and environmental field, minimising the risk of undesirable effects or possible toxicity.

However, among the disadvantages of this method, the risk of obtaining materials with low mechanical stability is certainly to be mentioned<sup>113,114</sup>. To overcome this disadvantage, recently, different strategies have been developed, for example the addition of other natural polymers, metal ions or functional units<sup>107</sup>

### 4.1.3 Chitosan bubbles for sustainable dye removal from water.

In the **chapters 1** and **3** the theme of environmental remediation, and in particular of water cleaning, has already been faced, with particular focus on heavy metal ions removal such as hexavalent chromium.

However, heavy metal ions are not the only worrying pollutants.

When the objective is to develop new technologies for purifying water, it must be considered that a real water sample can be affected on one hand by biological agents (viruses and bacteria) on the other, by chemical substances (heavy metals emerging pollutants and organic dyes).

In this chapter we will focus on the latter, trying to develop systems capable to resist to the presence of microbial agents of real samples water and remove organic dyes.

Organic dyes are extensively used in different industrial sectors, especially textile and tannery industry but also paper and pulp industry or dye manufacturing, so that they can be easily found in various industrial wastewaters even at high concentration levels. Recent studies have reported that, annually, about  $7 \times 10^7$  tons of synthetic dyes are produced worldwide, with over 10,000 tons of such dyes are used by textile industries<sup>115</sup>. Furthermore, the global textile market is estimated to grow in the next few years<sup>116</sup>. Unfortunately, the concentration of organic dyes in textile wastewater can be as high as 250 mg/L<sup>117</sup>, posing serious hazard for the environment.

At very high concentration level, dyes modify the colour of the water and increase biochemical and chemical oxygen demand, limit light penetration and impair photosynthesis and plant growth; at lower concentration range, however, they can promote toxicity, mutagenicity, and carcinogenicity and they enter the food chain, providing recalcitrance, bioaccumulation, and secondary pollution. In addition, they can cause skin irritation, allergies, or gastrointestinal and respiratory diseases<sup>115</sup>.

The chemical structure of organic dyes can be various, for example azo dyes, which are the most widespread class (over the 60% of the textile dyes), are characterized by the presence of at least one azo group, while acid dyes are water-soluble anions or basic dyes are water-soluble cations.

Despite their chemical variability, all the synthetic dyes have in common a high solubility in water, and the fact that their structure can be barely degraded, without the formation of

dangerous intermediate species. In particular, they are highly stable both under solar light and environmental oxidation, and do not undergo bioremediation.

For these reasons, conventional treatment options are frequently ineffective, and innovative advanced decontamination approaches are needed. Different strategies have been proposed in literature: coagulation, flocculation, advanced oxidation (Fenton or photo-Fenton), ion-exchange, electrochemical treatments, adsorption and biological (bacteria or enzymes or fungi or algae -assisted) degradation are some examples<sup>116</sup>.

Since it is desirable that the employed decontamination system is characterized by easiness of preparation and use, stability, fastness of dye removal and low cost, adsorption (that is a surface-based process in which adsorbed molecules or ions are attracted to a solid adsorbent surface) often is considered a viable option. Activated Carbon are the commercial standard for adsorption systems for the treatment of industrial wastewater, but their production and regeneration are characterized by high costs and require treatment at very high temperature. In addition, they derive from fossil fuels: all these characteristics pose limitations and doubts on their extended use.

On the contrary, the preparation and employment of the adsorption system should be characterized by a low environmental impact, suggesting that the use of natural materials, which can be processed according to sustainable chemical processes, is a virtuous strategy.

In this perspective, the use of hydrogel bubbles made of chitosan derived from food waste, as main component of multi-functional -systems, capable of adsorb pollutants, is appealing.

Generally, multi-functional systems are made by <sup>118,119</sup>:

- An **adsorbing unit**: a good adsorbent is a component with high water trapping ability, that can be easily recovered after use, and which is easy to manipulate. Obviously, it

should not release any toxic compounds in the surrounding aquatic environment, and it should be obtained through a simple, sustainable, and low-cost procedure.

- A **recognition unit**: molecular species that are able to interact in a quite specific way with the analyte or a class of analytes, they favour its capture and reduce its desorption.
- **photocatalyst**: consisting of plasmonic nanoparticles (NPs) or dielectric NPs able to promote photodegradation of pollutants through the capture of UV-visible light.

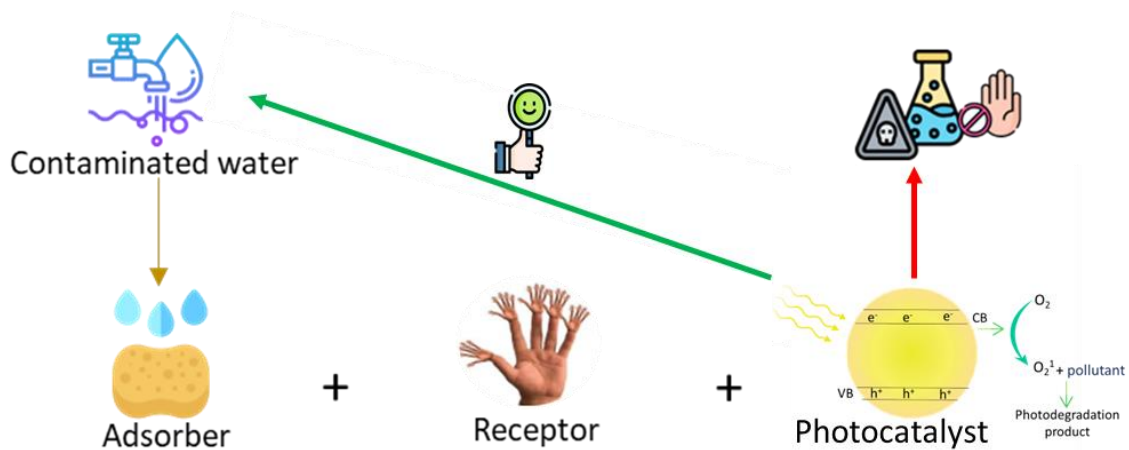


**Figure 4.3:** Schematic representation of nano-system used for water remediation.

The idea at the basis of this work is to use chitosan extracted from shrimp's shells to create physical natural hydrogel bubbles that can be used as **adsorbing unit** in multi-functional systems created to remove dyes from wastewater.

This is a win-win approach: on one hand what is considered a waste is converted into a high added-value product, on the other it is possible to improve water quality. Other advantages are tightly linked to the proposed system: chitosan is a biocompatible and biodegradable natural polymer, the preparation of the adsorbent system in the form of bubbles is extremely simple and guarantees the adsorbent removal just thanks the use of a common filtering system or tweezers. At the same time, the synthesis protocol is extremely versatile and, it can also enable the preparation of the adsorbent in other structures and geometrical forms, for example in the form of film. In addition, chitosan is characterized by an antimicrobial activity that can be exploited for further improvement of water quality<sup>120</sup>. This last aspect is a significant advantage in comparison to other natural biopolymers, such as pectin and alginate, from which it is possible to gain similar hydrogel-based adsorbents<sup>118,119</sup>.

Moreover, hydrogel bubbles can integrate several new functionalities.

For example, as previous illustrated, chitosan in standard conditions (in almost neutral pH) is considered a positively charged polymer, since its aminic units are protonated ( $pK_a \sim 6.5^{121,122}$ ), and this property make it ideal for interaction and adsorption of negatively charged molecules. In order to extend its activity in the case of positively charged pollutants, it is necessary to modify (increase) the pH of the environment: in this way it is possible to convert the aminic unit of the polysaccharide chain into  $NH^-$  groups and introduce negative charges on the hydroxyl groups, which are ideal for the interaction with positive species in water. Even if this could be an effective strategy, it requires a constant monitoring and adjustment of the pH of the wastewater from an external operator decreasing simplicity and immediacy of the decontamination system.

Our aim was to create a universal adsorbent, efficient in the adsorption of both positive and negative molecules. To pursue this scope, we included inside the chitosan matrix an additional functional unit which was able to improve the interaction with organic pollutants (in particular, synthetic dyes) thanks to the presence of an extended structure of conjugated  $\pi$  bonds. In particular, we inserted inside the hydrogel matrix a derivative of polythiophene, poly(3,4-ethylenedioxythiophene) polystyrene sulfonate (PEDOT:PSS), which is one of the most common and studied conductive polymer.

Moreover, with the aim to guarantee a complete dye removal in a reduced amount of time, and to exploit an efficient **optical nanoantenna unit for pollutant photodegradation**,  $TiO_2$  nanoparticles ( $TiO_2$  NPs), gold nanoparticles (AuNPs) and silver nanoparticles (AgNPs), were embedded into the chitosan matrix.

The possibility to add nanoparticles inside hydrogel bubbles, allow us to exploit the catalytic activity of these functional units under solar illumination, without the risk to release into the environment any possible toxic elements.

In this work, Methyl Orange (MO) and Methylene Blue (MB) have been selected, as references of negatively and positively charged dyes, respectively. MO is an allergenic substance that can cause eczema upon contact with the skin and its presence in living organisms is considered harmful; similarly, MB can cause eyes and skin irritation, its ingestion may cause gastrointestinal irritation with nausea, vomiting and diarrhoea, while inhalation can cause respiratory tract irritation. Other health hazards linked to chronic exposition to high concentration of MB are methemoglobinemia, cyanosis, convulsions, tachycardia, dyspnoea and mutagenic effects.

Their solutions have been treated with hydrogel bubbles made of pure chitosan (CH), chitosan+PEDOT:PSS (CH@PEDOT:PSS) where PEDOT:PSS has been added at different concentrations, chitosan+AgNPs (CH@AgNPs), chitosan+AuNPs (CH@AuNPs) and chitosan+TiO<sub>2</sub> NPs (CH@TiO<sub>2</sub>) where TiO<sub>2</sub> has been added at different concentrations.

**Table 4.1** summarizes all systems used in this work.

**Table 4.1:** Functional unit used to modify chitosan matrix, their concentration in the starting solution of chitosan 10g/L and short name used to indicate each system in this thesis.

Functional Unit (F.U.)	F.U. concentration	Bubbles short name
-	-	CH
AgNPs	-	CH@AgNPs
AuNPs	-	CH@AuNPs
TiO <sub>2</sub>	0.1 % (w/v)	CH@TiO <sub>2</sub> 0.1%
TiO <sub>2</sub>	1 % (w/v)	CH@TiO <sub>2</sub> 1%
PEDOT:PSS	0.1 % (v/v)	CH@PEDOT:PSS 0.1%
PEDOT:PSS	1 % (v/v)	CH@PEDOT:PSS 1%

The amount of adsorbed dye as function of time has been calculated.

After the reaching of equilibrium of the adsorption process, the dye solutions containing the hydrogels bubbles have been disposed under illumination using a solar simulator and the photodegradation capability of the different systems have been evaluated.

In this way, thanks to the employment of a system that pair adsorption properties with photodegradation capabilities, it was possible to achieve complete dye removal.

Moreover, to be sure to have a system that can be used in real water samples, without deteriorating upon exposure to viruses and bacteria that are generally present in real wastewater, the antibacterial and antifungal properties of chitosan hydrogels were proven with tests performed with *Pseudomonas Syringae pv. Phaseolicola* and *Alternaria Tenuissima*, respectively. This study has required the formulation of chitosan hydrogel in form of films.

The preparation of chitosan-based hydrogels in the form of film allowed us to do a further characterization of their mechanical properties and to better understand if and how the introduction of nanoparticles (AuNPs, AgNPs and TiO<sub>2</sub>) can influence them.

#### 4.1.4 Brief introduction of general chemical physical properties of PEDOT:PSS

Poly (3,4-ethylenedioxythiophene)polystyrene sulfonate (PEDOT:PSS) is a polymer constituted by two ionomers: poly(3,4-ethylenedioxythiophene), also known as PEDOT, and polystyrene sulfonate (Figure 4.4).

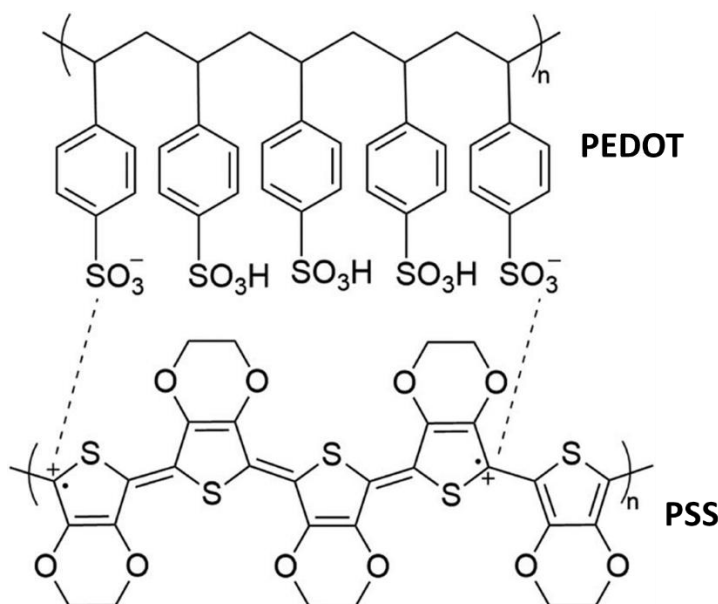


Figure 4.4: Chemical structure of Poly (3,4-ethylenedioxythiophene)polystyrene sulfonate (PEDOT:PSS).

The ionomer PEDOT is one of the most common and studied conductive polymer, recently used in a wide range of applications such preparation of sensors or organic electronics<sup>123</sup>, preparation of organic photovoltaics<sup>124</sup> or preparation of photo-catalysts for environmental remediation<sup>125</sup>.

PEDOT presents a lot of advantageous properties: it is characterized from a very high conductivity (400-600 S/cm), good stability in the oxidized state with a low oxidation potential, and it is possible to obtain highly transparent and thin oxidized films from it<sup>126</sup>.

It can be prepared via chemical or electrochemical polymerization approach, through the oxidative polymerization of its starting monomer, the ethylenedioxythiophene (EDOT)<sup>127</sup>.

However, this polymer is insoluble in water, and this makes difficult its use for a wide variety of interesting applications.

To overcome this obstacle for the applications that require the polymer dispersion, PEDOT is combined with polystyrene sulfonate, thus generating PEDOT:PSS.

In this compound, the component of PEDOT is characterized by a positive charged surface with a  $\pi$ -conjugated system, while the part of PSS is negative charged (Figure 4.4)<sup>115,128</sup>

In PEDOT:PSS, the two ionomers are bonded together with Columbic interactions and, generally, to stabilize the compound in water, poly(4-styrylsulfuric acid) (PSSH) in excess is required.

The most common PEDOT:PSS ratio in good aqueous dispersions is 1:2.5 wt.

#### 4.1.5 Brief introduction of chemical-physical properties of TiO<sub>2</sub>

Titanium dioxide, TiO<sub>2</sub>, is an inorganic compound that looks like a white odourless and non-combustible powder.

This compound appears as not very soluble particulate, and exists in 3 different polymorphic forms: brookite, anatase and rutile.

The most reactive polymorph is anatase, with a reactivity of 6 times of than of rutile, in generating ROS (Reactive Oxygen Species) when irradiated by UV light<sup>129</sup>. It is a wide band gap semiconductor, which is able to absorb light mainly in the UV region (band gap= 3.2 eV,  $\lambda=387$  nm)

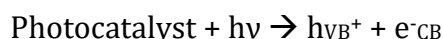
TiO<sub>2</sub> DEGUSSA P25, is a commercial product made of TiO<sub>2</sub> NPs, which are a mixture of rutile and anatase phase. It finds abundant use as white pigment and is one of the top 5 nanoparticles employed in consumer products<sup>130</sup>.

Moreover, TiO<sub>2</sub> NPs are also used in medicine, cosmetic, pharmaceutical and food products, as well as in solar cells as photoactive materials, and in contaminants water treatment<sup>131</sup>. Among the most interesting applications of recent years, there are those that exploit their high stability and photocatalytic properties.

Precisely these characteristics will be exploited in this study.

In general, a mechanism of photodegradation induced by a photocatalyst provides for different steps<sup>132</sup>:

1. The adsorption of an efficient photon leads to the generation of a hole in the valence band (VB), due to the transition of an electron from VB to the conduction band (CB):

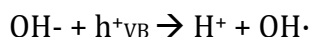


2. The O<sub>2</sub> presents in the solutions combine itself with the generated e<sup>-</sup>CB and the ionosorption of O<sub>2</sub> occurs:

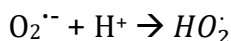


the recombination of e<sup>-</sup>CB and h<sup>+</sup>VB is prevented, and the oxidation of dye can happen.

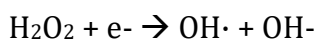
3. Production of OH· radicals through neutralization of hydroxyl groups by photo-holes takes place:



4. Neutralization of  $\text{O}_2^{\cdot-}$  generated in step 2 by protons, happens:



5. Oxygen dismutation and transient formation of  $\text{H}_2\text{O}_2$  occurs, followed by the decomposition of hydrogen peroxide with formation of other radicals OH·:



6. Oxidation of organic molecule can happen by OH· or holes:



In literature, the photocatalytic activity of  $\text{TiO}_2$  is attributed to the presence of anatase as predominant component in  $\text{TiO}_2$  NPs, or to the high surface area of nanoparticles<sup>133,134</sup>.

#### 4.1.6 Brief introduction of chemical-physical properties of AgNPs and AuNPs

Gold and silver nanoparticles are NPs obtained by reducing a precursor of noble metal such as  $\text{AgNO}_3$  (for AgNPs) and  $\text{HAuCl}_4$  (for AuNPs).

Both nanoparticles can assume different shapes as spherical, thin sheets, diamond or octagonal and, generally, have a size ranging between 1 and 100 nm.

The most interesting property of these nanoparticles is their ability to sustain surface resonance plasmons under illumination with visible light. Surface Plasmons are collective coherent oscillations of free electrons of the metal, induced by the oscillation of electromagnetic field of light incident on the metal nanoparticles surfaces. This oscillation causes a charge separation, and then a dipole oscillation, in the direction of magnetic field. When this oscillation reaches a maximum value at a certain specific frequency, a surface plasmonic resonance occurs (SPR), that causes a strong adsorption and scattering of light. AgNPs and AuNPs show a strong SPR band in the visible region. This is the reason why these nanoparticles

are good optical nano-antennas, and this ability makes them particularly suitable in the field of detection of chemical compounds, especially when in low concentration.

The same phenomenon could generate local hot spots that cause the photodegradation of organic molecules such as organic pollutants.

For these reasons, AgNPs and AuNPs are interesting not only in the analytical field, but also in the field of environmental remediation.

## 4.2 Experimental

### 4.2.1 Chemicals and Materials

All chemicals were used as received, without any further purification.

Sodium hydroxide (commercial grade), gold (III) chloride trihydrate ( $\text{HAuCl}_4 \geq 99.9\%$  trace metal basis), trisodium citrate dehydrate (99.0%), acetic acid (99%), nitric acid silver (I) salt ( $\text{AgNO}_3, \geq 99.0\%$ ) titanium dioxide ( $\text{TiO}_2$  DEGUSSA P25), Poly(2,3-dihydrothieno-1,4-dioxin)-poly(styrenesulfonate) (PEDOT:PSS), methyl orange (solid, dye content 85%) and methylene blue (solid, dye content > 75%) were acquired from Sigma- Aldrich.

Chitosan was extracted from local shop shrimp's shells as reported in *paragraph 2.2.2*.

In all experiments ultrapure Milli-Q water was used, obtained from a Milli-Q Integral 5 system. All glassware used for AuNPs synthesis were washed with fresh prepared aqua regia ( $\text{HNO}_3$  (conc.):  $\text{HCl}$ (conc.) 1:3).

### 4.2.2 Synthesis of CH hydrogel bubbles

0.10 g of chitosan was dissolved in 10 mL of 5% (v/v) acetic acid to obtain a 10 g/L solution. The dissolution process was accelerated thanks to the use of an ultrasonic bath or magnetic stirring. The prepared solution was then poured dropwise by a syringe in a solution of 3 M NaOH, used as a cross-linker. The crosslinking step lasted 6 hours, at the end of which the obtained bubbles were recovered and washed with Milli-Q water until a neutral pH was reached.

### 4.2.3 Synthesis of CH@PEDOT:PSS hydrogel bubbles

The same synthetic steps described in **4.2.2** were followed in the case of PEDOT:PSS-chitosan bubbles, with the only difference being the composition of the starting acidic chitosan solution. In fact, maintaining fixed the chitosan and the acetic acid concentrations (10g/L and 5% v/v, respectively), variable amounts of PEDOT:PSS commercial solution (Sigma Aldrich) were added in order to reach a concentration of 0,1%, 1%, 5% or 10 % v/v.

### 4.2.4 Synthesis of CH@TiO<sub>2</sub> hydrogel bubbles

The same synthetic steps described in **4.2.3** were followed. In this case, variable amounts of commercial  $\text{TiO}_2$  DEGUSSA P25 (Evonik) were added in order to reach a concentration of 0,1%, and 1 % w/v.

#### 4.2.5 Synthesis of AuNPs

AuNPs are synthesized as reported in *paragraph 3.2.2*.

#### 4.2.6 Synthesis of AgNPs

AgNPs were synthesized following the classical Turkevich procedure.

50 mL of AgNO<sub>3</sub> 0.01 M were placed on a heating plate under magnetic stirring. When the solution was boiling, 5 mL of Na<sub>3</sub>C<sub>6</sub>H<sub>5</sub>O<sub>7</sub> 1% (w/v) were added drop by drop: the solution turned from colourless to pale yellow. After 5 min. under vigorous stirring, the solution was recovered and put in a water bath down to room temperature, keeping the magnetic stirring.

To remove the excess of citrate, the obtained AgNPs were centrifuged at 12500 rpm for 15 min and re-suspended in Milli-Q water.

The reaction involved in the procedure is:

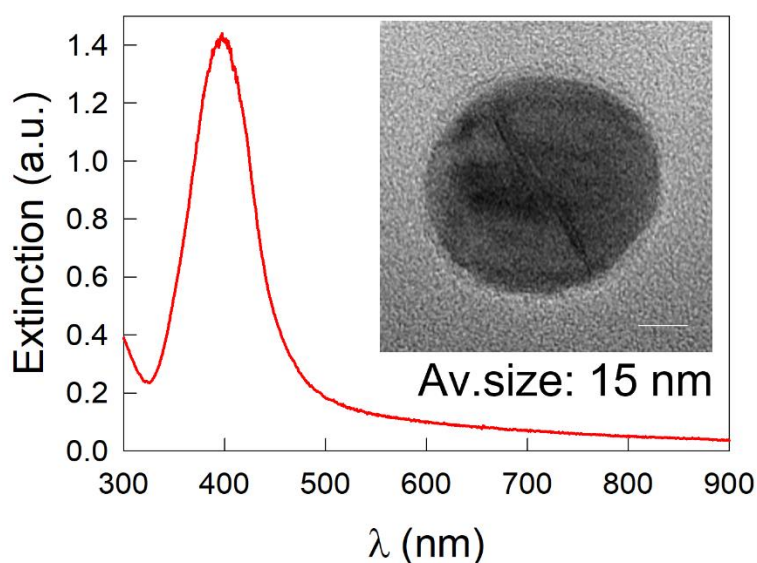


**Figure 4.5:** Uv-vis spectrum and average size of the synthesised AgNPs.

#### 4.2.7 Synthesis of CH@AuNPs and CH@AgNPs hydrogel bubbles

The same synthetic steps described in *4.2.2* were followed. In these cases, a solution of AuNPs or AgNPs were used instead of Milli-Q water, in order to obtain 10 mL of CH<sub>3</sub>COOH 5% with chitosan 10 g/L.

#### 4.2.8 Dyes adsorption tests

For each prepared bubbles, 23 hydrogel bubbles were added to 1 mL of methylene blue (MB) or methyl orange (MO) solutions with a concentration of  $10^{-5}$  M prepared using Milli-Q water (obtained from a Milli-Q Integral 5 system). The pH of the dye solutions was 5.6 and it became 6.2 after the bubble addition.

The variation of the absorption peak (at 660 nm for MB and at 460 nm for MO) was evaluated at regular time intervals of time after the addition of hydrogel bubbles by means of a UV-vis spectrometer (QE 65000 Ocean Optics).

The percentage of adsorbed pollutant was determined using the following equation:

$$\% \text{ Adsorbed} = \frac{(A_0 - A_t)}{A_0} * 100 \quad (4)$$

where  $A_0$  is the initial value of absorbance of the analyte (proportional to the value of its initial concentration) and  $A_t$  is the value of absorbance measured at time  $t$  after the mixing with the adsorbent in the dark. The obtained data were used for the calculation of  $q_t$ , which represents the amount of adsorbed pollutant per gram of dried adsorbent ( $\text{mg g}^{-1}$ ) at any time  $t$  (min), and for the calculation of  $q_e$  ( $\text{mg g}^{-1}$ ), which corresponds to the amount of adsorbed pollutant per gram of dried adsorbent after the reaching of the equilibrium between the processes of dye adsorption and desorption on the surface of the hydrogel bubbles under dark conditions and represents the equilibrium adsorption capacity of the tested systems.

In order to calculate the kinetic constant, the experimental data were fitted with the non-linear form of the pseudo-second order model for solid-liquid adsorption, according to the following equation:

$$q_t = \frac{(q_e^2 kt)}{(1 + q_e kt)} \quad (5)$$

where  $k$  corresponds to the pseudo-second order kinetic constant expressed in  $\text{g mg}^{-1} \text{min}^{-1}$ .

The adsorption performances were compared with the adsorption capability of analogous systems made of chitosan and activated carbon (DRACO), maintaining constant all the

experimental parameters (room temperature, sampling times, milliQ water,  $10^{-5}$ M dye concentration, no pH adjustment).

In order to get some more information about the interaction between chitosan and PEDOT (that is the most performing sample) with the organic dyes, the solutions pH was subsequently buffered at 6 and 5.6 using  $\text{CH}_3\text{COOH}$  and at 9.8-10 using  $\text{NaOH}$ .

Further experiments were conducted by preparing dye solutions using not ultrapure water, but mineral water (see **Table 3.2** in *chapter 3* for its chemical analysis).

#### **4.2.9 Dye photodegradation tests under solar illumination**

Photodegradation capabilities of the synthesized hydrogel systems were studied after the end of the adsorption tests. The MB and MO solutions containing hydrogel bubbles were placed under the light of a solar simulator (Abet Technologies, Sun 2000 Simulator, model: 11016), working with an illumination intensity equal to 1 sun (irradiance: 1.5 A.M., working distance: 5.2 cm) for 240 min. Photodegradation was studied by evaluating the variation of absorption peaks typical of the two dyes by means of UV-vis spectrometer. A comparison with pure MB and MO solutions under illumination with the same conditions was performed.

## 4.3 Results and discussions

### 4.3.1 MB and MO dye adsorption

Following the procedure reported in the *Materials and methods* section and schematized in **Figure 4.5**, it was possible to produce chitosan-based hydrogels characterized by a spherical shape and a diameter in the order of few millimetres (~3 mm).

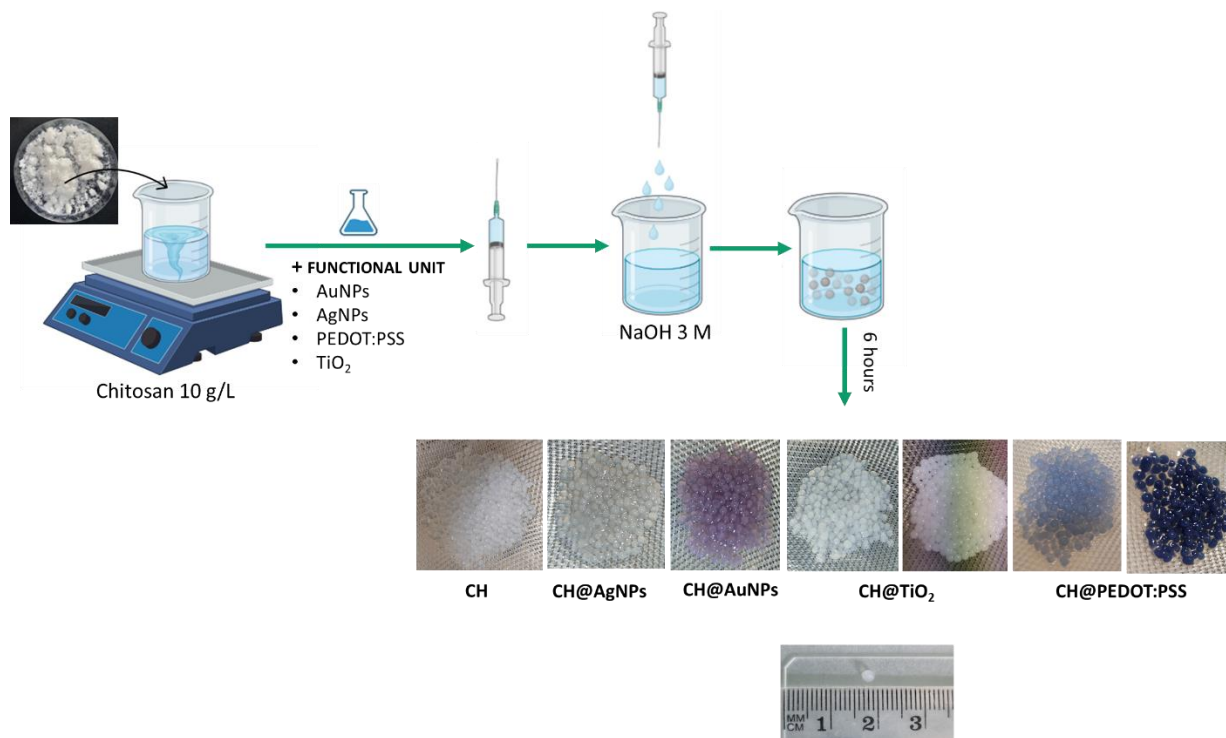


**Figure 4.5:** Scheme of the synthesis of CH, CH@AuNPs, CH@AgNPs, CH@TiO<sub>2</sub> and CH@PEDOT:PSS bubbles.

The final shape and dimension strongly depended on the pressure applied to the syringe piston, the dimension of the syringe needle and the fall distance of the chitosan acidic solution inside the alkaline medium used for jellification. In addition, the inclusion of functional units inside chitosan starting acidic solution (e.g. AuNPs, AgNPs, TiO<sub>2</sub> and PEDOT:PSS) can modify its viscosity and then, the size and shape of final bubbles. **Figure 4.6** represents three SEM images of a typical dried CH@TiO<sub>2</sub> bubbles at three different magnification and allows us to better appreciate the morphology of the bubble.

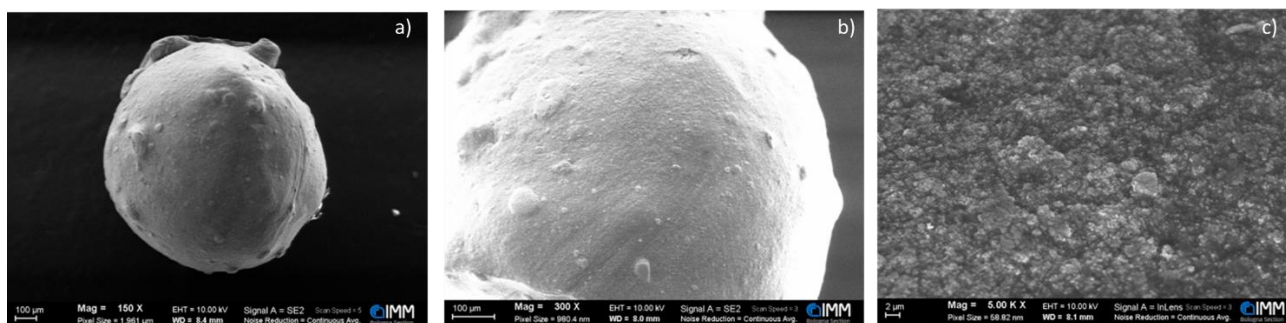


**Figure 4.6:** SEM image, kindly provided from Prof. Matteo Ferroni, of dried CH@TiO<sub>2</sub> bubbles at a)150x b)300x and c) 5.00K X.

The bubbles were tested as adsorbents and then as photocatalysts for dyes removal. In particular Methylene Blue (MB, 10<sup>-5</sup> M) and Methyl Orange (MO, 10<sup>-5</sup> M) were selected as examples of cationic and anionic dyes, respectively (**Figure 4.7**).



**Figure 4.7:** Chemical structure of Methylene Blue (MB) and Methyl Orange (MO).

In this paragraph, we first evaluate the adsorption capacity of the prepared samples.

Initially, the adsorption efficiency of different chitosan-based bubbles, containing variables amount of PEDOT:PSS, TiO<sub>2</sub>, AuNPs and AgNPs, was evaluated in not buffered (natural) conditions. Since the produced bubbles were characterized by different sizes and weights, to perform a truthful comparison between the different tested systems, the number of bubbles put in contact with the dye solution was maintained fixed and their weight was used to normalize the amount of adsorbed dye and calculate the adsorption capacity,  $q$  (mg/g), of each adsorbing system. In particular, the variation of the adsorption capacity as a function bubbles soaking time ( $q_t$ ) was evaluated, until the reaching of the adsorption equilibrium after 21.5 h. All the tested systems were characterized by a pseudo-second order kinetic behaviour: a fast adsorption occurred in the first period, followed by a decrease of the adsorption rate, until the reaching of a plateau.

From the data reported in **Figure 4.8a** and **4.8b**, it is evident that for both dyes the adsorption capability does not depend only from chitosan matrix but can be properly modified by

introducing in it functional units such as plasmonic nanoparticles (AuNPs and AgNPs), biocompatible and semiconductor nanoparticles (TiO<sub>2</sub> NPs) and eco-sustainable polymeric blends (PEDOT:PSS).

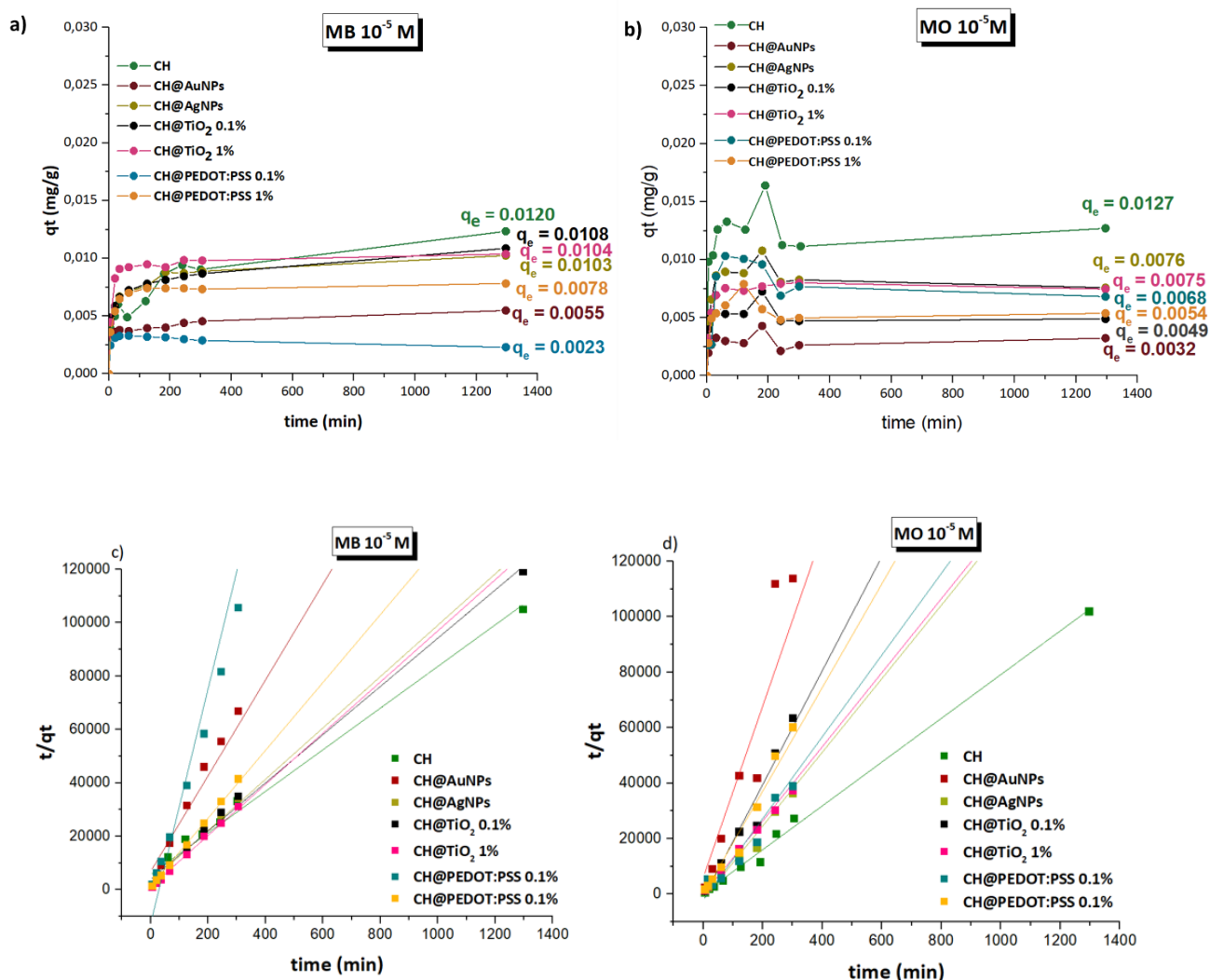


**Figure 4.8:** Comparison between the adsorption behavior of different types of chitosan-based bubbles during the interaction with MB and MO  $10^{-5}$  M solutions. **a)** Variation of the adsorption capacity of pure chitosan bubbles and chitosan bubbles functionalized with AuNPs, AgNPs, TiO<sub>2</sub> NPs (0.1 and 1% w/v) and PEDOT:PSS (0.1 and 1% v/v) as a function of bubbles soaking time inside a MB  $10^{-5}$  M solution; **b)** Variation of the adsorption capacity of pure chitosan bubbles and chitosan bubbles functionalized with AuNPs, AgNPs, TiO<sub>2</sub> NPs (0.1 and 1% w/v) and PEDOT:PSS (0.1 and 1% v/v) as a function of bubbles soaking time inside a MO  $10^{-5}$  M solution; **c)** pseudo-second order kinetic model for adsorption of MB with pure chitosan and different functionalized chitosan bubbles; **d)** pseudo-second order kinetic model for adsorption of MO with pure chitosan and different functionalized chitosan bubbles.

Moreover, the samples containing MB were characterized by a more regular adsorption trend, while MO led to a fast and high adsorption at the beginning, followed by an evident desorption process before the reaching of equilibrium. Nevertheless, in the case of both dyes all the experimental data can be satisfactorily fitted according to the linearized form of the pseudo-

second order model (**Figures 4.8c and 4.8d**) and it was possible to calculate the theoretical values of the equilibrium adsorption capacity, showing a good agreement with the experimental data.

The pure chitosan bubbles resulted to be a discrete adsorbent system both for MO (% adsorption=47.3%,  $q_e = 0.0127$  mg/g) and MB (% adsorption= 52.13%,  $q_e = 0.0123$  mg/g), without showing a clear preference/specificity for positively or negatively charged dyes. The reason could be linked to the fact that in natural conditions (i.e. without any external pH buffering), the pH of the dye solution was equal to 6.2 and the chitosan chains were only slightly protonated. As a result, the electrostatic attraction with negatively charged species in solution (i.e. MO<sup>-</sup>) was limited, as well as the electrostatic repulsion towards positively charged species (i.e. MB<sup>+</sup>). In addition, since chitosan crosslinking was performed through reaction with NaOH, some hydroxyl groups can remain entrapped inside the hydrogel matrix and compensate the eventual positive charge on the polymeric network and favour interaction with positive MB<sup>+</sup> species in solution.

The addition of nanoparticles (AgNPs, AuNPs and TiO<sub>2</sub> NPs) as well as the addition of the polymer blend PEDOT:PSS, inside the chitosan hydrogel matrix modifies the adsorption performances of the bubbles.

In order to quantify the effect of the NPs or the conductive polymer, we calculated the normalized adsorption percentage: pure chitosan bubbles, which corresponded to the not functionalized adsorbent, were considered a sort of reference material and their weight was used to normalize the amount of all the other adsorbent systems. The obtained data are plotted in **Figure 4.9**, which illustrates that functionalization led to different behaviours in the case of MO and MB.

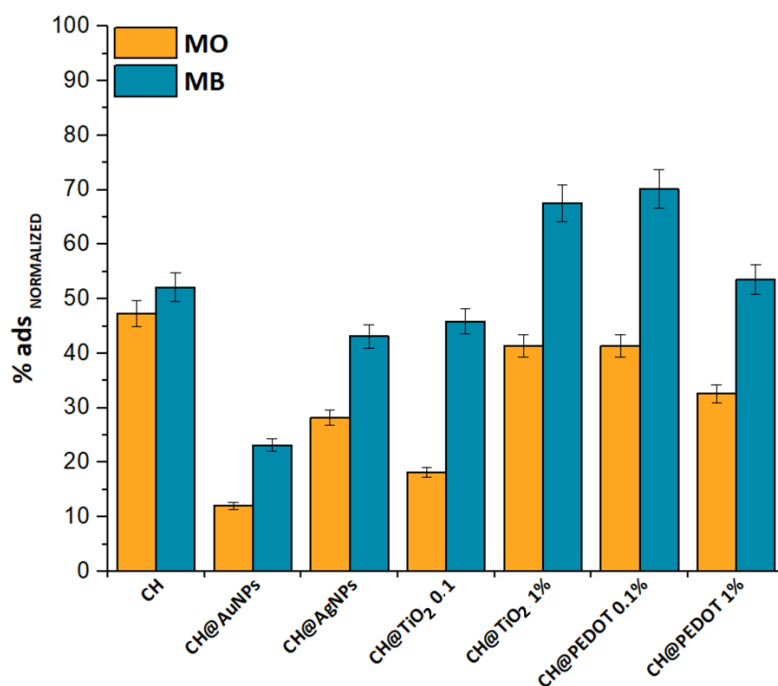


**Figure 4.9:** Variation of the normalized adsorption percentage of MB and MO according to chemical composition of chitosan-based bubbles.

When AgNPs and AuNPs are introduced into chitosan bubbles, as a result there has been a reduction of normalized % adsorption respect pure chitosan bubbles, both for MB+ and MO-. In both cases, this decrease is more pronounced for AuNPs ( $\%ads_{Normalized}(MB+) = 23.16\%$ ;  $\%ads_{Normalized}(MO-) = 12.03\%$ ) than for AgNPs ( $\%ads_{Normalized}(MB+) = 43.14\%$ ;  $\%ads_{Normalized}(MO-) = 28.2\%$ ).

When the analyte is MO ( $pK_a = 3.39$ ), which at the considered pH ( $pH = 6.2$ ) is negatively charged, this is an expected behaviour: in fact, as a result of adopted synthetic procedure, both NPs are negatively charged, electrostatic repulsion between the analyte and the nanoparticles can be originated.

In the case of MB+, instead, the opposite results were expected. However, the results reported in **Figure 4.9** disregard our expectations: this could be justified by the fact that the insertion of nanoparticles inside the polymeric matrix, could adversely affect the porosity of the material. Therefore, electrostatic interactions alone would no longer be sufficient, thus causing a decrease in efficiency. This would explain also the difference between AgNPs and AuNPs that are characterized by a larger distribution size (**Figure 3.1 section 3.2.2** and **Figure 4.5 section 4.2.6**).

However, the role of plasmonic nanoparticles, that are not particularly efficient in adsorption tests, will be fundamental for residual MB photodegradations.

The normalized adsorption percentage of MB<sup>+</sup> significantly increases when TiO<sub>2</sub> 1% (w/v) is added into biopolymer bubbles, passing from 52.13% when chitosan pure hydrogel is used, to 67.42% when titania nanoparticles are added. In literature<sup>132</sup> is reported that at pH < 7 TiO<sub>2</sub> is positively charged while at pH > 7 is negatively charged. The pH of the explored solution is 6.2, that is close to the discriminating pH value 7, this means that probably TiO<sub>2</sub> NPs start to acquire some negative charges and then are capable to establish electrostatic attraction with MB, by promoting dye adsorption.

The decrease of adsorption in MO<sup>-</sup> (41.3%) seems to confirm our hypothesis.

Nevertheless, when TiO<sub>2</sub> is added at 0.1% (w/v) the adsorption capability of the systems does not differ so much from the reference but, on the contrary, the obtained result seems to fall into the error bar. Probably it could be due to too low TiO<sub>2</sub> concentration that is not enough to establish efficient interactions with MB<sup>+</sup>, but are sufficient to repulse MO<sup>-</sup>, also assisted by the presence of the already mentioned OH<sup>-</sup> residues in hydrogels.

In the case of functionalization of chitosan bubbles with PEDOT:PSS, we initially evaluated two concentrations (0.1% (v/v) and 1% (v/v)) in order to better compare the behaviour of the obtained bubbles with those enriched with TiO<sub>2</sub>. In **section 4.3.3**, instead, we will discuss the behaviour of bubbles with higher content of PEDOT:PSS.

In both cases, the adsorption is very similar or only slightly enhanced in comparison to pure chitosan bubbles. In the case of negatively charged MO, a reduction of dye adsorption was observed, in comparison to pure chitosan bubbles. The reason could be the insurrection of an electrostatic repulsion between MO<sup>-</sup> and negative charged of PSS. Nevertheless, MO adsorption is not zero, thanks to the interaction with the chitosan matrix.

### **4.3.2 MB and MO dye photodegradation**

In this paragraph the results obtained from photodegradation tests will be discussed.

The possibility to remove the residual dye through photodegradation after overnight adsorption, was explored with a solar simulator at an irradiance of 1 sun. The overnight adsorption is required to ensure the adsorption equilibrium between the dye and photocatalyst.

Photodegradation is a process in which organic molecules as MB and MO are converted into non-toxic products such as CO<sub>2</sub>, sulphate, nitrate, or ammonium ions.

It has been verified that auto-photodegradation of MB and MO does not occur when the solutions alone are irradiated under solar simulator for 8 h.

The catalytic activity of each bubble for MB or MO photodegradation was evaluated by plotting  $C/C_0$  in function of time, where  $C$  is the dye concentration at time  $t$ , and  $C_0$  is the starting concentration of dye after overnight adsorption.

**Figure 4.10** shows the degradation of all prepared systems both for MB and MO. All the tested systems are capable to completely degrade MB within two hours, while only systems containing  $TiO_2$  NPs can photodegrade MB. The systems CH, CH@AuNPs, CH@AgNPs and CH@PEDOT:PSS are not capable to degrade MO, and then they are not reported in the graph for clarity.

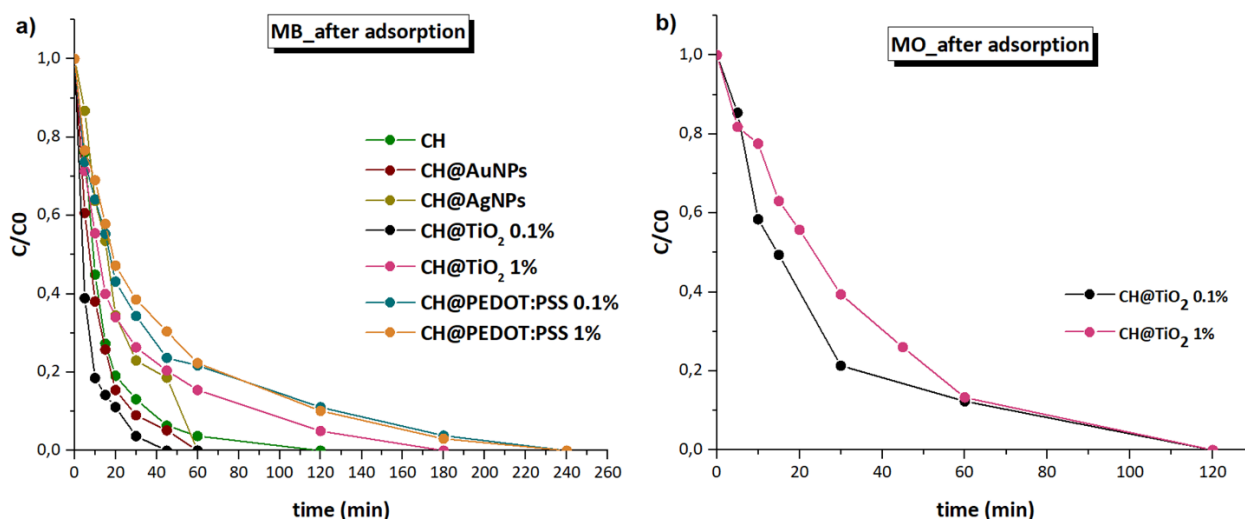


**Figure 4.10:** Comparison between the photocatalytic behaviour of different types of chitosan-based bubbles during the interaction with MB and MO solutions. a)  $C/C_0$  of pure chitosan bubbles and chitosan bubbles functionalized with AuNPs, AgNPs,  $TiO_2$  (0.1 and 1% w/v) PEDOT:PSS (0.1 and 1% v/v) as a function of photodegradation time inside a MB solution, after overnight adsorption; b)  $C/C_0$  of pure chitosan bubbles and chitosan bubbles functionalized with AuNPs, AgNPs,  $TiO_2$  (0.1 and 1% w/v) PEDOT:PSS (0.1 and 1% v/v) as a function of photodegradation time inside a MO solution, after overnight adsorption.

The reaction of photodegradation for both dyes follow a pseudo-first order kinetic and to better compare different systems behaviour and evaluate their catalytic activity, the reaction rate constant,  $k$ , was calculated from the equation:

$$\ln(C_0/C) = kt \quad (6)$$

**Table 4.2:** photodegradation kinetic constant calculated from each system using the equation (6).

SYSTEM	k(MB)	k(MO)
CH	0.05478 ± 0.00445	-
CH@AuNPs	0.06636 ± 0.00609	-
CH@AgNPs	0.04064 ± 0.00432	-
CH@TiO2 0.1%	0.10173 ± 0.01094	0.03584 ± 0.00445
CH@TiO2 1%	0.0232 ± 0.0022	0.03254 ± 0.00119
CH@PEDOT:PSS 0.1%	0.01654 ± 0.00127	
CH@PEDOT:PSS 1%	0.01809 ± 8.506E-4	

When CH@AuNPs and CH@AgNPs systems are used, the removal of residual MB is completed within one hour. Both nanoparticles, in fact, are well known to be very efficient plasmonic optical nano-antennas able to concentrate the electromagnetic field of the incident light in their surroundings and leads to MB photodegradation (**Figure 4.11**). The difference in rate between the two nanoparticles could be attributable to the different aggregation state of the nanoparticles inside the bubbles as well as to their different distribution of dimensions. In fact, the concentration of electromagnetic field correlated to incident field, is much greater in the spaces between the nanoparticles, the so-called “hot spots”, and therefore the photodegradation could be favoured when the NPs are aggregated.

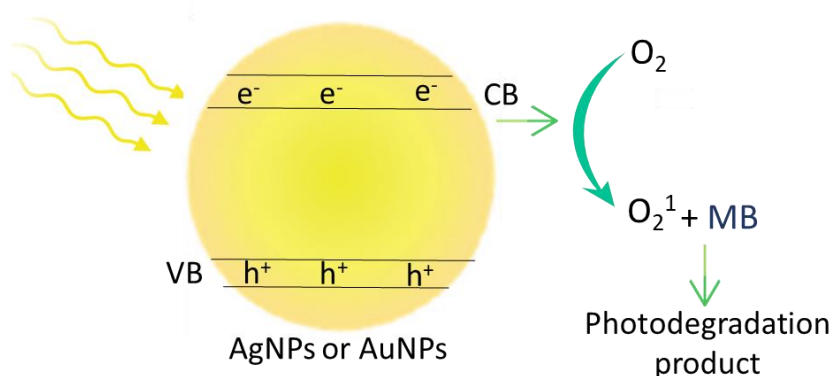


**Figure 4.11:** Schematic representation of the effect of plasmonic nanoparticles on MB photodegradation.

The use of bubble containing TiO<sub>2</sub> both in concentration 0.1 % (w/v) and 1% (w/v) allows to degrade not only MB but also MO.

According literature<sup>132,135,136</sup>, the catalytic degradation process for MB, as well as for MO, induced by TiO<sub>2</sub> seems to be a “surface location” process. This means that the initial oxidation of the organic dye occurs on the surface of the catalyst rather than in solution. This hypothesis

also explains why in the first hour, the photodegradation of MB, which is a cationic dye, is faster than the photoinduced degradation of MO, which is an anionic dye. At experimental pH (6.2), in fact, the TiO<sub>2</sub> nanoparticles begin to assume an increasing number of negative charges, thus resulting tied more effectively to negatively charged molecules like MB.

However, **Figure 4.10** shows that the degradation efficiency decreases as the amount of TiO<sub>2</sub> NPs increases from 0.1 % to 1%. This behaviour is more pronounced for MB than for MO.

In general, the photodegradation rate of titania nanoparticles increases as the amount of TiO<sub>2</sub> increases within certain limits, and then remains constant or decreases.

The decrease is due to the combination of two phenomena: on one hand, when all the pollutant molecules were adsorbed on the catalyst surface, the further addition of the latter has no effect on the efficiency of photocatalysis, since it is not involved in the process. On the other hand, the excess of titania leads to a greater opacity of the bubbles that adversely affects interaction with incident light and causes a higher NPs aggregation, which reduces the free surface area available for interaction with the dye.

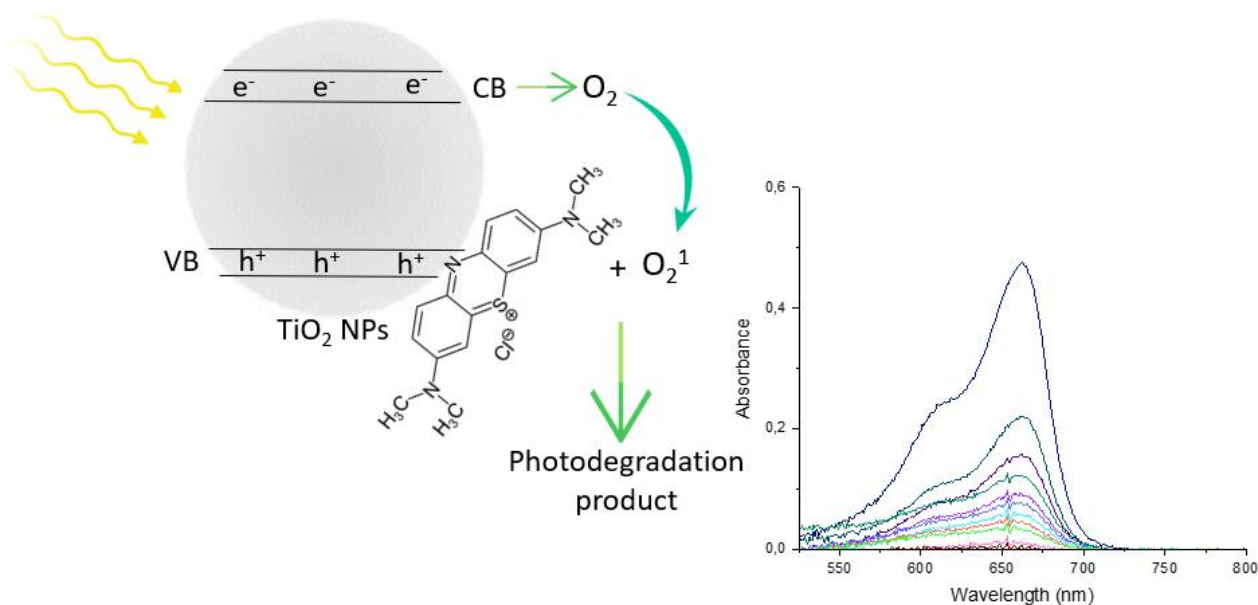


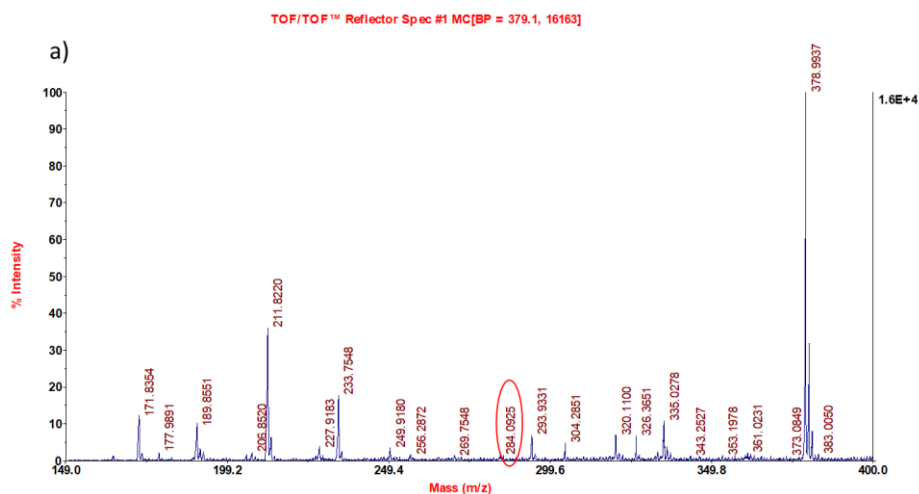
**Figure 4.12:** Schematic representation of the suggested photodegradation mechanism of organic dye induced by TiO<sub>2</sub> NPs inside chitosan bubbles. The dye (MB in the case of the figure) is adsorbed by TiO<sub>2</sub> NPs, and the reaction of photodegradation induced by solar light occurs on catalyst surface.

Moreover, the unexpected activity of bubbles containing only chitosan in MB photodegradation is surprising, in fact it is comparable to that of analogous bubbles loaded with AuNPs and even better than bubbles with AgNPs. The origin of this enhanced activity is currently under

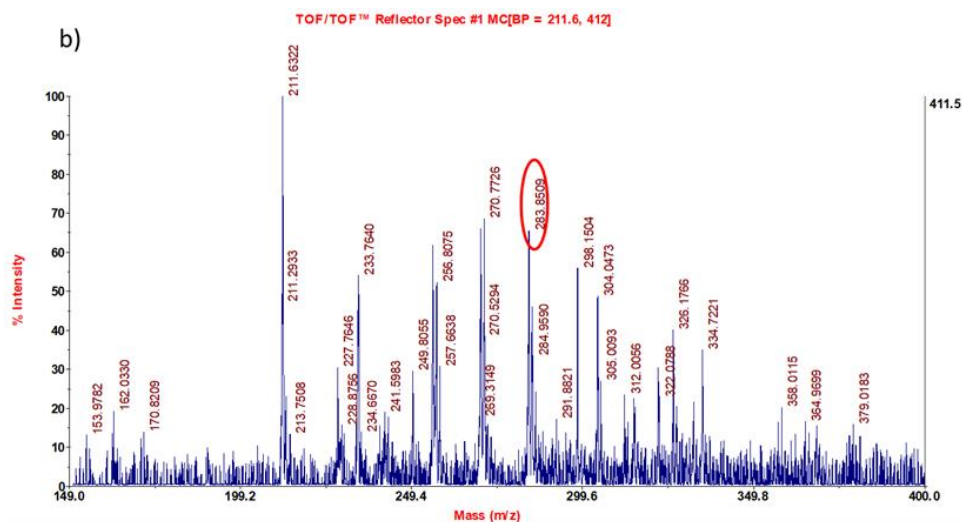
investigation and to the best of our knowledge, has never been observed before. One of the possible reasons is linked to the origin of the material: the used chitosan is not pure, but it derives from food waste; consequently, it can contain some impurities (i.e. metals) that can be precious for catalytic purposes.

The mechanisms of photodegradation for CH and CH@TiO<sub>2</sub> were investigated through mass-spectrometry data kindly provided by Dott. Alessandra Gianoncelli of the Department of Molecular and Translational Medicine of the University of Brescia. (**Figure 4.13**). The idea is that to verify the presence or the disappearance of dye molecules inside dried bubbles or inside the residual solution, by evaluating the peak at ~ 284 m/z typical of MB+ ions.

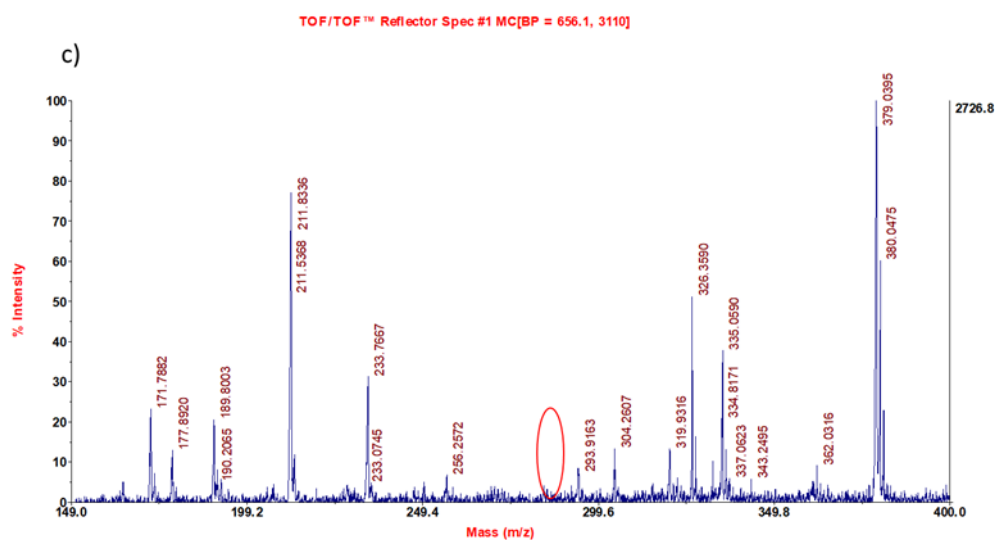
### MB solution after CH bubbles photodegradation treatment



### CH bubbles after photodegradation



## MB solution after CH@TiO<sub>2</sub> 0.1% bubbles photodegradation treatment



## CH@TiO<sub>2</sub> 0.1% bubbles after photodegradation

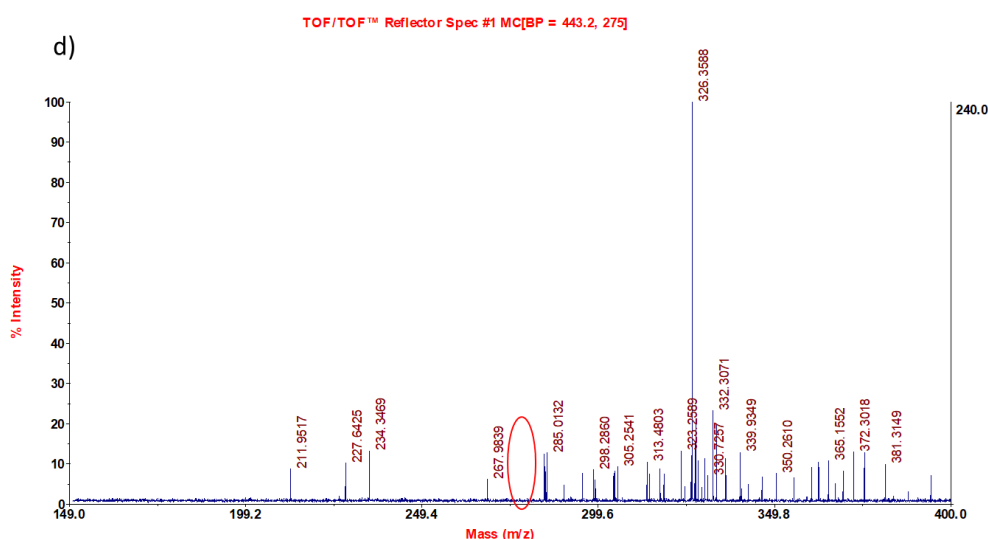


**Figure 4.13:** **a)** Mass spectrum of the solution of MB after 120 min. of treatment of CH bubbles under solar simulator. **b)** Mass spectrum of the CH bubbles after 120 min. of treatment of MB solution under solar simulator. The presence of the peak of MB at 284 m/z confirms the adsorption of MB and the fact that the photodegradation of MB occurs only in the solution. **c)** Mass spectrum of the solution of MB after 60 min. of treatment of CH@TiO<sub>2</sub> bubbles under solar simulator. **d)** Mass spectrum of the CH@TiO<sub>2</sub> bubbles after 60 min. of treatment of MB solution under solar simulator. The absence of the peak of MB at 284 m/z confirms that the photodegradation of MB occurs on catalyst surface after adsorption.

The mass-spectroscopy data confirm that what we observe in the case of CH bubbles, is a true photodegradation. In fact, the absence of the characteristic peak of MB at 284 m/z in the residual dye solution (**Figure 4.13a**), proves that what it is observed with UV-vis spectroscopy it is not attributable to a discoloration of MB due to the lamp of the solar simulator. Moreover, the mass spectrum on the dried CH bubble recovered after 120 min of photodegradation underlines that the catalytic degradation of the dye occurs only for the molecules in solution

and does not concern the molecules adsorbed inside the bubbles that remains in the original form (clear visible peak at 284 m/z), thus indicating that adsorption and photodegradation are two separated phenomena.

Finally, the spectra reported in **Figure 4.13c** and **4.13d** confirm the proposed mechanism for the photodegradation induced by CH@TiO<sub>2</sub>. Unlike what was observed in the case of pure chitosan bubbles, in fact, when dried CH@TiO<sub>2</sub> bubbles are analysed, no bands attributable to MB is visible, confirming that the photodegradation of the organic dye occurs on catalyst surface after adsorption.

Finally, the introduction of a semiconductor such as PEDOT:PSS seems to greatly decrease the effectiveness of photo-catalysis, which is not only worse than the bubbles containing the nanoparticles (Au, Ag and TiO<sub>2</sub>) but it looks even worse than the degradation induced by chitosan alone.

However, we decide to further investigate their adsorption capabilities, as discussed in the following paragraph.

### **4.3.3 In-depth study on the adsorption capacity of CH@PEDOT bubbles**

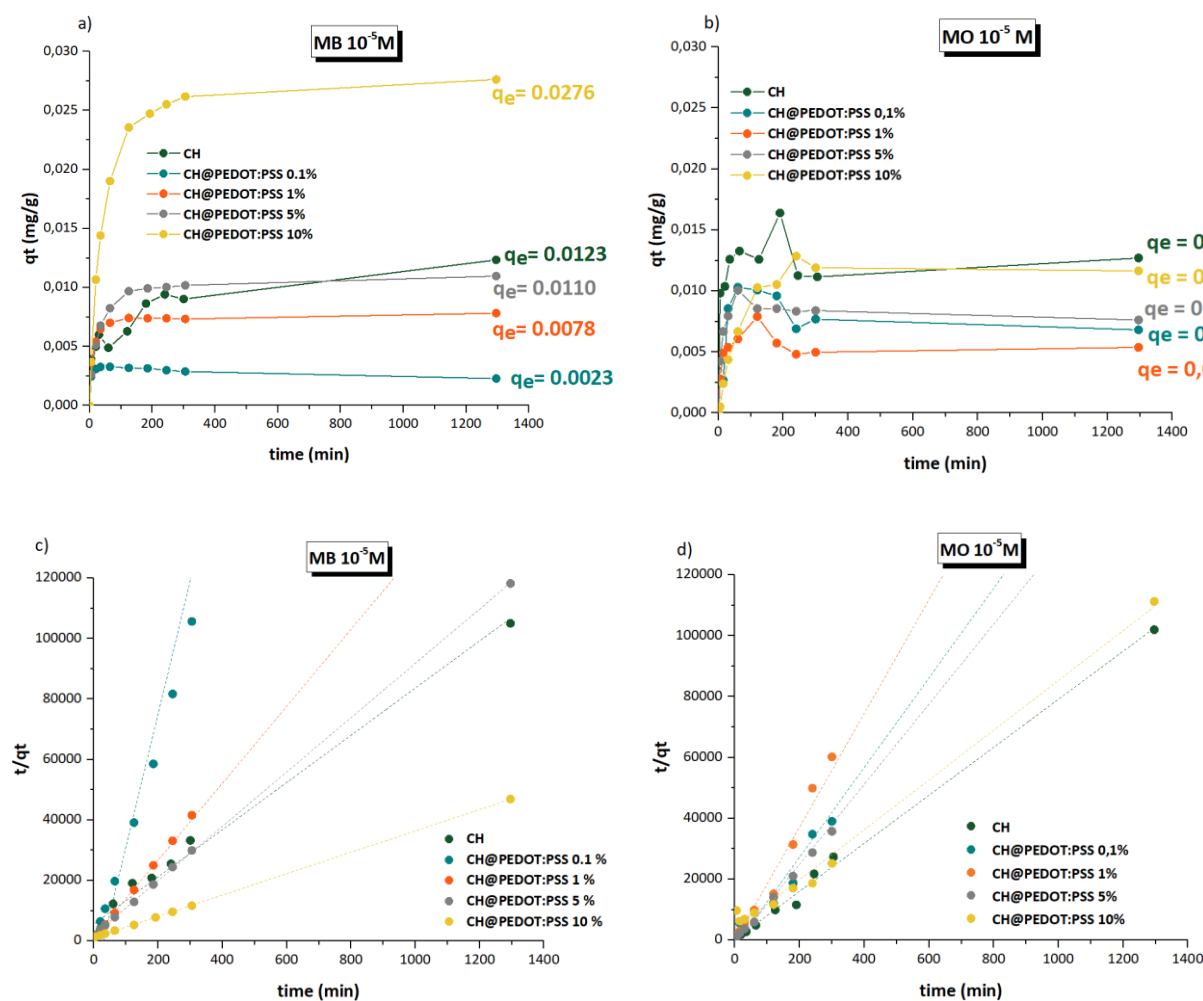
From its discovery in the seventies, PEDOT has found numerous applications, especially for the preparation of sensors or organic electronics<sup>123</sup>. More recently, thanks to the exploitation of its hole-conduction capability, it has been used for the preparation of organic photovoltaics<sup>124</sup>, and, thanks to its oxidation properties, it has been employed in the field of photo-catalysis, also for environmental remediation<sup>125</sup>.

Related to dye removal, its exploitation as adsorbent has been investigated only marginally<sup>137</sup> and deserve further studies. Da Silva et al. investigated the possibility of using PEDOT in combination with polyvinylidene fluoride (PVDF) mats, which serve as mechanical supports, for the adsorption of Methyl Orange (MO), an azo dye commonly used as a pH indicator in research laboratories, which has found extensive application in the textile, printing, pharmaceutical, plastics, and food industry. Despite pristine PVDF membranes do not show any activity in dye adsorption, thanks to their functionalization with PEDOT they are able to significantly reduce the concentration of MO in water, especially when the pH is ~ 3. In this case, it has been mainly exploited an electrostatic interaction between the positive surface charge of the adsorbent (the pH influences the state of protonation of PSS, and then the charges on the PSS chains) and the negative charge of the dye. Because of the electrostatic nature of the interaction between the adsorbent and the dye, the proposed system is quite specific towards

MO or analogous negative dyes. A more universal adsorbent is desirable, in order to enable the simultaneous removal of different synthetic dyes, and the exploitation of  $\pi$  interaction between the conjugated system of PEDOT and the benzene units of various synthetic dyes could be a successful strategy. In addition, as we see previously, PEDOT is generally available in formulation with polystyrene sulfonate (PSS), which is characterized by a very low value of pka ( $pka \sim 1$ ), meaning that these units are negatively charged guaranteeing a good electrostatic interaction also with positively charged pollutants.

In the *paragraph 4.3.1* we have already shown the behaviour of PEDOT:PSS chitosan hydrogels, when the concentration of PEDOT:PSS is very low (0.1 or 1% w/V).

Subsequently, we compared the above mentioned bubbles CH@PEDOT:PSS (0.1 and 1%) with bubbles with a concentration of semiconductor of 5% (v/w) and 10% (v/w). The results obtained for both MB and MO are summarized in **Figure 4.14**.



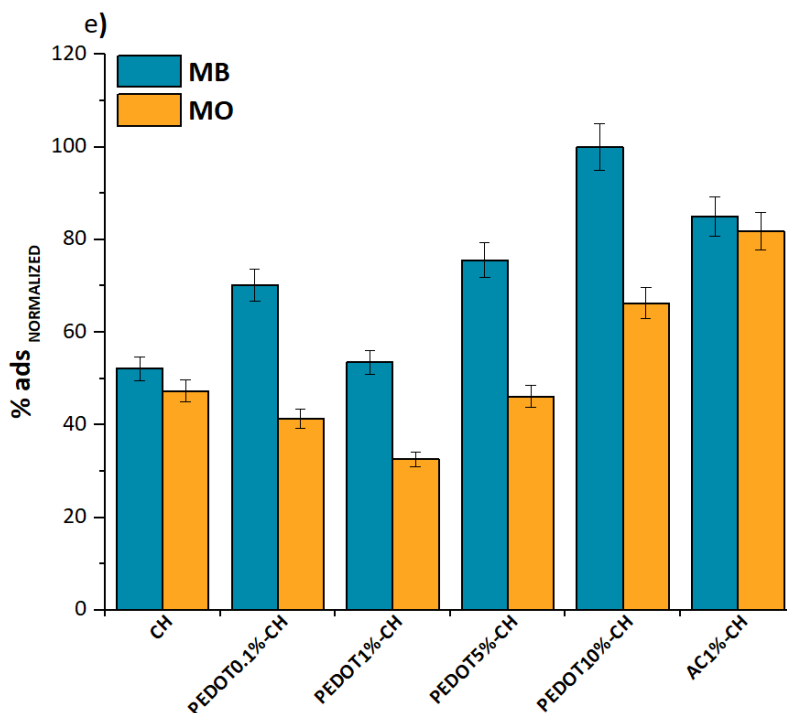


**Figure 4.14:** Comparison between the adsorption behaviour of different types of chitosan-based bubbles during the interaction with MB and MO  $10^{-5}$  M solutions. **a)** Variation of the adsorption capacity of pure chitosan bubbles and chitosan bubbles functionalized with PEDOT:PSS (0.1-10% V) as a function of bubbles soaking time inside a MB  $10^{-5}$  M solution; **b)** variation of the adsorption capacity of pure chitosan bubbles and chitosan bubbles functionalized with PEDOT:PSS (0.1-10% V) as a function of bubbles soaking time inside a MO  $10^{-5}$  M solution; **c)** pseudo-second order kinetic model for adsorption of MB whit different chitosan and chitosan-PEDOT:PSS bubbles; **d)** pseudo-second order kinetic model for adsorption of MO whit different chitosan and chitosan-PEDOT:PSS bubbles; **e)** variation of the normalized adsorption percentage of MB and MO according to chemical composition of chitosan-based bubbles.

The obtained results confirm a different behaviour in the case of MB and MO.

In fact, when the positively charged MB was considered, the normalized adsorption percentage tended to increase when the amount of PEDOT:PSS raised.

Multiple could be the reasons of this behaviour: on one hand, polystyrene sulfonate units are negatively charged, and they can favour an electrostatic interaction with MB<sup>+</sup> ions in solution and foster its adsorption; on the other, PEDOT is characterized by an extended conjugated system that can enable non-electrostatic  $\pi$ - $\pi$  interactions with the aromatic moieties of the organic dye<sup>138</sup>.

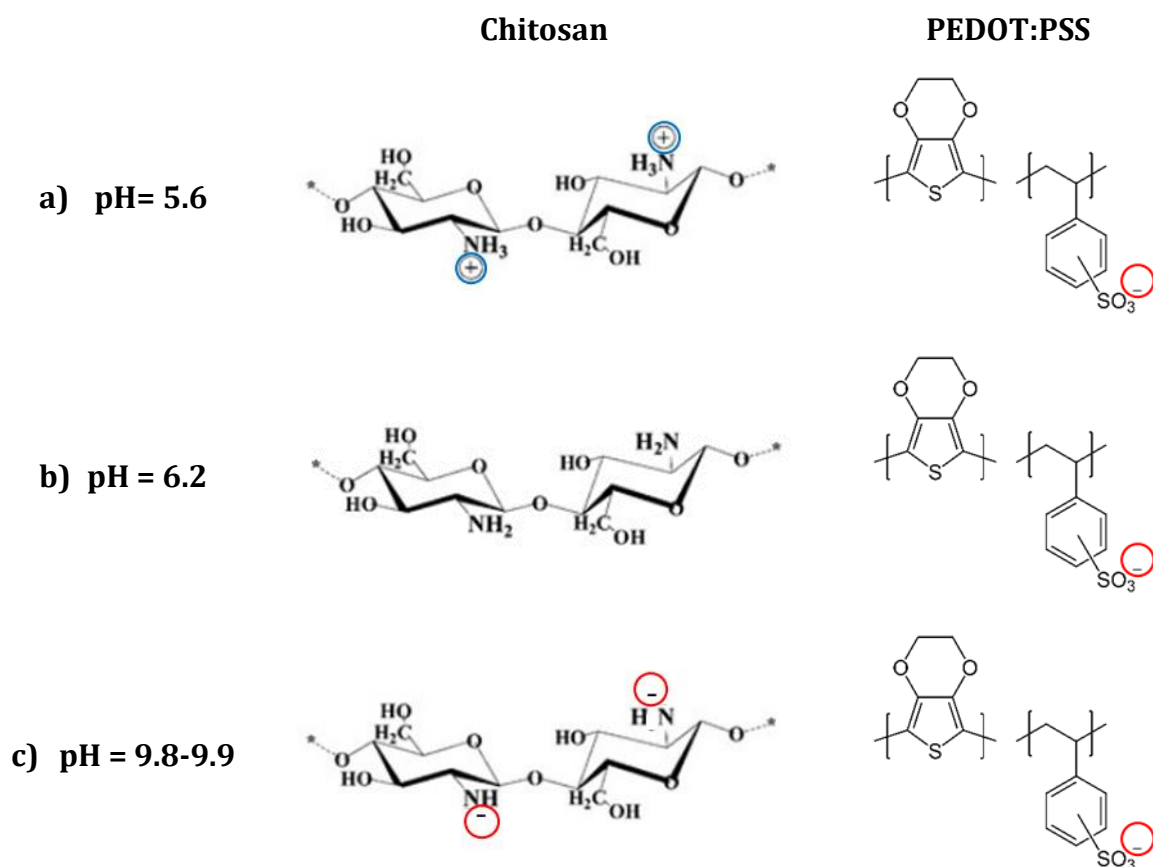


**Figure 4.15:** Structure of chitosan and PEDOT:PSS at different pH.

When the negatively dye is considered, MO, also when the content of PEDOT:PSS is 5% a reduction of dye adsorption was observed, in comparison to pure chitosan bubbles, in line with the observation that there are electrostatic repulsions between  $\text{MO}^-$  and negative charged of PSS. Nevertheless, when the PEDOT:PSS concentration was increased up to the 10%, a significant increase of adsorption was observed in comparison to pure chitosan bubbles, indicating that in these conditions the contribution of non-electrostatic forces based on  $\pi$ - $\pi$  interactions became prevalent. Anyway, the enhancement of adsorption was significantly more contained in comparison to MB.

Interestingly, the adsorption performances against MB of chitosan bubbles containing PEDOT:PSS at 10% were higher also than those of similar chitosan bubbles containing Activated Carbon (1% w/v. This concentration was selected because higher AC content led to unstable bubbles), which in the form of free powder can be considered the golden standard for pollutants adsorption in industrial and commercial systems. Their high adsorption capacity is linked to their high surface area and porosity, with the presence of many adsorption sites available for chemical species free in solutions. For this type of system any electrostatic

interaction was not expected, as confirmed by the very similar values of normalized adsorption % obtained in the case of MB (85%) and MO (82%).

Although, the creation of not-specific adsorbent could be desirable, especially in view of application in real water systems characterized by the simultaneous presence of different and differently charged pollutants, we tried to modulate the adsorption capacity of the chitosan-PEDOT:PSS tested systems by modifying the pH of the solution. In this way, it was possible to get some insights in the adsorption mechanism and individuate the best conditions to maximize the adsorption process for each organic dyes. For this scope, we considered 2 different pH values in addition to the natural one of the dye solutions (pH= 6.2): an alkaline pH of 9.8-9.9, and a more acidic value of 5.6. Unfortunately, it was not possible to work in more acidic conditions reaching values of pH that were lower than the pKa of MO (3.39, in order to protonate it and nullify the negative charge on the sulfonate group) because in those conditions the bubbles are not stable and tend to dissolve. Furthermore, we restricted the investigation to pure chitosan bubbles and chitosan bubbles with a PEDOT:PSS content equal to the 10%, since they were the most performing systems in not-buffered conditions.

Inside the investigated pH range, all the tested bubbles maintained a second order adsorption behaviour, considering both MO and MB solutions, as shown in **Figures 4.16a** and **4.16b**, plotting the variation of the value of  $q_t$  as a function of contact time. Interestingly, the value of adsorption equilibrium capacity  $q_e$  significantly vary according to the pH value of the dye solution and according to the type of dye (positively or negatively charged).

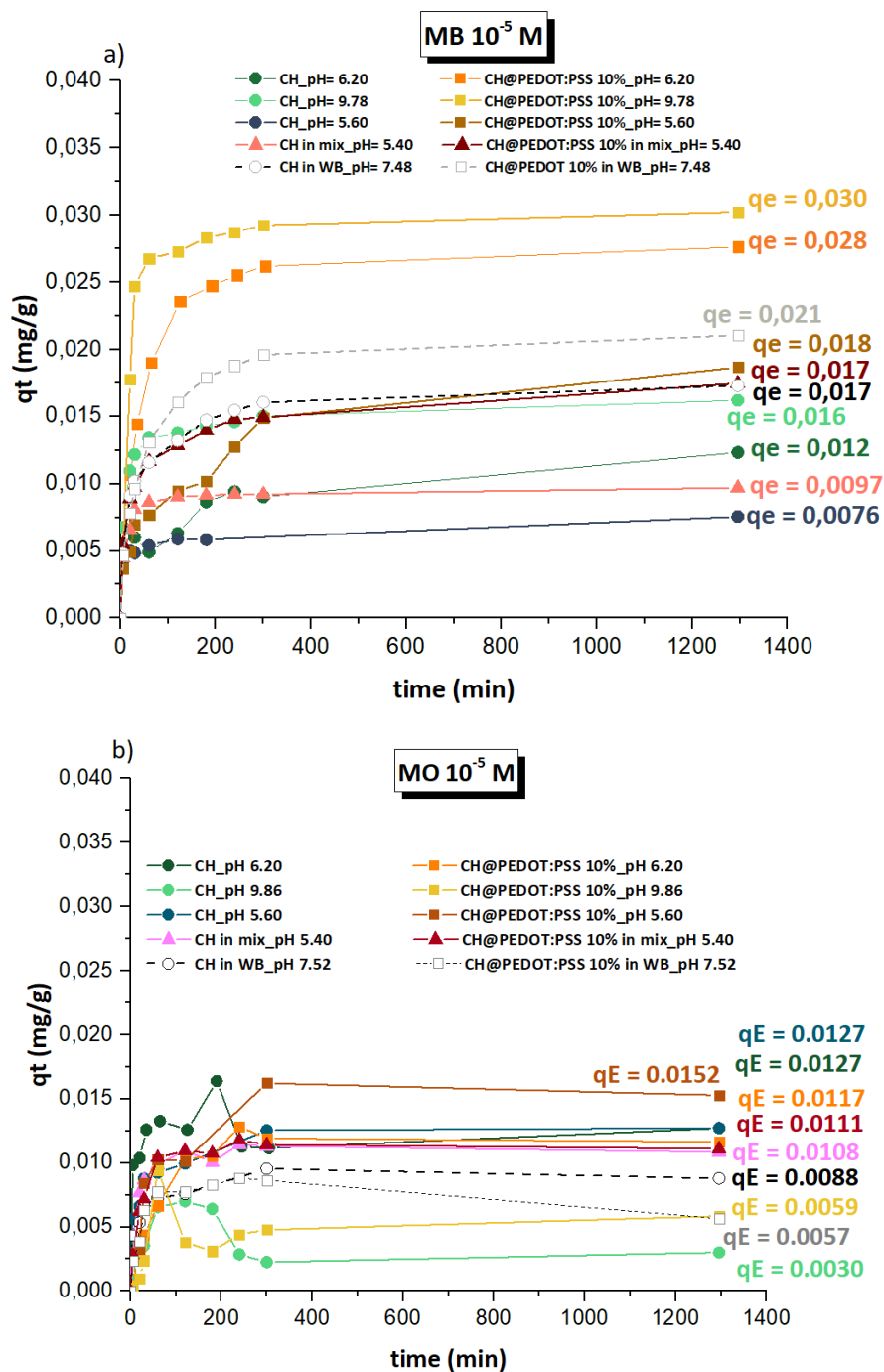


**Figure 4.16:** Comparison between the adsorption behaviour of CH@PEDOT:PSS 10% bubbles at different pH during the interaction with MB and MO  $10^{-5}$  M solutions. **a)** Variation of the adsorption capacity of pure chitosan bubbles and CH@PEDOT:PSS 10% at different pH, as a function of bubbles soaking time inside a MB  $10^{-5}$  M solution; **b)** Variation of the adsorption capacity of pure chitosan bubbles and CH@PEDOT:PSS 10% at different pH, as a function of bubbles soaking time inside a MO  $10^{-5}$  M solution.

As visible in **Figure 4.16a**, in the case of MB, by increasing the pH value it was possible to enhance the adsorption of the bubbles, especially in the case of pure chitosan. In fact,  $q_e$  passed from 0.0076 mg/g at pH 5.6 to 0.0162 mg/g at pH 9.8, reaching a value that was more than the double. This behaviour could be explained considering that in alkaline medium the positive

charges localized on the  $\text{NH}_3$  groups of chitosan were nullified, limiting the electrostatic repulsion between them and positive  $\text{MB}^+$  in solution. (Scheme 4.15b) The variation of  $q_e$  had a similar trend also in the case of chitosan bubbles containing PEDOT:PSS 10% (higher value of  $q_e$  for alkaline pH), but it was less evident:  $q_e$  passed from 0.0187 mg/g at pH 5.6 to 0.03 mg/g at pH 9.8, with a relative increase limited to the 62%. This fact demonstrates that in the case of functionalization, electrostatic interactions between chitosan chains and dye in solution were less important but prevailed electrostatic interactions between  $\text{MB}^+$  and  $\text{PSS}^-$  or  $\pi$ - $\pi$  interactions between PEDOT and the organic dye.

In the case of MO an opposite behaviour was observed: a lowering of adsorption capacity was recorded when the pH was increased. This fact was valid for both pure chitosan bubbles and PEDOT:PSS functionalized ones: in the first case,  $q_e$  passed from 0.0127 mg/g at pH 5.2 to 0.0030 mg/g at pH 9.9, with a relative decrease of the 75%, while in the case of PEDOT-containing bubbles  $q_e$  passed from 0.0153 mg/g at pH 5.2 to 0.0059 at pH 9.9, with a relative decrease of 62%. Also for MO, the variation of  $q_e$  as a function of pH could be explained considering electrostatic forces at the basis of the interaction between the adsorbent and the dye. At high values of pH (9.9), both MO and chitosan were negatively charged, they electronically repelled each other, and adsorption was possible only through weak forces, such as Van der Waals or H-bonds. Despite in the case of functionalized bubbles additional repelling negative charges were present due to polysulfonate units, at high value of pH higher adsorption was obtained ( $q_e = 0.0059$  mg/g versus 0.0030 mg/g) thanks to  $\pi$ - $\pi$  interactions between PEDOT ions and aromatic rings of MO. At low values of pH (6.2 and 5.6), instead, the number of positive charges of the chitosan polymeric network increased, favouring the interaction with  $\text{MO}^-$  in solution and increasing its adsorption. Between the two values of acidic pH no differences of  $q_e$  were observed, since no variation of the chitosan polymeric chain from an electrostatic point of view occurred. Furthermore, in acidic conditions of pH 5.6 bubbles containing PEDOT:PSS outperformed pure chitosan bubbles, indicating the persistence of the contribution of  $\pi$ - $\pi$  interactions. (Scheme 4.15a and 4.15c)

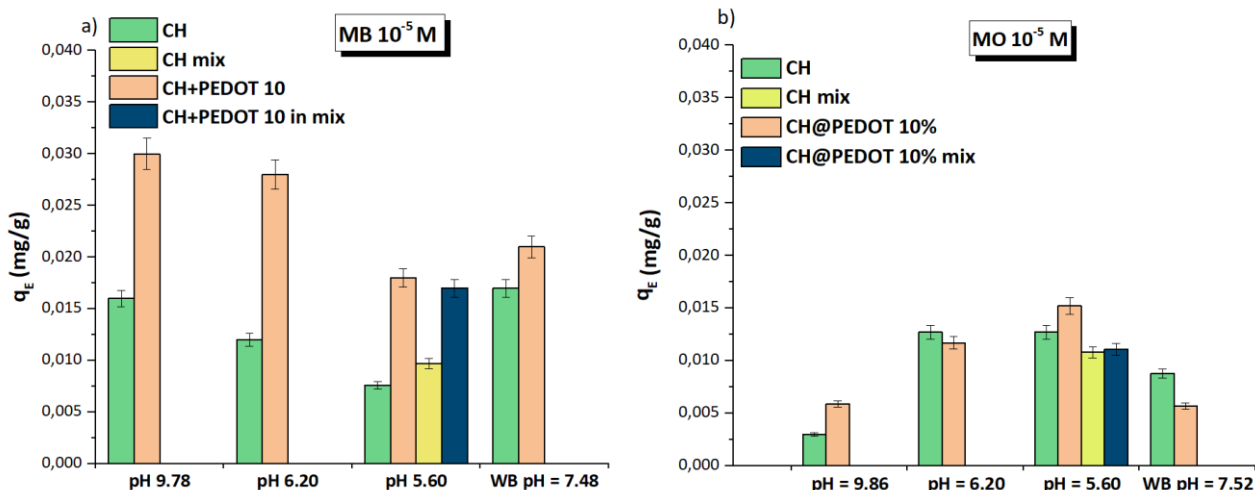


**Figure 4.17:** Variation of the equilibrium adsorption capacity ( $q_e$ ) of pure chitosan and chitosan-PEDOT:PSS (10%) bubbles as a function of solution pH.

As shown in **Figure 4.17**, in order to investigate the behaviour of the synthesized bubbles in experimental conditions more similar to real world conditions, we analysed their adsorption capacities in acidic conditions when both the dyes were simultaneously contained inside the solution (see date indicated as CH and CH@PEDOT 10 mix).

Interestingly, the bubbles were able to efficiently adsorb both MB and MO, without any significant reduction of  $q_e$ , in comparison to the values obtained when a single dye was considered. If we consider the adsorption of MB in presence of MO, in the case of PEDOT:PSS containing bubbles  $q_e$  was lowered of only the 6.5 %, while in the case of pure chitosan bubbles a slight increase of the 28% was recorded, in comparison to pure MB solution.

It was evident that MO did not hinder MB adsorption. MB, instead, slightly reduced MO adsorption, since  $q_e$  was reduced of the 15% in the case of pure chitosan bubble and of 27.5 % in the case of PEDOT:PSS-containing bubbles. This behaviour could be due to the fact that MB molecules saturated some adsorption sites and limit their availability for  $\pi$ - $\pi$  interactions with MO.

With the aim to prepare true-to-life samples, we independently dissolved MB and MO in mineral water (see **Table 4.3** for its chemical composition) in order to reach the same  $10^{-5}$  M concentration and we tested pure chitosan and chitosan-PEDOT:PSS 10% bubbles (WB pH = 7.48 in **Figure 4.17**).

**Table 4.3:** Chemical composition of bottled water. Chemical-physical constants: Water temperature at the source: 10.8°C · pH at the source: 7.60 · specific electrical conductivity at 20°C: 91  $\mu\text{S}/\text{cm}$  · fixed residue at 180°C: 60 mg/L · Hardness °f 5.9 · free CO<sub>2</sub> at the source: 6.0 mg/L.

<b>Substances dissolved in one litre of water expressed in ions</b>			
Ca <sup>2+</sup>	11.2 mg/L	SO <sub>4</sub> <sup>2-</sup>	5.6 mg/L
Mg <sup>2+</sup>	3.5 mg/L	NO <sub>3</sub> <sup>-</sup>	3.8 mg/L
Na <sup>+</sup>	2.0 mg/L	Cl <sup>-</sup>	2.0 mg/L
K <sup>+</sup>	0.70 mg/L	F <sup>-</sup>	< 0.1 mg/L
HCO <sub>3</sub> <sup>-</sup>	50 mg/L	SiO <sub>2</sub>	7.1 mg/L

Also in this case, a satisfactory adsorption was maintained in the case of pure chitosan bubbles, while PEDOT-containing bubbles showed a more environment-sensitive behaviour.

In the case of MO, for pure chitosan bubbles a value of  $q_e$  intermediate to that measured at pH 9.9 and that of 6.2 was obtained, as expected considering that the pH of the obtained solution was 7.48. In the case of PEDOT functionalized bubbles, instead, a more limited adsorption was achieved, probably because of the interference from other ionic species contained in the solution. A similar trend was observed for MB. In the case of pure chitosan bubbles the value of  $q_e$  obtained in mineral water was increased in comparison to solution prepared in Milli-Q water (solution with pH 6.2), thanks to the elimination of all the positive charge localized on the polymeric chain and the electrostatic repulsion with MB<sup>+</sup> in solution. The adsorption increase was even higher than that obtained in the case of alkaline solution prepared in milli-Q water, indicating that in this case ions contained inside the mineral water can favour MB<sup>+</sup> adsorption. In the case of PEDOT-PSS containing bubbles, instead, a reduced value of  $q_e$  was achieved (significantly lower than those measured both at pH 9.8 or 6.2), suggesting again a competition during adsorption between aqueous ions and dye molecules. This systematic reduction of the adsorption capacity in the presence of competitive chemical species that was observed in the case of both the dyes, independently from their charge, was a further confirmation of the fact that PEDOT:PSS contribute to dye adsorption not only through electrostatic forces, which were linked to the charge of the adsorbed species, but also through not-charge dependent forces, as such as  $\pi$  - $\pi$  interactions.

## 4.4 Synthesis and characterization of chitosan hydrogels in form of films

In the following paragraph will be discussed the synthesis and mechanical properties characterization of chitosan hydrogel in form of films. Moreover, will be reported the experimental tests on the antimicrobial activity of the obtained hydrogel.

### 4.4.1 Materials and Methods

#### 4.4.1.1 Synthesis of CH, CH+AuNPs, CH+AgNPs and CH+TiO<sub>2</sub> films

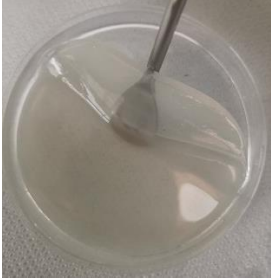
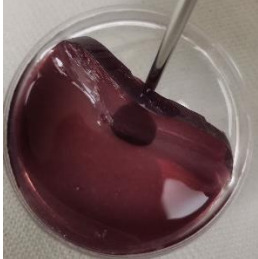
To prepare CH film, 0.900 g of chitosan were dissolved in 5% CH<sub>3</sub>COOH w/v in order to obtain a solution of concentration 30 g/L. The dissolution of biopolymer was favoured by the use of an ultrasonic bath.

The dissolved solution was poured into a Petri dish and covered with NaOH 3 M to ensure the physical crosslinking. After 6 hours, NaOH was removed, and the obtained film was washed with Milli-Q water until pH = 7.

To prepare the functionalized films, the same synthetic steps are followed, but in the case of CH+TiO<sub>2</sub> film, a fixed amount of TiO<sub>2</sub> DEGUSSA P25 was added in order to reach a concentration of 0.1% w/v, while in the case of CH+AuNPs and CH+AgNPs, solution of AuNPs and AgNPs (prepared according to section 3.2.2 and 4.2.7 respectively) were used instead of Milli-Q water.

All films were prepared in wet and dry forms (**Table 4.4**). In particular, the dry form is obtained from wet form after slow and complete drying under the hood.

**Table 4.4:** Summary of films tested for mechanical properties.

<b>System</b>	<b>Dry form</b>	<b>Wet form</b>	<b>Short Name</b>
<b>Chitosan</b>			<b>CH</b>
<b>Chitosan + AuNPs</b>			<b>CH+AuNPs</b>
<b>Chitosan + AgNPs</b>			<b>CH+AgNPs</b>
<b>Chitosan + TiO<sub>2</sub> 0.1% w/v</b>			<b>CH+TiO<sub>2</sub></b>

#### 4.4.1.2 Mechanical tests on chitosan films

These tests were performed in collaboration with Prof. Stefano Pandini, of the Department of Mechanical and Industrial Engineering of University of Brescia.

Mechanical tests were performed in uniaxial drive mode with the electromechanical dynamometer Instron 3366 to determine the hardness (or elastic modulus) and the resistance of materials.

Both for dry and wet hydrogels, strips 40mm x 10 mm were cut.

In the case of dry films, they were mounted on paper frames to facilitate handling (**Figure 4.18a**) and the precise value of length, width and thickness were measured with a microscope and a digital micrometre.



**Figure 4.18:** a) paper frames prepared for the strips 40mm x 10 mm obtained from dry films. b) 40mm x 10 mm strips cut from wet films.

In the case of wet films, the use of paper frame is not necessary, and width, thickness and length were measured with a calibre (**Figure 4.18b**). In this case, the clamps used for the tests, were coated with silicon covers to avoid a compromise of the results due to knurling. During the tests, the samples were kept moist by wetting them with Milli-Q water.

For both types of samples, the distance between the two ends was 40 mm.

The displacement speed was 1 mm/min for dry samples and 10 mm/min for wet samples.

#### 4.4.1.3 Antifungal and antibacterial tests

These tests were performed in collaboration with Dott. Daniela Bulgari, of the Department of Molecular and Translational Medicine of the University of study of Brescia.

Antifungal tests were conducted only on wet chitosan films, that were prepared and washed under biological hood to prevent data distortions due to external contaminations.

For antifungal tests, the prepared films were laid on a Petri dish containing a culture medium with *potato dextrose agar* (PDA). A “dowel” of a fungal stain *Alternaria tenuissima*, was put at the centre of each film and the samples were incubated for 7 days at 26°C.

All tests were carried out in duplicate and compared with a reference in which *A. tenuissima* has been grown on PDA without any chitosan films.

The antibacterial tests were carried out on chitosan starting solutions (CH, CH+AgNPs, CH+AuNPs and CH+TiO<sub>2</sub>), before the jellification, that is in absence of NaOH. Also in this case, the solutions were prepared under biological hood.

100 µL of liquid culture of the pathogenic bacterium *Pseudomonas Syringae pv. Phaseolicola* were inoculated on Luria-Bertani (LB) Agar Plate. The LB plate was incubated at 26°C for 24h in order to obtain the formation of bacterial film. 200 µL of each chitosan solutions were placed on the colonized plate and were incubated overnight at 26°C.

## 4.4.2 Results and discussions

### 4.4.2.1 Mechanical behaviour of chitosan-based films

In this paragraph the results obtained from mechanical tests will be reported.

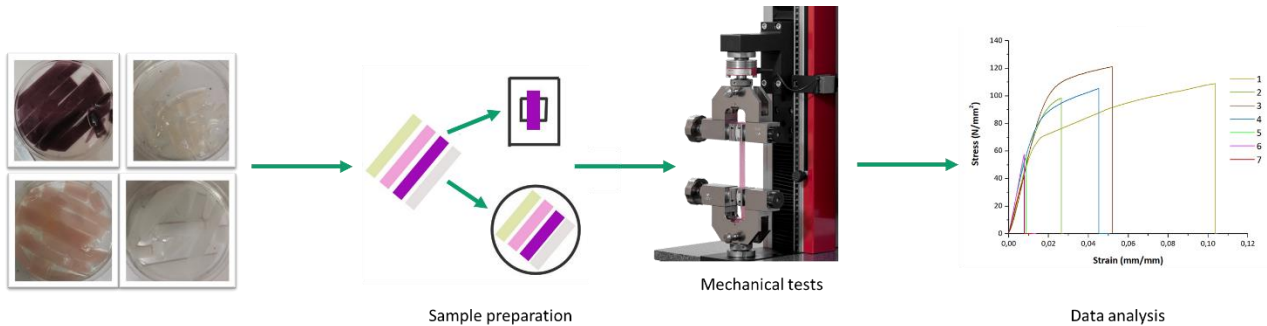


**Figure 4.19:** Schematic representation of experimental procedure for mechanical tests.

For each film, in its dry or wet version, a minimum of three and a maximum of five replicas were done.

These mechanical tests allow us to define two fundamental parameters for each film: the **strain** of the sample, that is a deformation calculated as the ratio between the force-induced displacement applied during the experiment and the initial length of the sample (mm/mm), and the **stress**, calculated as the force applied to a material divided by the material's cross-section area (N/mm<sup>2</sup>):

$$\text{strain} = \frac{L - L_0}{L_0} \quad (6)$$

$$\text{stress (N/mm}^2\text{)} = \frac{F}{A_0} \quad (7)$$

where: F = force (N)

$A_0$  = original cross section area (mm<sup>2</sup>)

$L_0$  = original length (mm)

L = length after load is applied

The plot of stress vs strain is a diagram that allows us to calculate how much force a material can withstand before failure or permanent deformations occur.

**Figure 4.20** represents the stress vs strain graph for **dry** films:

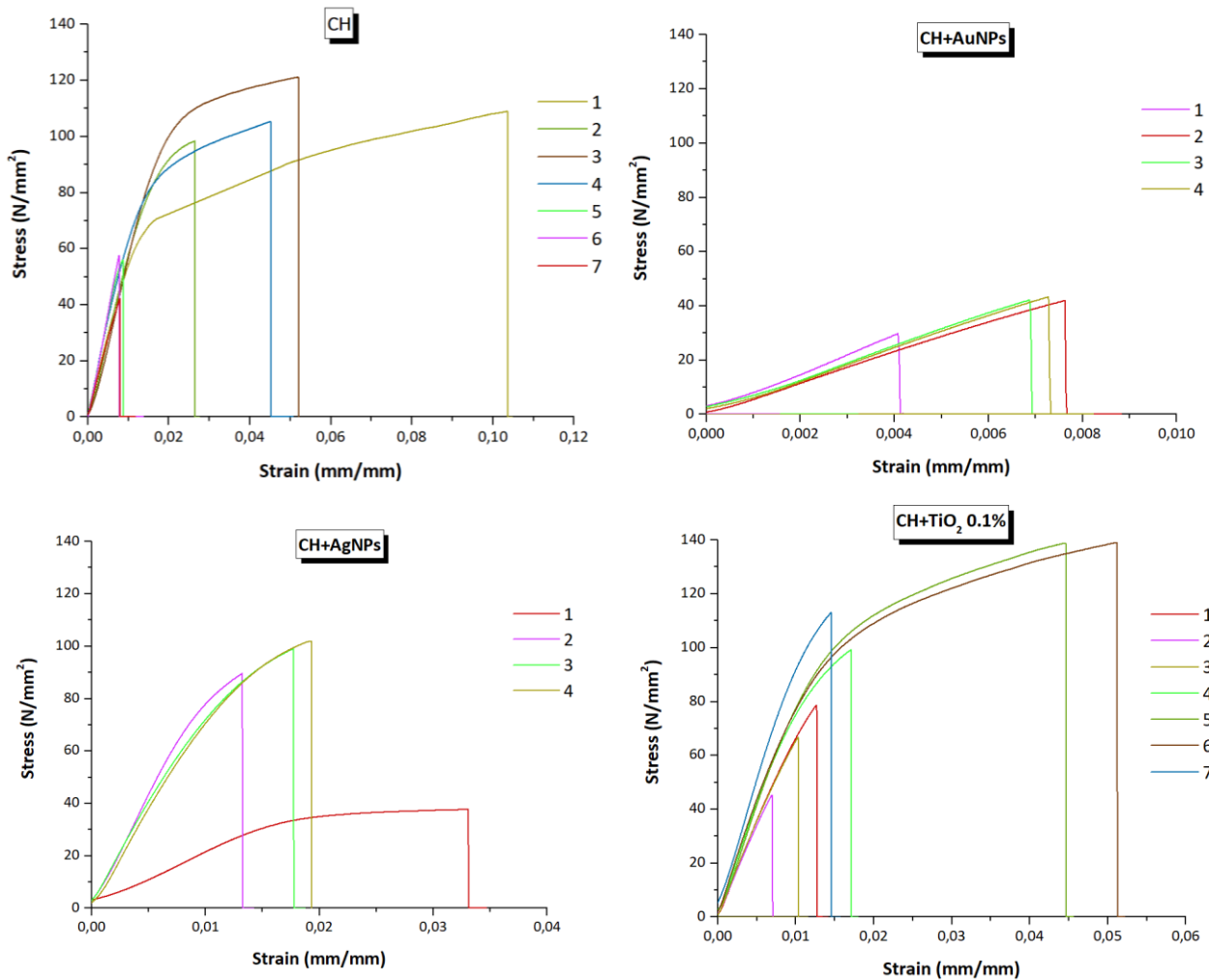


**Figure 4.20:** Stress vs Strain curve for **dry** films.

As we saw in **Figure 4.20**, a typical diagram presents a first straight section, whose angular coefficient represents the elastic modulus of the analysed material. The elastic modulus exploits the relationship between the tension applied on the sample and the subsequent deformation in the case of monoaxial load conditions and of “elastic” behaviour of the material. The greater is the elastic modulus, the greatest is the resistance of material to deformation; on the contrary the material will be defined “yielding”.

The maximum value of stress defines the resistance of material, while the maximum strain at the maximum stress corresponds to fracture deformation.

These three parameters for dry films were summarized in **Table 4.5** and **Figure 4.21**.

**Table 4.5:** Elastic modulus, resistance and fracture deformation for each **dry** system  $\pm$  the standard deviation.

System	Elastic Modulus (Mpa)	Resistance (Mpa)	Fracture deformation
CH	6600 $\pm$ 810	84 $\pm$ 31	0.036 $\pm$ 0.035
CH+AuNPs	6500 $\pm$ 600	39 $\pm$ 6	0.006 $\pm$ 0.002
CH+AgNPs	8000 $\pm$ 700	101 $\pm$ 10	0.024 $\pm$ 0.014
CH+TiO <sub>2</sub> 0.1%	8000 $\pm$ 1100	97 $\pm$ 36	0.022 $\pm$ 0.018

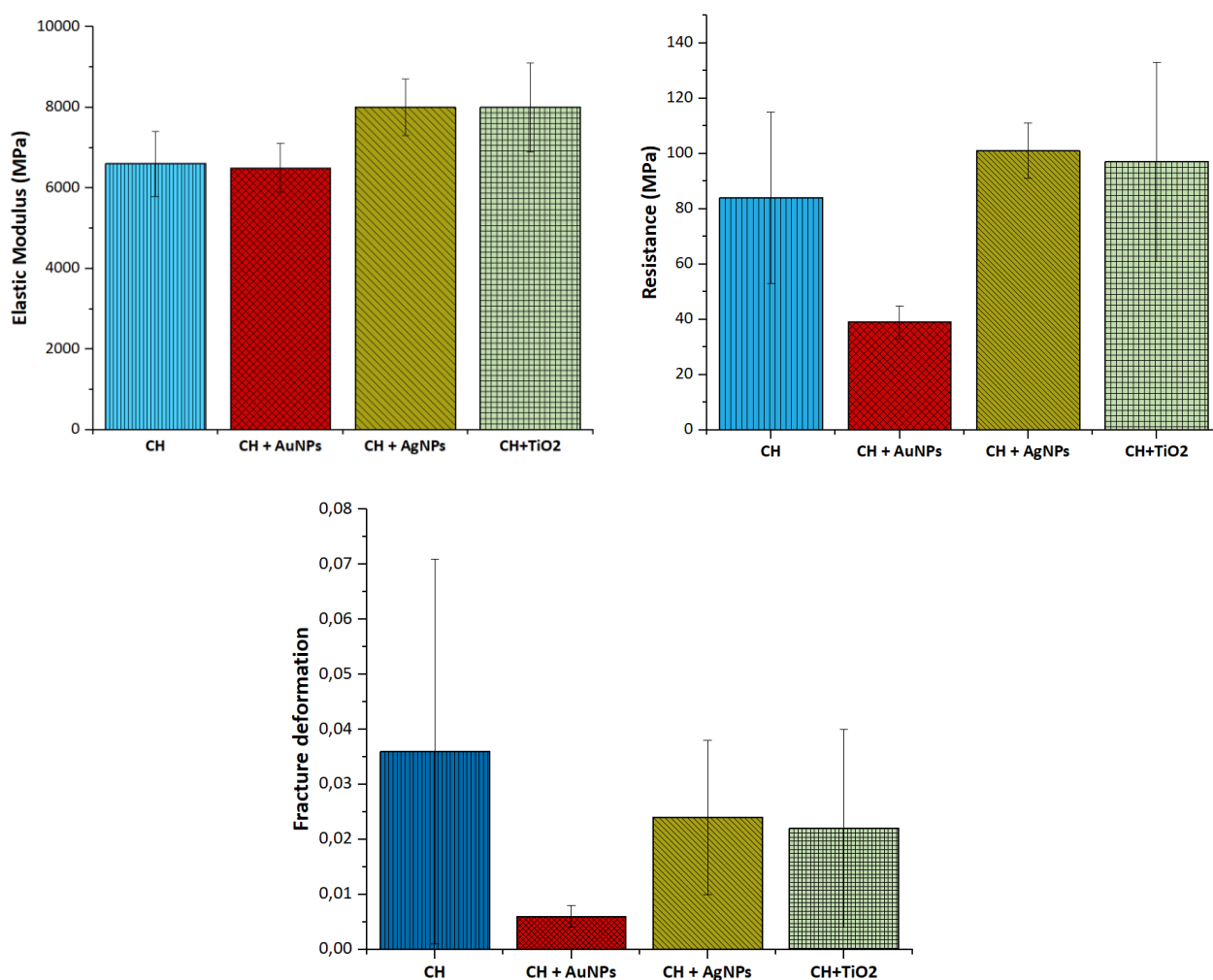


**Figure 4.21:** Comparison between the value of Elastic modulus, Resistance and Fracture deformation for the different **dry** systems.

The obtained results are characterized by a not negligible standard deviation, especially for the fracture deformation. This is attributable to the synthetic procedure that doesn't allow to control the homogeneity of the sample in all directions.

The matrix material, represented by the film of pure chitosan (CH), has good mechanical properties even if presents a certain fragility. In all cases, the addition of nanoparticles inside

the matrix seems to worsen the response to fracture deformation with a minimum value reached when AuNPs are added, which also adversely affect the resistance of the film. However, the insertion of gold nanoparticles does not affect the elastic modulus.

On the contrary, the addition of TiO<sub>2</sub> and AgNPs, causes an increase in the elastic modulus suggesting a more effective reinforcement of the matrix; while, also taking into account the high standard deviation, they don't seem to significantly affect the resistance.

**Figure 4.22, 4.23 and Table 4.6** show the results obtained for wet hydrogels.

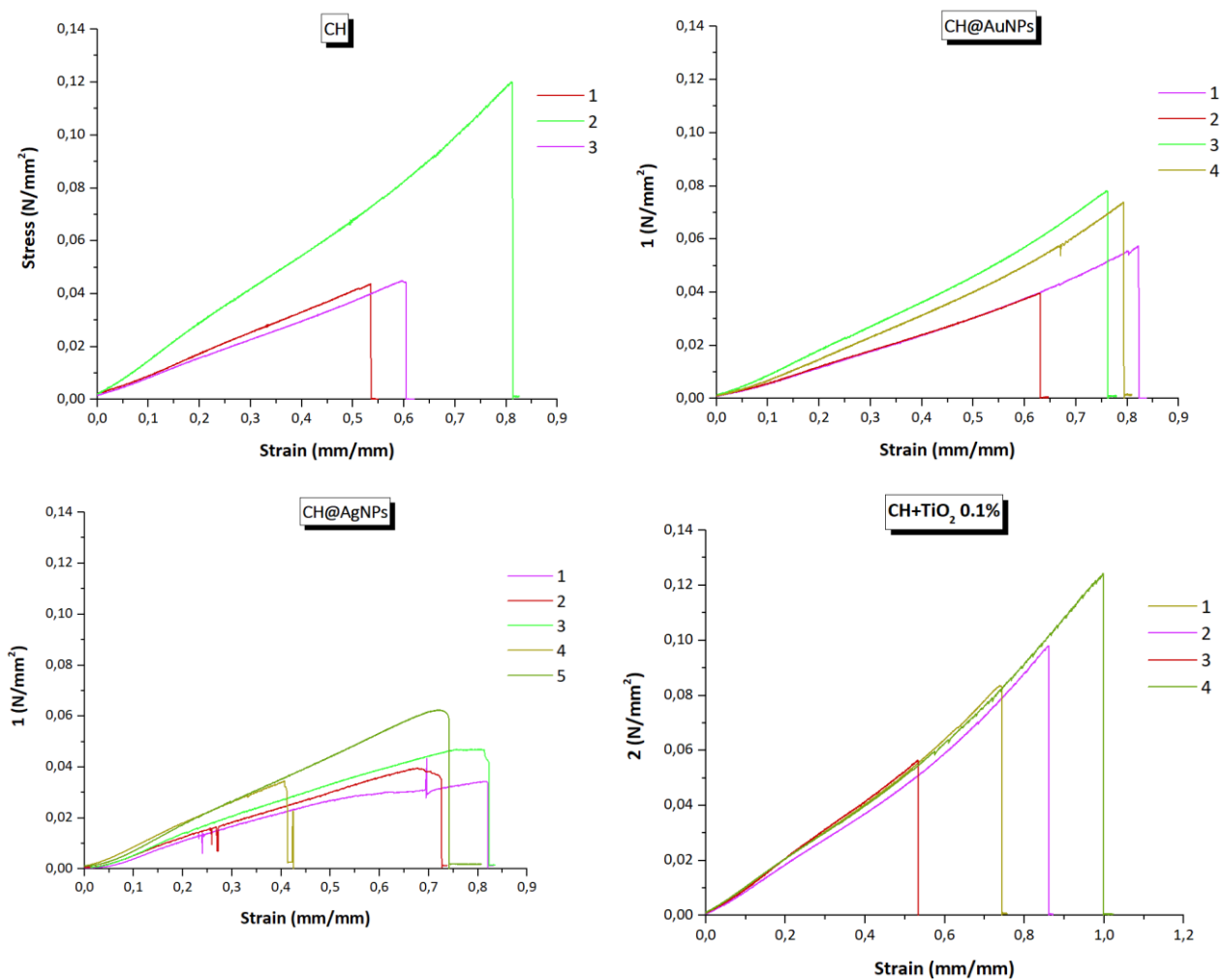


**Figure 4.22:** Stress vs Strain curve for **wet** films.

**Table 4.6:** Elastic modulus, resistance and fracture deformation for each **wet** system  $\pm$  the standard deviation.

System	Elastic Modulus (Mpa)	Resistance (Mpa)	Fracture deformation
CH	97 $\pm$ 40	0.07 $\pm$ 0.04	0.65 $\pm$ 0.15
CH+AuNPs	57 $\pm$ 14	0.06 $\pm$ 0.02	0.75 $\pm$ 0.08
CH+AgNPs	68 $\pm$ 18	0.05 $\pm$ 0.01	0.69 $\pm$ 0.19
CH+TiO <sub>2</sub> 0.1%	88 $\pm$ 9	0.09 $\pm$ 0.03	0.78 $\pm$ 0.20

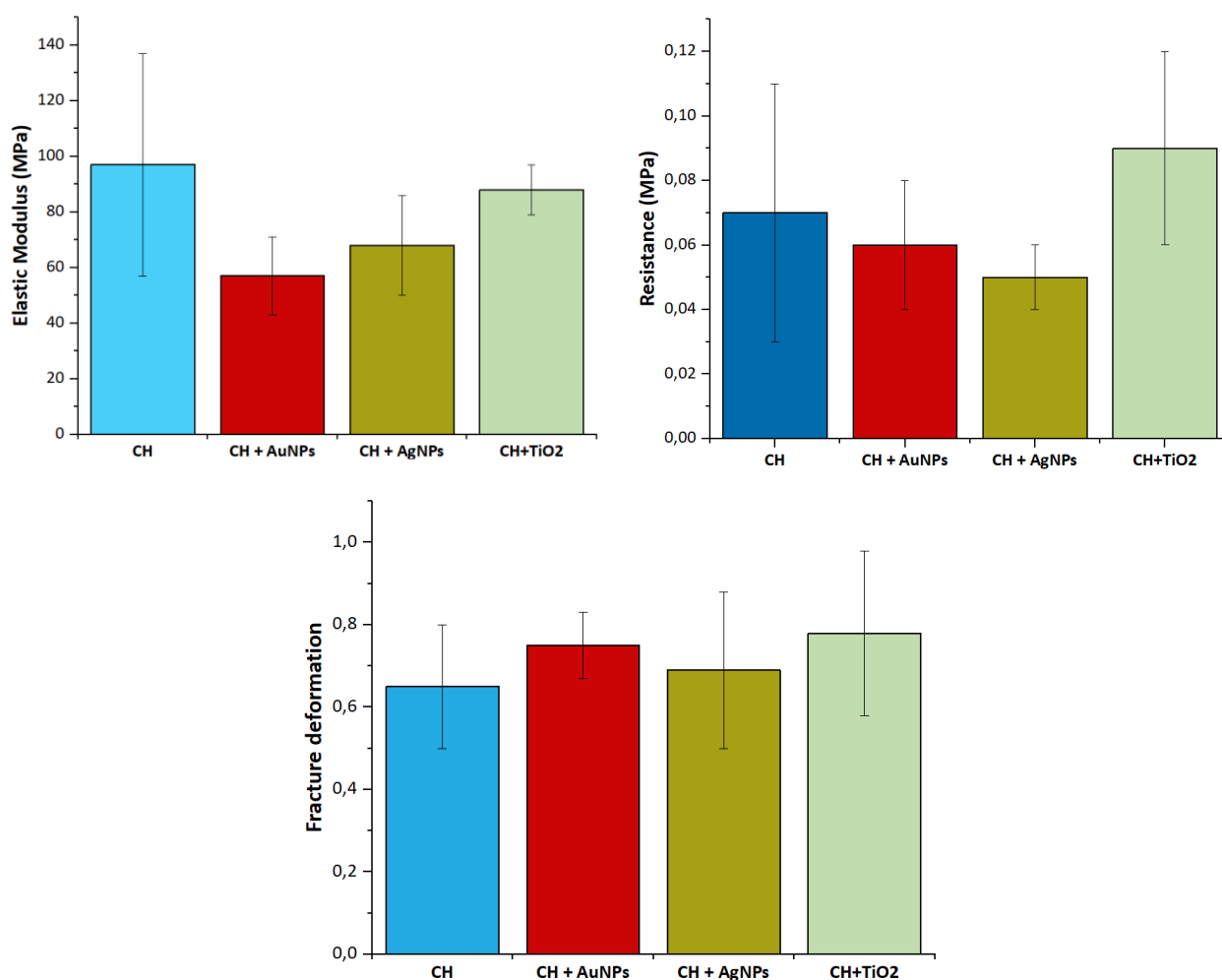


**Figure 4.23:** Comparison between the value of Elastic modulus, Resistance and Fracture deformation for the different **wet** systems.

CH and CH+ TiO<sub>2</sub> films present value of elastic modulus that are considerably higher than that presented by the sample CH+AuNPs and only slightly higher than that loaded with AgNPs. Then, it can be said that for these materials in the wet form the addition of NPs to chitosan matrix had negative effect on the elastic modulus, contrary to what could be expected from the typical behaviour of particle composite.

Finally, deformation has no significant deviations from pure chitosan, while there is an important improvement in resistance when TiO<sub>2</sub> is added, and a decline in resistance with the introduction of AgNPs, even if all values fall into the error bar preventing to make an absolute comparison.

In conclusion, the mechanical tests on chitosan-based films open the door to the use of chitosan hydrogels for real-world practical applications, which require a good resistance and mechanical stability, such as food protective films in the field of food packaging, or as adsorbent membrane in the field of environmental remediation. In this perspective, especially the data acquired on dry films become relevant. In particular, the pure chitosan hydrogel shows good mechanical properties, and the addition of NPs does not affect the fracture parameters; instead, the observation of the other two parameters demonstrates that the addition of AgNPs makes the materials more incline to deformation, while the addition of TiO<sub>2</sub> makes it more resistant.

#### 4.4.2.2 Antifungal activity tests

The antifungal activity tests were carried out in duplicate and only on wet films, evaluating the growth of *A. Tenuissima* placed at the centre of the chitosan films laid on a PDA plate and incubated for 7 days at 26°C. For all samples, the experimental procedure described in **section 4.4.1.3** was carried out, with the only exception of one of the replicas of CH+AuNPs film (**Figure 4.24**).

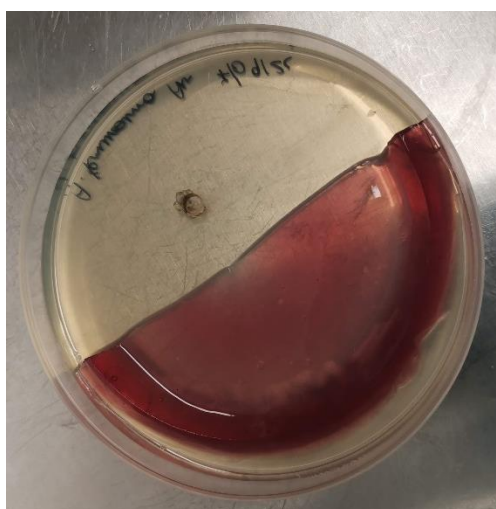


**Figure 4.24:** Particular of the film CH+AuNPs split in two part and treated with a different experimental procedure.

In fact, as we see in **4.24**, one of the two selected films broke in two parts during the deposition on PDA plate, so resulting in a lower radial surface in comparison with the other specimens. For

this reason, it has been chosen to place the *A. Tenuissima* “dowel” on the side of PDA plate film-free and to evaluate if the fungal radial growing is stopped when the hydrogel is reached.

**Figure 4.25** summarized the obtained experimental results.

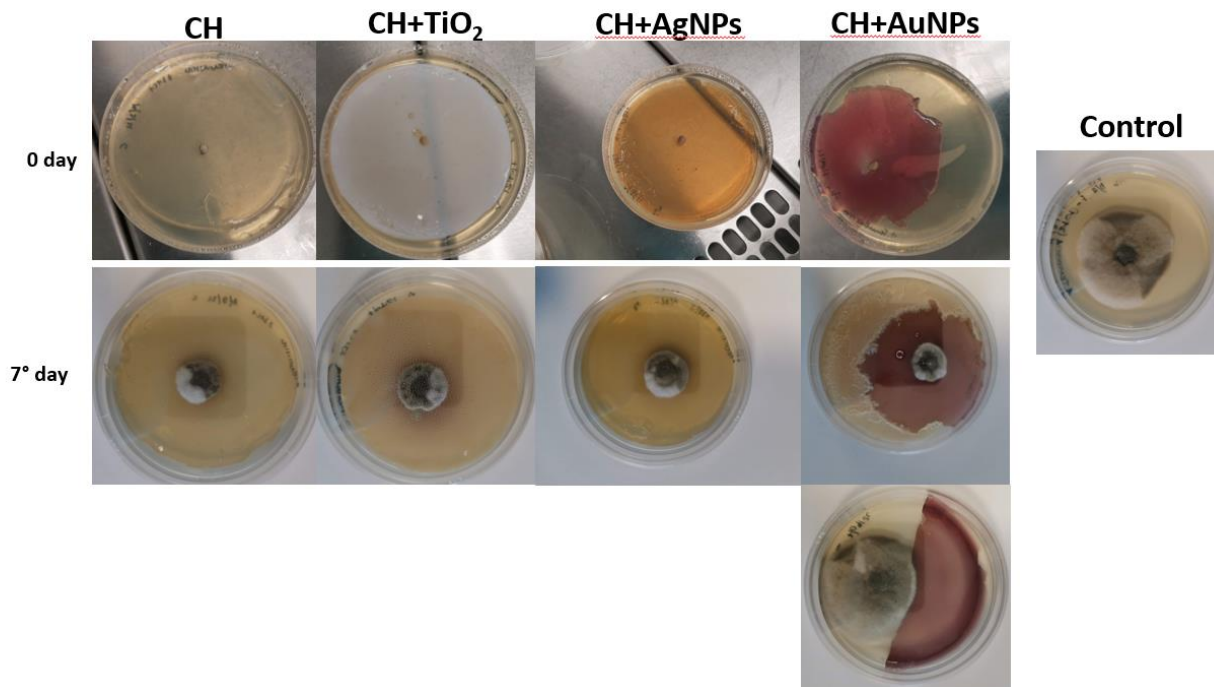


**Figure 4.25:** Results of the experiment with *A. Tenuissima* after 7 days of incubation at 26°C.

From the figure above, it is clear that the plate containing the first replica of CH+AuNPs film has a fungal contamination., in fact, unlike all the other plates where the fungal growth is limited only to the centre of the film on which the inoculum was deposited, in the sample in question it is evident that the fungus has also grown all around the film, where the inoculum had not been deposited. The accidental displacement of the plate during the incubation period, resulting in the spreading of the spores, could be an explanation of what was observed. However, if we exclude the contamination occurred on the portion of PDA plate film-free, it is still possible measure the diameter of growing of fungus placed in the centre of the hydrogel.

Obviously, from such observation the second replica of the film CH+AuNPs is excluded from such observation, for which, as already mentioned, a different protocol has been adopted.

After 7 days of incubation, for each film, in fact, the growing diameter of *A. Tenuissima* were measured and compared with the reference (PDA plate without films). The results are summarized in **Table 4.7**

**Table 4.7:** Mean radial growth of *A. Tenuissima* on chitosan films: the results are obtained by measuring the diameter of each specimen's radial growth of the fungus and are the mean of two replications.

SYSTEM	MEAN RADIAL GROWTH
CONTROL	5.10 ± 0.14
CH	1.87 ± 0.07
CH + TiO <sub>2</sub>	2.01 ± 0.01
CH + AgNPs	1.87 ± 0.14
CH + AuNPs	2.4 ± 0.14

Both the numeric and visual results confirm that in all cases the fungal growing seems to be extremely slowed down, without significant differences between the different types of chitosan hydrogel. This means that, the observed results are attributable only to chitosan matrix and are not influenced by the functional units introduced in it, even if these units have an antimicrobial nature as in the case of AgNPs.

This is justifiable by admitting that the introduced substances remain entrapped inside the film without protruding from the surface, limiting their direct contact with fungi.

Moreover, it is interesting to note that, in the case of half-cut CH+AuNPs film, the fungal growing is stopped from the presence of the hydrogel.

However, the presence of a halo of growth under the film, led us to remove each film from the PDA plate and evaluate the growth of *A. Tenuissima* under hydrogels (**Figure 4.26**).

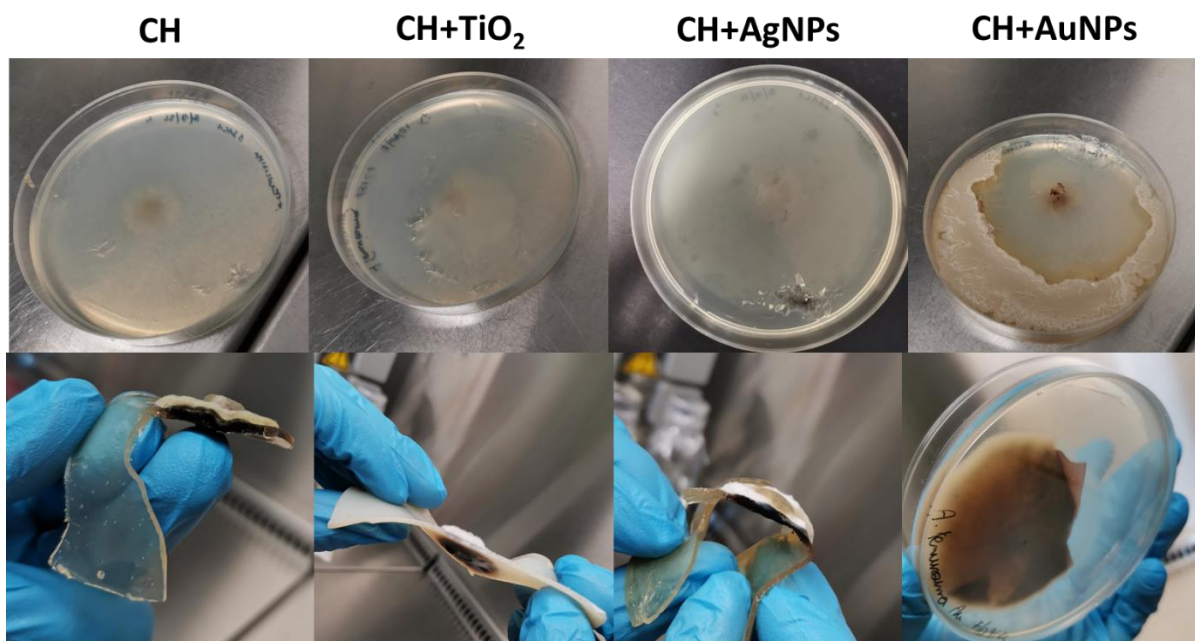


**Figure 4.26:** halo of growth under the chitosan films due to the penetration of *A. Tenuissima* inside the films.

In all cases, the fungus seems to have managed to pass the film, penetrating inside the hydrogel and reaching the layer of PDA below. However, while for the CH film, the halo retains the same magnitude of radial growth on the hydrogel, in the case of the CH+AgNPs sample this halo is even smaller.

This means that the fungus seems effectively penetrate the film, but in this case, its growth through the hydrogel is actually slowed down when inside it there is an antimicrobial substance (e.g. AgNPs).

Finally, to be sure that the observed halo is only the result of the pressure due to the fungal growth on the film, and that its growth is actually slowed, following the removal of the hydrogel, the plates have been incubated for a few more days (**Figure 4.27**).

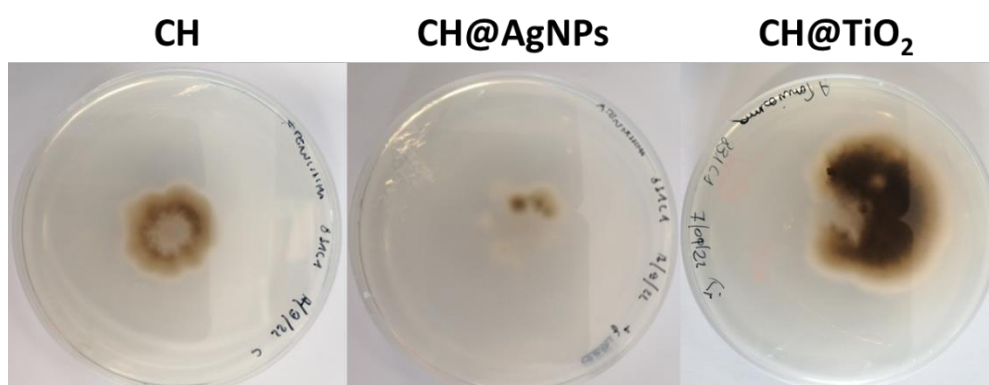


**Figure 4.27:** halo of growth under the chitosan films after a few days of further incubation at 26°C.

The unchanged size of the growth halo after further incubation, confirm that *A. Tenuissima* can cross the hydrogel barrier, but its growth is significantly slowed by the antimicrobial action of the film that, in this case, it is more or less high depending on the type of functional unit introduced in it.

#### 4.4.2.3 Antibacterial activity tests

To better evaluate the antimicrobial activity of the prepared materials, and to be sure that it is not due to the effect of NaOH used as polymer crosslinking, tests with the gram-negative bacterium *Pseudomonas syringae pv. phaseolicola* were carried out directly on the chitosan starting solution, according to the experimental procedure reported in *section 4.4.1.3*.

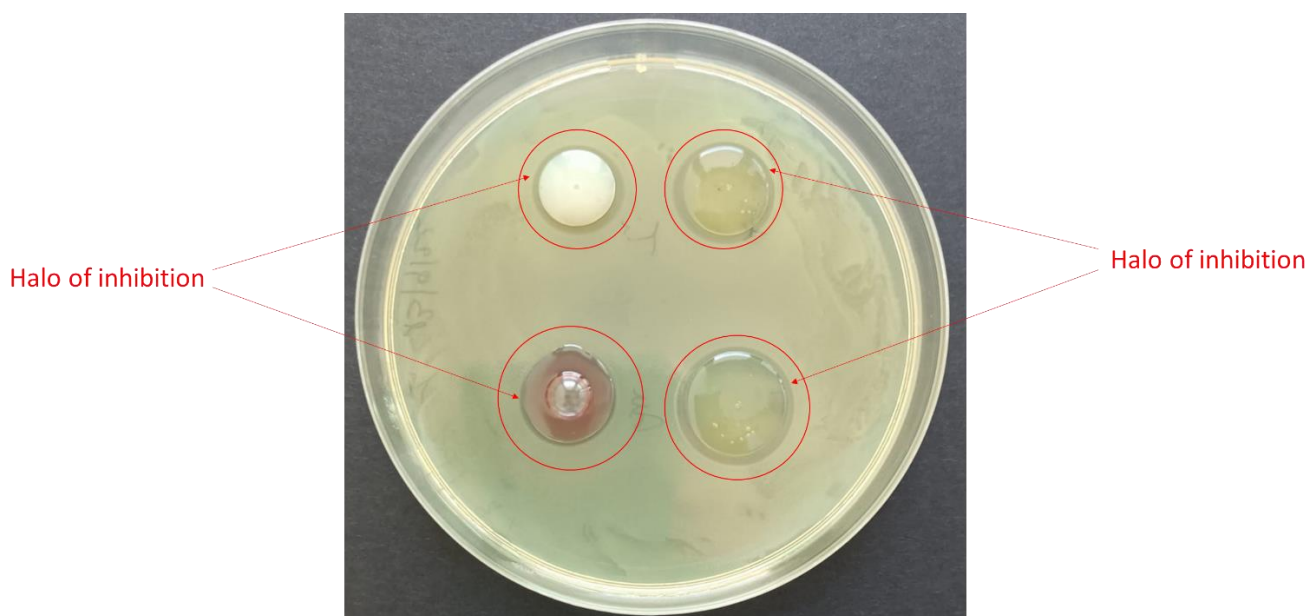


**Figure 4.28:** LB plate inoculated with *Pseudomonas syringae pv. phaseolicola* on which chitosan solutions before jellification with NaOH were added (from left to right, from top to bottom: CH+TiO<sub>2</sub>, CH+AgNPs, CH+AuNPs, and CH). The halos of inhibition due to the bactericidal activity of all solutions are well visible and are underlined from the red circles in the figure.

The presence of transparent inhibition halos around the LB plate with *Pseudomonas*, confirms the antibacterial activity of each solution (**Figure 4.28**).

Such antibacterial activity appears to be attributable solely to chitosan and it is poorly affected by the added functional units.

Inhibition halos are similar for all four solutions tested. Such halos could, therefore, be due to the release of the only chitosan molecules (not crosslinked with each other), which obviously have a bactericidal action in the LB soil.

## 4.5 A preliminary study on chitosan bubbles containing CsPbBr<sub>3</sub> perovskite, used for MB removal

In this paragraph the preliminary data of an exploratory study on use of lead halide perovskites (PVK), stabilized in chitosan hydrogel, for the removal of organic pollutants in aqueous matrix, will be reported. This study has been conducted in collaboration with Dott. Giammarco Roini of the department of information engineering of the University of Brescia.

Lead halide Perovskites, with the general chemical formula APbX<sub>3</sub> (where A is an organic or inorganic monovalent cation and X is a halide ion) are a particular class of semiconductors that are known especially for their great optoelectronic properties, and their efficiency in photo conversion <sup>139,140</sup> and they are widely used for the production of materials with high light adsorber efficiency and photovoltaic applications <sup>141</sup>.

In particular, CsPbBr<sub>3</sub> is one of the most studied lead halide perovskites, in fact it has been largely used in lasers <sup>142</sup>, light-emitting diode<sup>143,144</sup>, solar cells<sup>145,146</sup>, and photodetectors<sup>147,148</sup>. This PVK exhibits a band gap of 2.3 eV and has a great carrier transport capability and, therefore, can easily generate holes and vacancies by exciting electrons from valence band (VB) to conductive band (CB). In particular, the electrons in CB have a carrier mobility lifetime product of  $1.7 \cdot 10^{-3} \text{ cm}^2/\text{V}$ , while the same parameter for hole is about  $1.3 \cdot 10^{-3} \text{ cm}^2/\text{V}$ <sup>149</sup>. Moreover, this type of PVK has the advantage to be more stable than the organic perovskites, and this makes them perfect for the production of long-life devices.

In this study, we exploited the photophysical properties of CsPbBr<sub>3</sub> to catalyse the degradation of MB induced by solar light. In particular, CsPbBr<sub>3</sub> has been synthesised in form of nanocrystals, from its starting salts PbBr<sub>2</sub> and CsBr, combined with each other in four different molar ratios: 1 (PVK(1)), 1.9 (PVK(1.9)), 2.9 (PVK(2.9)) and 3.9 (PVK(3.9)).

Each obtained nanocrystal powder, then, has been introduced into chitosan bubbles (**Figure 4.29**). The encapsulation inside millimetric hydrogel has two main scopes: on one hand, reducing the risk of dispersion of this material into the environment, and on the other hand the polymeric matrix is used as protection to stabilize PVK in contact with water. The limited stabilization of Lead Halide Perovskites in water, in fact, remains one of the greatest limits of these materials.

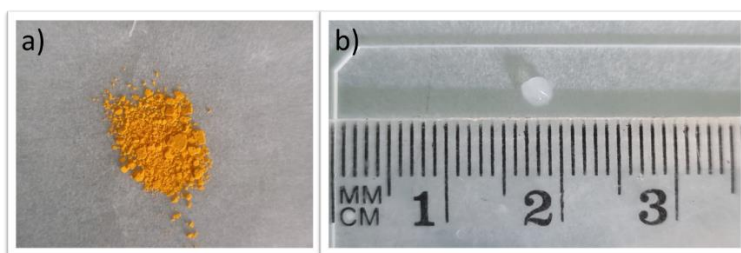


**Figure 4.29:** a) CsPbBr<sub>3</sub> powder and b) chitosan@PVK bubbles obtained from the procedure described in *section 4.2.2*

Since this is a preliminary study, it was decided to consider only the MB as pollutant and make a comparison between the systems obtained with PVK with the reference system composed by the simple chitosan matrix.

Therefore, it was decided to treat this paragraph separately from the others and the part relating to materials and methods will be given below instead of *Section 4.2*.

#### 4.5.1 Experimental: synthesis of CsPbBr<sub>3</sub> and CH@PVK bubbles

All chemicals were used without any further purification.

PbBr<sub>2</sub> (99.999%, perovskite grade), CsBr (99.999%, perovskite grade), dimethylformamide (DMF) and methanol (MeOH), were purchased from Sigma Aldrich.

In all experiments ultrapure Milli-Q water was used, obtained from a Milli-Q Integral 5 system.

For the synthesis of CsPbBr<sub>3</sub>, PbBr<sub>2</sub> and CsBr were dissolved in DMF at 75°C and MeOH at 50°C, respectively, in order to obtain PbBr<sub>2</sub> 0.017 M and CsBr 0.035 M solutions.

Under magnetic stirring, a defined amount of PbBr<sub>2</sub> was mixed with a defined amount of CsBr in order to obtain PVK(1) when the amount of PbBr<sub>2</sub> was equal to CsBr, PVK(1.9) when the amount of PbBr<sub>2</sub> was equal to 1.9 time the amount of CsBr, PVK(2.9) when the amount of PbBr<sub>2</sub> was equal to 2.9 time the amount of CsBr and PVK(3.9) when the amount of PbBr<sub>2</sub> was equal to 3.9 time the amount of CsBr.

The obtained solution was kept on heating plate until the complete evaporation of solvents and the obtained powder was washed with 2-propanol to eliminate solvent residue and was left to dry (**Figure 4.30a**).

For the synthesis of the bubbles (CH@PVK), the same procedure described in *section 4.2.2* was followed. In this case, a fixed amount of each synthesized PVK was added, in order to reach a concentration of 1% w/v inside the bubble (**Figure 4.30b**).

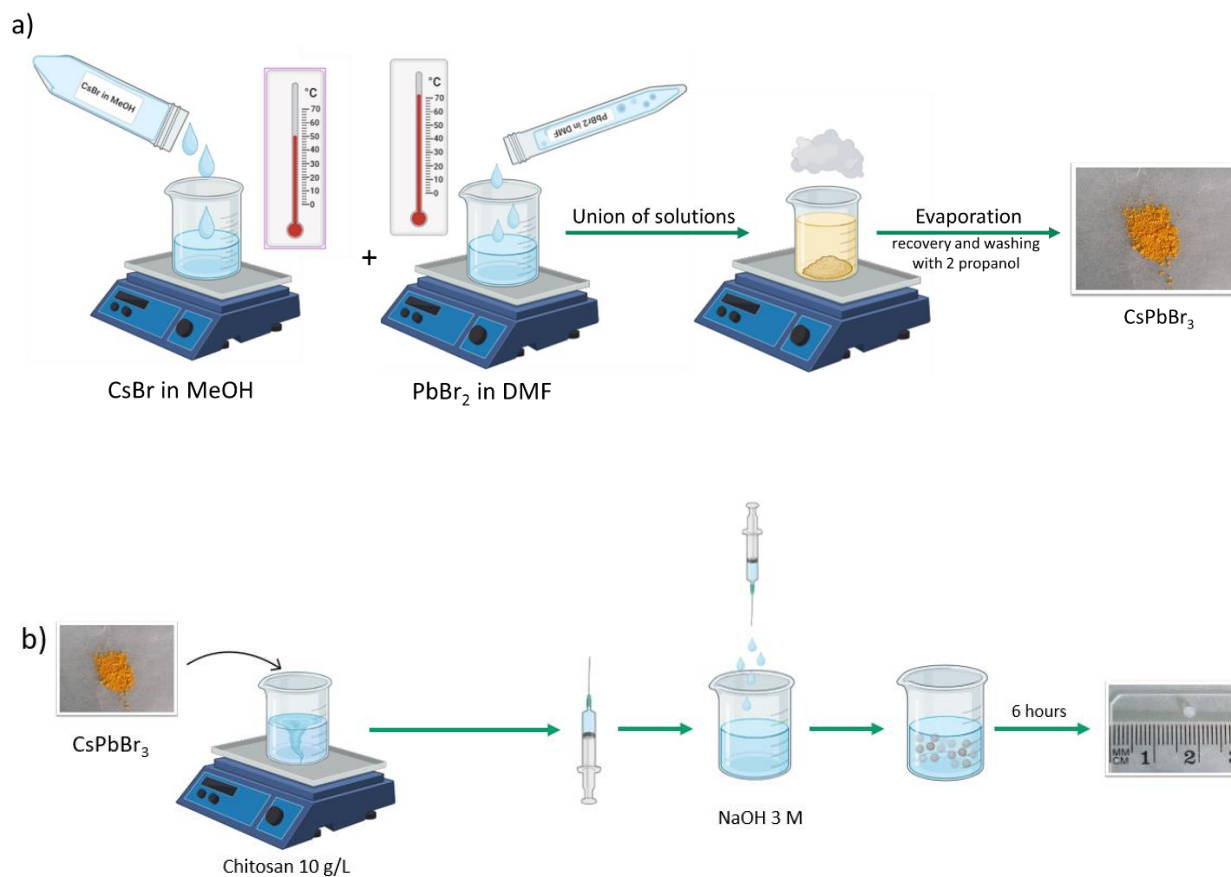


**Figure 4.30:** Schematic representation of the synthetic procedure for a) CsPbBr<sub>3</sub> nano-powder and b) CH@PVK bubbles.

## 4.5.2 Results

Following the procedure described in *section 4.2.8* and *4.2.9*, for each system an assessment of the adsorption capacity was first made.

**Figure 4.31** summarizes the obtained results.

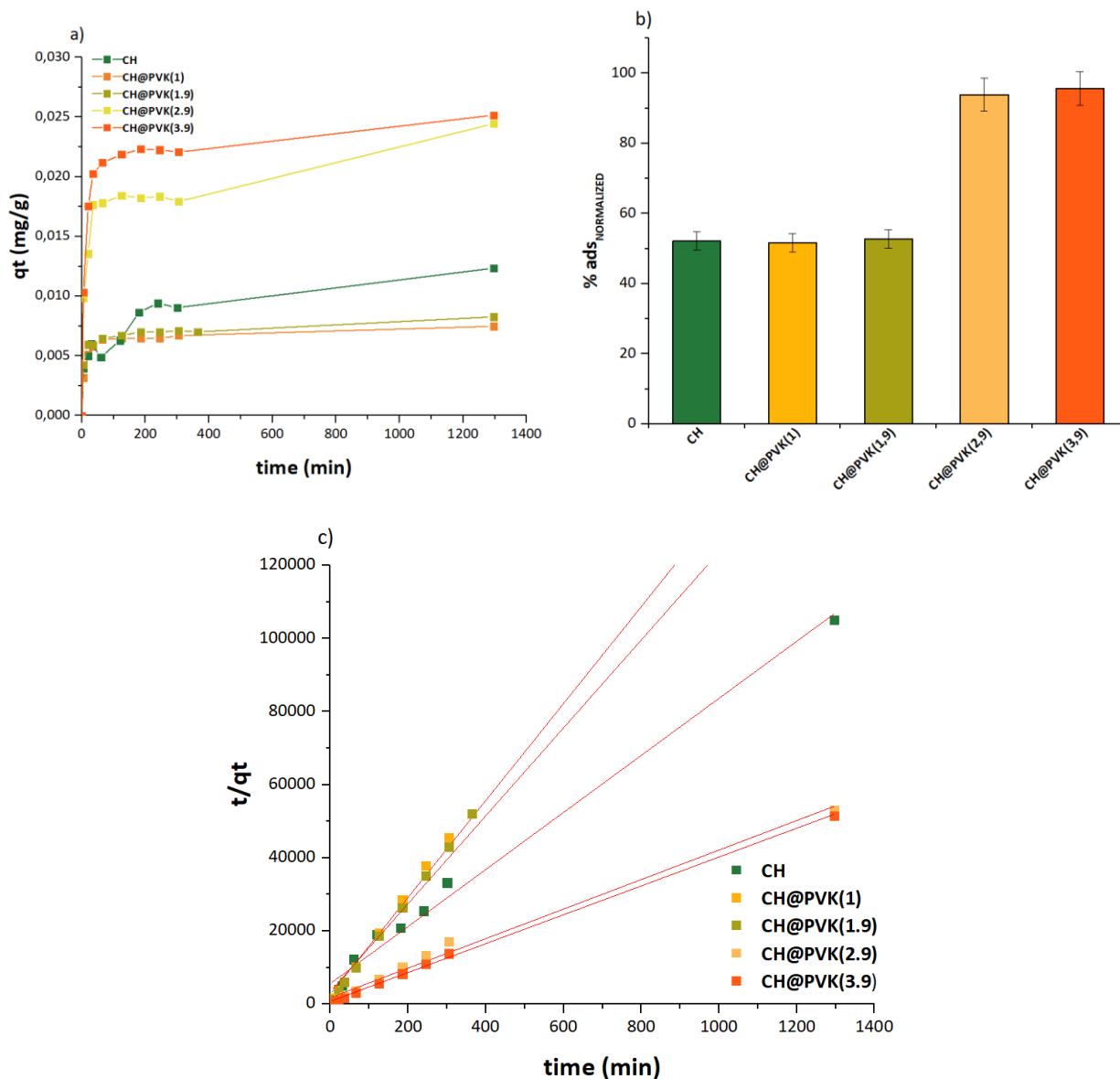


**Figure 4.31:** Comparison between the adsorption behaviour of different types of PVK chitosan-based bubbles during the interaction with MB solutions. **a)** Variation of the adsorption capacity of pure chitosan bubbles and chitosan bubbles functionalized with PVK (1-1.9; 1%w/v) as a function of bubbles soaking time inside a MB  $10^{-5}$  M solution; **b)** variation of the normalized adsorption percentage of MB according to chemical composition of PVK chitosan-based bubbles; **c)** pseudo-second order kinetic model for adsorption of MB with different chitosan and chitosan-PVK bubbles.

CH@PVK(1) and CH@PVK(1.9) systems show an adsorption behaviour similar to that of the polymeric matrix alone. However, the addition of PVK 2.9 and 3.9 enables to almost double the adsorption capacity of the hydrogel, leading us to think that not only the PVK is effectively inside the bubbles, but also that it has a key-role in the adsorption process.

To confirm that the increase in the adsorption is effectively attributable to the perovskite, nano powders of PVK were put directly in contact with MB solution  $10^{-5}$  M. In this case, two possible

amounts of PVK were evaluated: 1% and 10%. The percentage of dye remained in solution, after 5 min of contact between MB and Perovskite are reported in **Figure 4.32**.

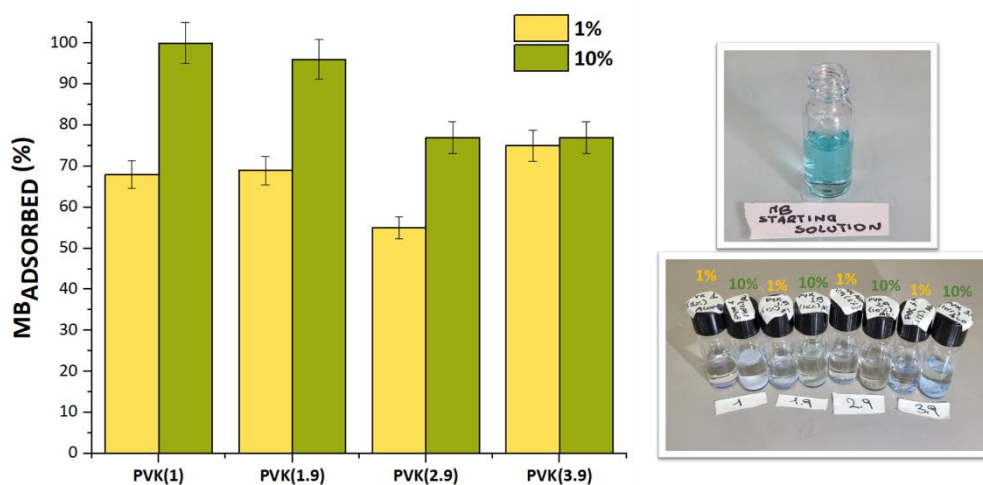


**Figure 4.32:** Percentage of adsorption of MB after direct contact between PVK nano-powder and a solution of MB  $10^{-5}$ M.

From **Figure 4.32** it is clear that 5 minutes of contact between the dye and perovskite powder are enough to obtain a significant MB adsorption for all tested systems. The higher adsorption is reached when the PVK used is PVK 1 and when PVK loading is 10% and this opens the future perspectives that, probably, a higher amount of PVK inside the bubbles could significantly improve the adsorption capability of the hydrogels.

The sample CH@PVK(1) shows a higher MB adsorption compared to the samples with other molar ratios, up to reaching the complete removal of methylene blue after 5 min (LLD – Low Limited Detection). However, if we focus on the adsorption due only to the 1% loading, the data seem to be coherent with those obtained with the bubbles, with the only exception of PVK 2.9. Probably the interaction PVK-chitosan matrix plays a fundamental role. Therefore, as a future perspective, this aspect deserves certainly to be deepened, for example by varying the type of pollutant, or increasing the amount of perovskite introduced into chitosan bubbles.

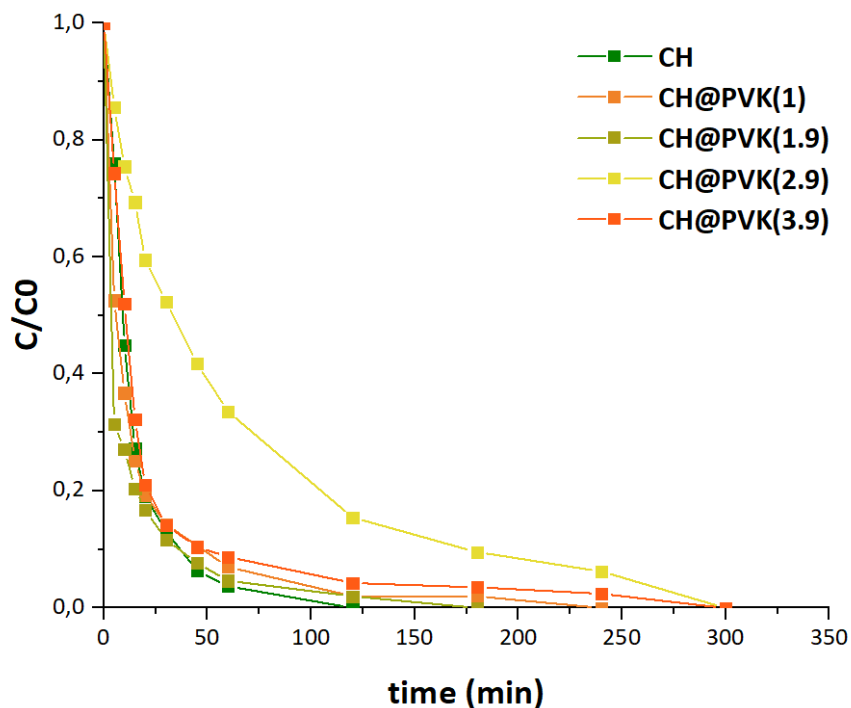


**Figure 4.33.:**  $C/C_0$  of pure chitosan bubbles and chitosan bubbles functionalized with PVK (1-3.9) 1% w/v as a function of photodegradation time inside a MB solution, after overnight adsorption.

**Figure 4.33** shows the results of photodegradation tests, obtained after overnight adsorption as described in previous paragraph.

The different systems tested behave very similarly to the reference system (CH), with the exception of samples CH@PVK(2.9) and CH@PVK(1.9).

The introduction of perovskite inside the bubbles, induce a photodegradation that generally required much time than that employed by the pure chitosan bubbles, but in all cases a full degradation of the dye is obtained within 300 minutes, with the 97% of organic molecule degraded in the first 120 minutes. The kinetic of dye degradation is quite similar to kinetic of photodegradation induced by the reference sample (CH) with two interesting exception: CH@PVK(2.9) slows down considerably the degradation of the pollutant in the first 120 minutes compared to the other systems, then moves from 84% to 100% MB removal in the remaining two hours, that is the which is the portion of time when other systems slow down their effectiveness. On the contrary, the system CH@PVK(1.9) shows an interesting acceleration in dye degradation, that is degraded until 70% in the first 5 minutes of reaction, with respect to 50% induced by CH system.

These data demonstrate that the presence of Lead Halide Perovskite inside chitosan bubbles, can modify the activity in the adsorption and photodegradation of organic dyes. The modification of chitosan matrix ability to act as adsorber and photocatalyst through the

selected pollutant, is a demonstration that PVK is still present in the bubbles even if in contact with water, letting us foresee good opportunities in the stabilization of perovskites in water. A more deepened study will be surely done.

Finally, to be sure that the prepared bubbles do not release  $\text{CsBrPb}_3$  in water, a sample of Milli-Q water, in which bubbles were immersed for more than 3 days, was analysed with TXRF. The analysis was kindly provided by Bruker in Germany, and the sample was sent already deposited on Plexiglass. The results are shown in **Figure 4.34**

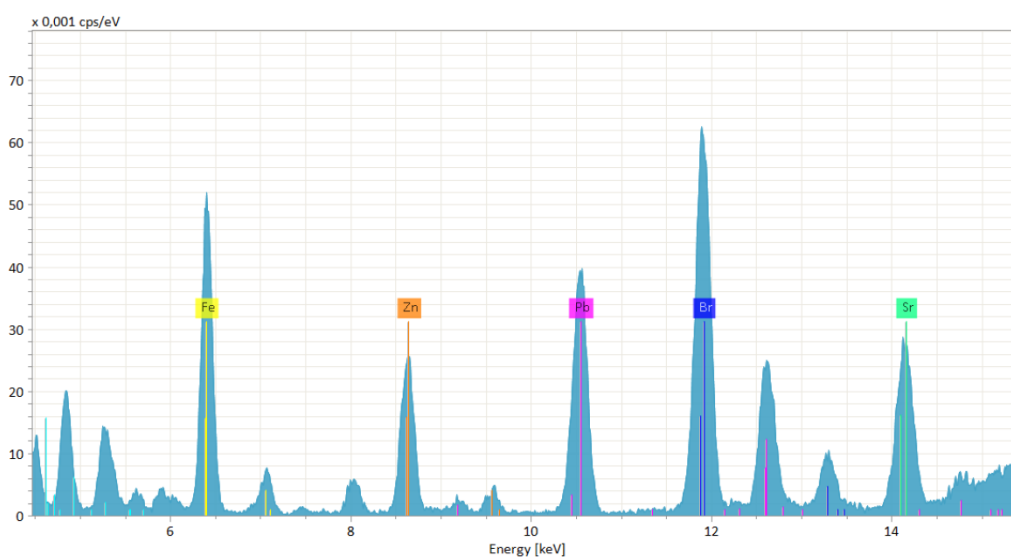


**Figure 4.34:** TXRF spectra of an aliquot of Milli-Q water in which CH@PVK bubbles were immersed for more than 3 days.

The presence of Fe, Sr, and Zn peaks, in addition to those attributable to Pb and Br, and the absence of signals related to Cs, suggest that those observed are actually peaks due to contamination related to sample preparation and shipment, rather than the actual presence of  $\text{CsPbBr}_3$  in water.

## 4.6 Conclusions

In this Chapter, we have investigated on the use of all-in-one systems based on chitosan hydrogels in form of bubbles, for capture and degradation from water of Methyl Orange (MO) and Methylene Blue (MB), two industrial organic dyes opposite in charge.

The use of chitosan extracted from food crustacean's shells using chemical method with HCl and NaOH, allows us to obtain a system with discrete adsorption capability, without showing a clear specificity for negatively (MO) or positively (MB) charged dyes.

The introduction of nanoparticles as AuNPs, AgNPs and TiO<sub>2</sub> NPs inside the bubbles, as well as the addition of biocompatible and environmental-friendly polymeric blend endowed with an extended  $\pi$ -conjugated system as PEDOT:PSS, modifies the performance of bubbles in adsorption, demonstrating that the adsorption capability does not depend only on the chitosan matrix, but can be properly modified.

A direct comparison between the effect of the conductive polymer or NPs on adsorption ability, was possible by calculating the normalized adsorption percentage of dye, in which the weight of pure chitosan bubbles was considered as reference materials and used as normalization factor.

The results demonstrate that by incorporating TiO<sub>2</sub> NPs and PEDOT:PSS, it is possible to enhance the normalized adsorption percentage when positive charged dye is involved, up to reach a percentage > 90% when PEDOT:PSS is introduced into chitosan hydrogel at the concentration of 10% v/v.

However, all the investigated systems are less efficient than reference CH, in removal of MO that is an anionic dye, with the only exception of CH@PEDOT:PSS(5-10%), in which the adsorption capability increases as the percentage of PEDOT:PSS increases. This demonstrates that in this type of bubbles, not only electrostatic interactions are involved in the adsorption mechanism, but also non-electrostatic forces based on  $\pi$ - $\pi$  interaction.

Moreover, a more in-depth study on the best adsorption system, CH@ PEDOT:PSS, shows that the electrostatic interactions can be modulated by varying the pH of the solution in which the bubbles are immersed. In this way, it is possible to play both on the charge of matrix, and on the charge of the functional unit inside, setting the most suitable parameters for the target pollutant.

Finally, the plasmonic nanoparticles, AuNPs and AgNPs, are not particularly efficient in adsorption of dyes, but are fundamental in MB photodegradation.

Under solar simulator, in fact, all systems are capable to degrade MB in just over two hours, and particularly unexpected is the activity of bubbles containing only chitosan, whose catalytic activity in MB degradation is comparable to that of analogous bubbles loaded with AuNPs and even better than bubbles with AgNPs. The origin of this activity, confirmed also by mass-spectroscopy, is currently under investigation.

On the other hand, CH@TiO<sub>2</sub> bubbles are the only systems capable to degrade MO.

This study demonstrates that food waste can be recovered and transformed into value-added materials for environmental remediation, whose functional properties can be rationally designed and controlled by a synergistic combination of individual, active components, such as polymer blends or photocatalytic nanoparticles. In particular, the preliminary study on our system loaded with CsPbBr<sub>3</sub>, is a clear proof that systems such as those used in this thesis can be beneficial not only from the water remediation point of view, but also because they have such properties that can be apparently stabilize challenging materials such as perovskite.

Finally, the demonstrated good mechanical properties and the confirmed antimicrobial activity of chitosan matrix, open the door to the use of chitosan-based hydrogel not only in the real contaminated wastewater but also in other field of applications such as, for example, food packaging.

# Chapter 5

---

## 5. Preliminary study of chitosan nanoparticles-induced resistance against *Tobacco Necrosis Virus* in *Phaseolus Vulgaris*

In this chapter, the antiviral activity of chitosan nanoparticles (CsNPs), used as resistance inductors of *Tobacco Necrosis Virus* (TNV) inoculated on *Phaseolus vulgaris* leaves, was evaluated.

Chitosan nanoparticles were synthesized both starting from extracted chitosan (see **section 2.2.2**) and starting from commercial chitosan Bio-basic, used as reference sample.

In this case, it was decided to avoid the use of the commercial chitosan Sigma Aldrich due to the difficulties in its dissolution discussed in the **Chapter 2**. Moreover, it was decided to compare the two chitosan with the most similar **DD** (see more information in chapter 2).

To synthesize CsNPs, the ionotropic gelation technique was used, and three concentrations of NPs were evaluated: 1, 2.5 and 5 mg/mL. The dimension and the morphology of the obtained CsNPs were verified through **Atomic Force Microscopy (AFM)**.

In particular, in this exploratory study, we demonstrated that CsNPs, synthesized according to the procedure reported in the following, are not phytotoxic for the plant *Phaseolus Vulgaris*, but, on the contrary, they seem to induce a mechanism of resistance in plants. In particular, we verified that when the plant *Phaseolus Vulgaris* is treated with CsNPs and is infected with **TNV** it has an extremely reduced number of necrotic lesions.

This work was carried out in collaboration with Dott.ssa Daniela Bulgari of the Department of Molecular and Translational Medicine of the University of study of Brescia.

## 5.1 Introduction

Nowadays, environmental sustainability represents one of the hottest topics in a great number of fields.

The abatement of CO<sub>2</sub> emissions and water remediation, that we discussed in previous chapters, are just two of the top themes of the scientific research in recent years<sup>150-154</sup>.

In fact, in 2020 FAO highlights an urgent need to protect more efficiently plants health to promote not only the environmental wellness, but also the economic development<sup>155</sup>.

Actually, indeed, about 40% of food crops is lost every year due to plant diseases that often adversely affect also the quality of food products<sup>156</sup>.

These plant diseases often result in a decrease in the yield of the seasonal product, appearance of necrotic lesions and stains on the product or limited plant growth, leading to significant economic losses.

On the other hand, in the last 10 years, the constant increasing worldwide population, has led to triplicate the demand of agriculture products, at the point that the demand for food products is estimated to grow by 60% by 2050<sup>157</sup>.

For these reasons, the research of new effective technologies for the protection of crops, is a practical and moral imperative.

Up to now, fertilizers and pesticides have been widely used to overcome this situation, and in recent years, genetically modified crops to be disease-resistant, are increasingly employed in farming communities. For example, in the United States alone the use of pesticides has reached 516 million pounds<sup>158</sup>.

If on the one hand such intensive use of pesticide and fertilizers protects food crops from plant diseases, on the other hand it decreases severely not only the quality of food generated from crops, but also and especially the soil fertility<sup>159</sup>.

This, therefore, results not only in a higher risk to human health but also in a destabilization of the ecosystem (i.e. marine environment, soil microbial flora)<sup>160</sup>.

For these reasons, changing conventional practices with smart agriculture protocols, is an urgent issue. In this regard, the use of nanotechnologies for a sustainable agricultural development could be a valid alternative <sup>158</sup>.

As described in **chapter 1**, in the last few years, nanotechnologies have aroused a greater interest in many scientific areas and their application in agricultural field is one of that.

In fact, in the last 10 years, nano fertilizers and nano pesticides were preferred to traditional chemical plants protection products such as azadiractina, phosphorus, valydamycin, urea or sulphur. Moreover, a great number of nanoparticles as Ti, Ag, Fe, Mo, Si, Zn and, especially, Cu are becoming increasingly successful in prevention of plant diseases <sup>161-166</sup>.

In addition, Cu nanoparticles have proved to be effective even against fungal and bacterial pathogens as *Aspergillus nyger*, *Phytophthora infestance*, *Xanthomonas campestris* and *Xanthomonas oryzae* at low concentration<sup>166167168</sup>. In this case the antibacterial activity of nanoparticles is related to the mechanism of generation of **ROS (Reactive Oxygen Species)**<sup>169</sup>.

The efficiency of Cu-based compounds and CuNPs in the prevention of food crop diseases, has led to the increasing use of these technologies especially for biological agriculture field, in which the employ of traditional pesticides is not allowed.

However, because of the massive use of these products, the concern of the European community, linked to possible bioaccumulation of this heavy metal, is growing.

Thus, to prevent this consequence, the European Union has recently modified its regulation and imposed a lower limit for CuNPs employment, whose annual maximum limit has passed from 6 Kg/ha to 4 Kg/ha <sup>170</sup>.

In response to this call, therefore, an additional alternative is needed, based primarily on environmentally friendly practices and substances.

Chitosan nanoparticles (CsNPs) synthesized from food waste could be a valid choice.

The antiviral activity of chitosan is already well known<sup>171-173</sup> and it is probably linked to the presence of free amino groups and positive charges on deacetylated units. The same feature makes chitosan suitable for antifungal, antibacterial and antiviral application.

The -NH<sub>2</sub> groups contained in deacetylated units, in fact, in solution are commonly protonated and confer to the biopolymer the capacity of interacting with the negative charges of biological membranes of plants, and thus to penetrate more efficiently inside them and stimulate the plant organism at immune level<sup>174</sup>.

In this way, chitosan is capable to act as general elicitor (or **Microbe-Associated Molecular Pattern-MAMP**) generating a no-host defence answer, by binding pattern recognition receptors and, thus triggering in the plant a **Systemic Acquired Resistance (SAR)**<sup>175</sup>.

This SAR is salicylic acid-dependent and, in the case of chitosan, acts as follow: increase of cytosolic Ca<sup>2+</sup>, oxidative burst (**ROS**), synthesis of ABA (abscisic acid), photoalexine and

pathogenesis related proteins (**PRR**), which then lead to a local **hypersensitivity reaction (HR)**. This HR induces the production of salicylic acid and thus activates SAR<sup>176</sup> (**Figure 5.1**).

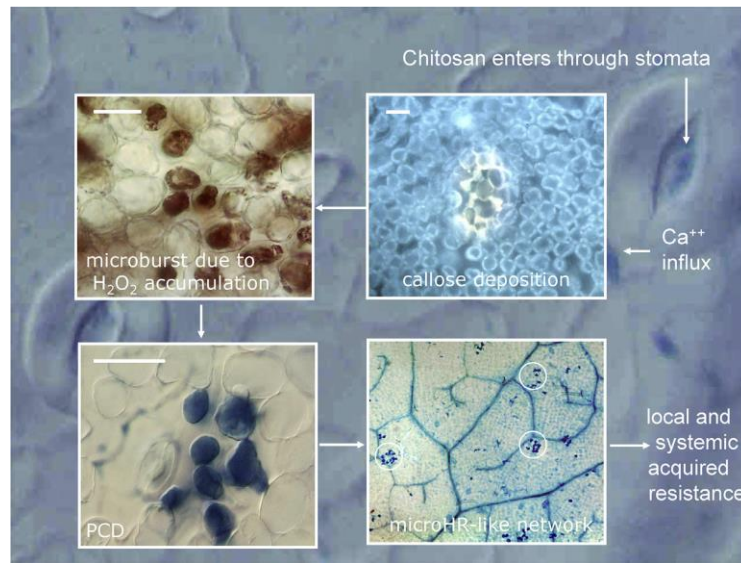


**Figure 5.1:** Hypothesis of Localized Acquired Resistance (LAR) and Systemic Acquired Resistance (SAR) induced by chitosan. When chitosan is sprayed on leaves, it can enter in the cells and causes Ca<sup>2+</sup> influx with a consequent callose deposition and microburst due to H<sub>2</sub>O<sub>2</sub> accumulation. In this way there is the death of some cells (PCD, at the bottom on the left) that generates LAR and SAR<sup>176</sup>.

Based on this state of the art, the aim of this work was to synthesize CsNPs starting from food waste and to test them in preliminary way as resistance inducers against *Tobacco Necrosis Virus* in *Phaseolus Vulgaris* plants.

### 5.1.1 Tobacco Necrosis Virus (TNV).

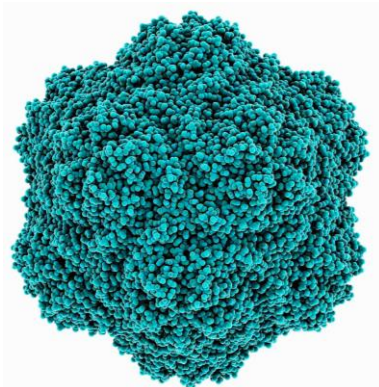


**Figure 5.2:** TNV capsid photograph

The *Tobacco Necrosis Virus* (TNV) is a necrovirus belonging to the family of *Tambusviridae* (**Figure 5.2**). Different cultures of TNV have been sequenced but, to the best of our knowledge, only two have characteristics different enough to be considered two different species: TNV-A (*Alphanecrovirus*) and TNV-D (*Betanecrovirus*). This subdivision is based on the immunologic cross-reactivity due to their envelop proteins. The different types of TNV are then associated with smaller viruses that are called satellite viruses, because they need the TNV virus (defined in this case as "helper") for their propagation<sup>177</sup>.

TNV has an uncapped and unsegmented genome consisting of a single stranded linear positive-sense RNA (Class IV of Baltimore) of 3.8 kb that lacks a poly A tail and replicates itself with the help of its own RNA-dependent RNA polymerase<sup>178</sup>.

The viral genome of TNV is encapsulated into uncoated icosahedral particles of approximately 26-28 nm diameter with symmetry T=3. Satellite virus cultures (satTNV) also have 17 nm particles, encoding a capsid protein that assembles into a T = 1 particle<sup>179</sup>.

This virus is naturally present in the roots of a wide range of plants and the symptoms are generally different depending on the type of TNV that infect the plant.

In *P. Vulgaris* leaves, as well in high number of plant species, TNV infection causes localized necrotic lesions due to HR elicited by viral coat protein. These lesions appear 3-4 days after infection and are quickly quantifiable, so this pathosystem is widely used to assess the level and mechanisms of resistance of plants induced by viral infection <sup>178</sup>.

This virus is easily transmitted by mechanical inoculation to a wide range of plants. Moreover, zoospores of its natural vector, the chytrid fungus *Olpidium brassicae*, are also an important

source of infection<sup>180</sup> In fact, the viral particles are able to attach themselves outside the spores and when the fungus penetrates the roots of the plant, the virus is transmitted concomitantly causing the infection.

In this work the TNV-D was employed.

## 5.2 Experimental

### 5.2.1 Chemicals and Materials

All chemicals were used as received, without any further purification.

Acetic acid (99%), Sodium Tripolyphosphate (TPP- technical grade, 85%), sodium thioglycolate ( $\geq 96.5\%$ ) and EDTA was purchased from Sigma Aldrich.

Commercial chitosan was acquired from Bio-Basic.

Extracted chitosan was obtained from local shrimps 'shells as reported in *paragraph 2.2.2*.

For the preparation of CsNPs, Milli-Q water was used, obtained from a Milli-Q Integral 5 system.

### 5.2.2 Synthesis of chitosan nanoparticles (CsNPs)

CsNPs were synthesized at three different concentrations: 1 mg/mL, 2.5 mg/mL and 5 mg/mL.

For the synthesis of the samples, 0.001 g, 0.025 and 0.05 g of chitosan were weighed and dissolved in 10 mL of  $\text{CH}_3\text{COOH}$  3% v/v on stirring plate.

When chitosan is completely dissolved, 2.5 mL of tripolyphosphate (TPP) 0.1 % w/v were added drop by drop, keeping the magnetic stirring at 800 rpm and room temperature, for 1 h.

At the end of the reaction, the solutions were recovered, centrifugated at 10000 rpm and resuspended in Milli-Q water.

Finally, the obtained NPs were washed three times in order to eliminate excess of TPP and stored in the fridge at 4°C. They are stable for about 15 days.

### 5.2.3 Atomic force microscopy (AFM) characterization

The dimension and morphology of the prepared nanoparticles were analysed with atomic force microscopy (AFM).

10  $\mu\text{l}$  of the samples were spotted on a freshly cleaved round shaped MICA sheet (Grade V-1, thickness 0.15 mm, size 10 x 10 mm) and air dried over a plate heated at 37-40°C for 5 minutes. Dried samples were then imaged in tapping mode with NaioAFM (Nanosurf AG) equipped with Multi75AI-G (Budget Sensors) tip (Resonant Frequency  $\approx 75$  kHz; Force Constant  $\approx 3$  N/m). Images were collected over different length scales (scan size ranged from 1  $\mu\text{m}$  to 15  $\mu\text{m}$  with a scan speed of ranged from 0.8 sec/line to 1 sec/line).

#### **5.2.4 CsNPs Phytotoxicity test**

For the phytotoxicity tests of nanoparticles obtained for both chitosan (extracted and Bio-basic), CsNPs were administered to *P. Vulgaris* leaves through nebulization.

The sample leaves were examined before the treatment and after 24 hours.

#### **5.2.5 Preparation of TNV inoculum**

For the preparation of inoculum, 0.02 g of TNV-infected leaves of *Phaseolus Vulgaris* were lyophilized and placed in a mortar (autoclaved at 120 °C for 20 min) containing 2 mL of buffer (for 1 L of phosphate buffer solution 0.05 M at pH = 7 : 1.2g of DIECA; 0.4 g of EDTA and 0.6 f of sodium thioglycolate.  $6.5 < \text{pH}_{\text{final}} > 7.5$ ).

For the inoculum, 2 concentrations were evaluated:

- 1:3 dilution (500 µL of inoculum and 1 mL of buffer);
- 1:9 dilution (500 µL of 1:3 dilution and 1 mL of buffer).

Silicon carbide is finally added to both dilutions to facilitate the entry of the virus.

#### **5.2.6 Tobacco necrosis virus (TNV)- Administration**

To evaluate the effects of CsNPs on TNV infection, 6 leaves of *P. Vulgaris* were treated with extracted CsNPs, 6 with Bio-basic CsNPs and 6 with water.

The procedure was carried out by spraying the NPs directly on the leaf.

H<sub>2</sub>O treatment is necessary to simulate possible mechanical lesions caused by nebulization that could also induce HR.

Then, the inoculum was administrated on each sample mechanically, through rubbing with gloves, spreading it evenly over the leaves.

An evaluation of damages due to virus was done after 3 days.

## 5.3 Results and discussions

As shown in **paragraph 5.1**, the aim of this preliminary study is that to evaluate if CsNPs are efficient as general elicitor against TNV inoculated on target plant of *P.Vulgaris*.

In **Figure 5.3** a general scheme of the experimental procedure followed in this study, is reported.

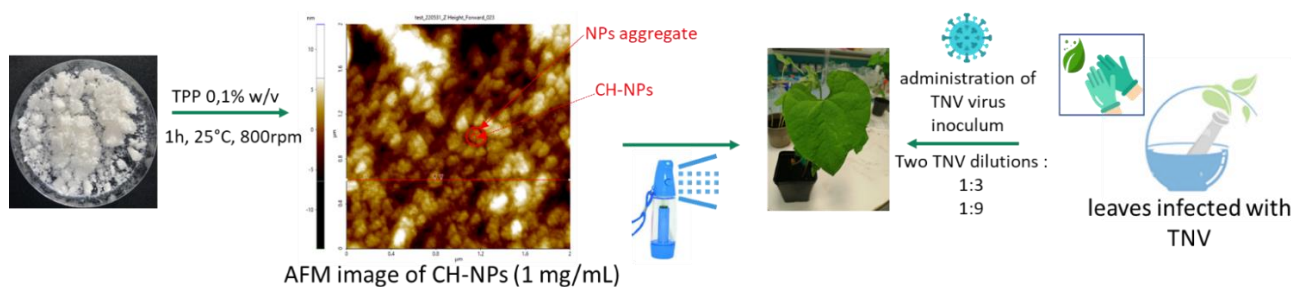


**Figure 5.3:** General scheme of the experimental set-up for the application of CsNPs on *P.Vulgaris* leaves and administration of TNV. CsNPs, synthesized through ionotropic gelation method, using TPP as reductant agent, are characterized with AFM and then sprayed on samples leaves. After 24 h, the inoculum prepared starting from *P.Vulgaris* infected leaves were administered on the samples.

AFM analysis of CsNPs synthesized at three different concentrations (1, 2.5 and 5 mg/mL) allows us to select the best concentration adapted to our need. At concentrations of 2.5 and 5 mg/mL, in fact, the resulting NPs appear too aggregate and big with difficulties to resuspended them after centrifugation, and that would negatively affect our experiment.

For this reason, *in vivo* experiments on *P. Vulgaris* leaves, were carried out only with 1 mg/mL CsNPs for both chitosans (extracted and Bio-basic).

In **Figure 5.4** the AFM image for the selected sample is reported.

CsNPs present a classical spherical morphology with a diameter between 1 and 100 nm.

Although the NPs appear perfectly resuspended in Milli-Q water after centrifuge, AFM image shows the formation of aggregates. This is due to the image acquisition protocol itself.

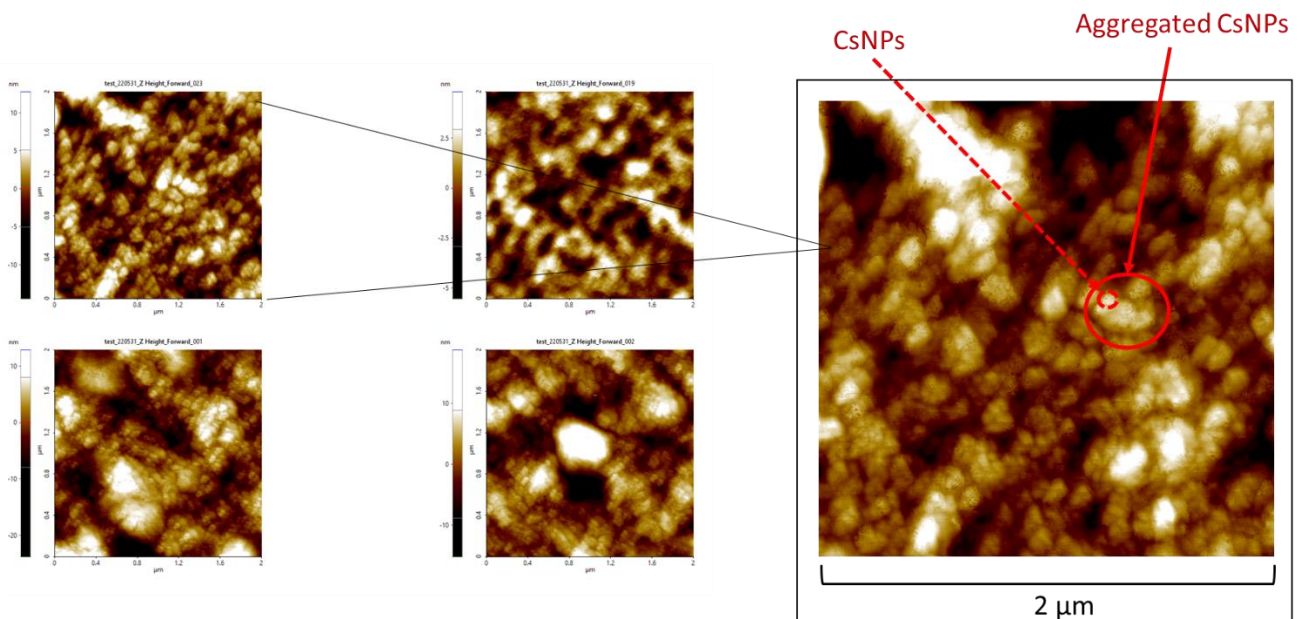


**Figure 5.4:** AFM image acquired for CsNPs 1 mg/mL. On the image on the right, it is possible to see a cluster of aggregate NPs (red solid line circle) and a single nanoparticle (red circle with dotted line) that has clearly a spherical morphology.

With no possibility to record the AFM image in liquid phase, in fact, it was necessary to dry the sample on a MICA sheet and the drying process probably induced nanoparticles aggregation. However, we can suppose that CsNPs have a good dispersion in solution, so we decided to proceed with *in vivo* experiments.

As anticipated in **section 5.2.5**, it has been necessary to test the phytotoxicity of CsNPs before proceeding with the actual experiment and inoculate the virus on the leaves.

When positive charged NPs are used, indeed, there is the risk that penetrating biological membranes, they can cause damage to the cell. These damages generally, appear as necrotic spots, chlorotic strains, wilting, until plant death within 24 hours from administration.

From **Figure 5.5**, it is clear that this not happens neither for nanoparticles obtained from extracted chitosan either for that obtained from the commercial Bio-Basic.

Therefore, we can conclude that, none of the prepared nanoparticles are phytotoxic for our samples, and then it was possible to proceed with the first preliminary tests of antiviral activity.

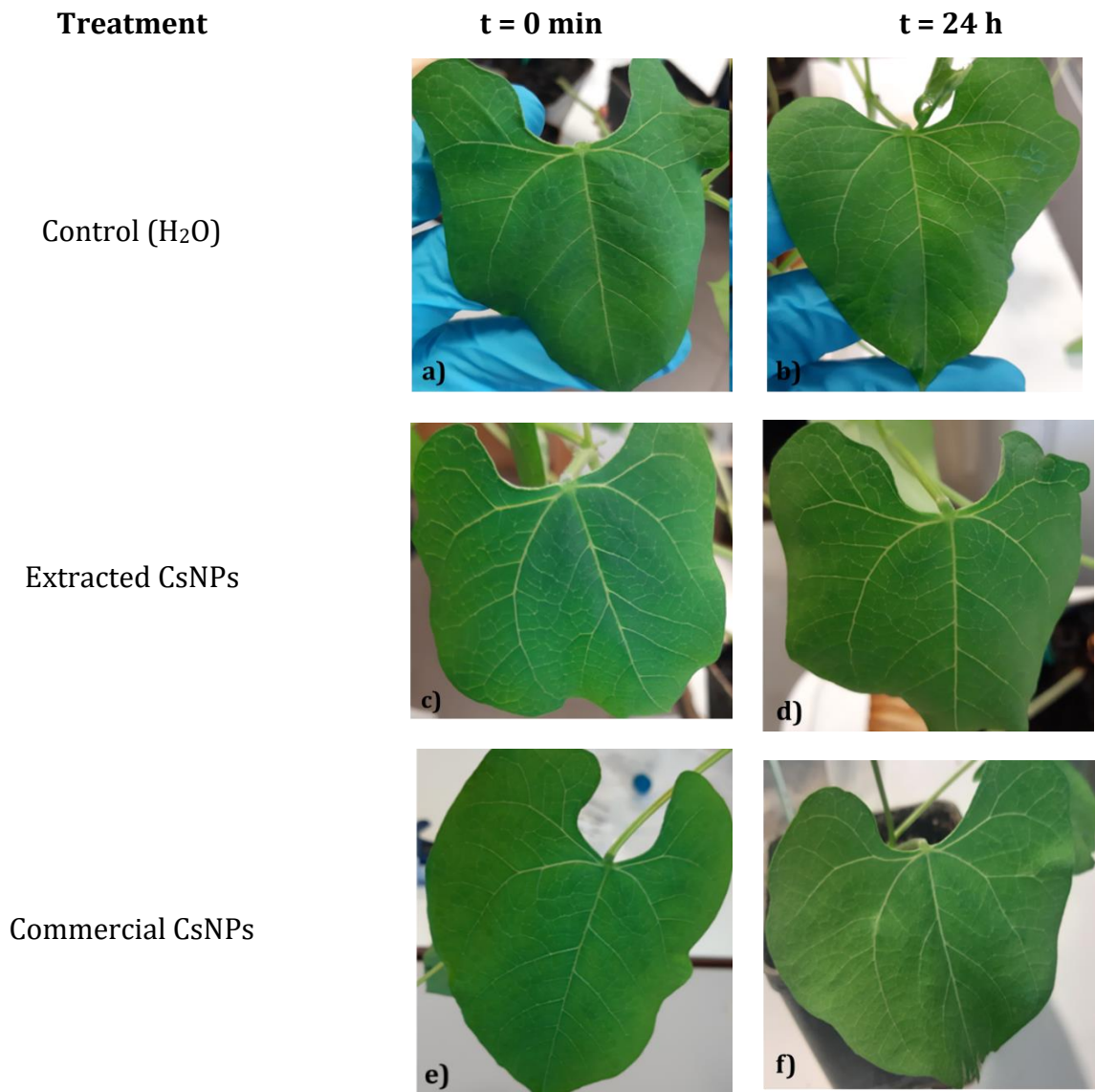


**Figure 5.5:** Results of the tests of phytotoxicity of extracted CsNPs (c and d) and Bio-Basic CsNPs (e and f). The absence of necrotic spots, chlorotic strains, wilting and plant death after 24 hours of administration is a clear signal of no-phytotoxicity for both samples.

In **Figure 5.6**, it is possible to see a comparison between *P. Vulgaris* leaves treated with H<sub>2</sub>O, or nanoparticles obtained from extracted chitosan (CH-ext) and commercial chitosan Bio-Basic (CH-BB). *P. Vulgaris* leaves, inoculated with TNV at 1:3 concentration, are visible in **Figures 5.6 a, b and c**), and *P. Vulgaris* leaves treated at the same way with TNV at 1:9 concentration are visible in **Figures 5.6 d, e and f**). The evaluation of damages was done by observing the leaves with microscope after 3 days of inoculation.

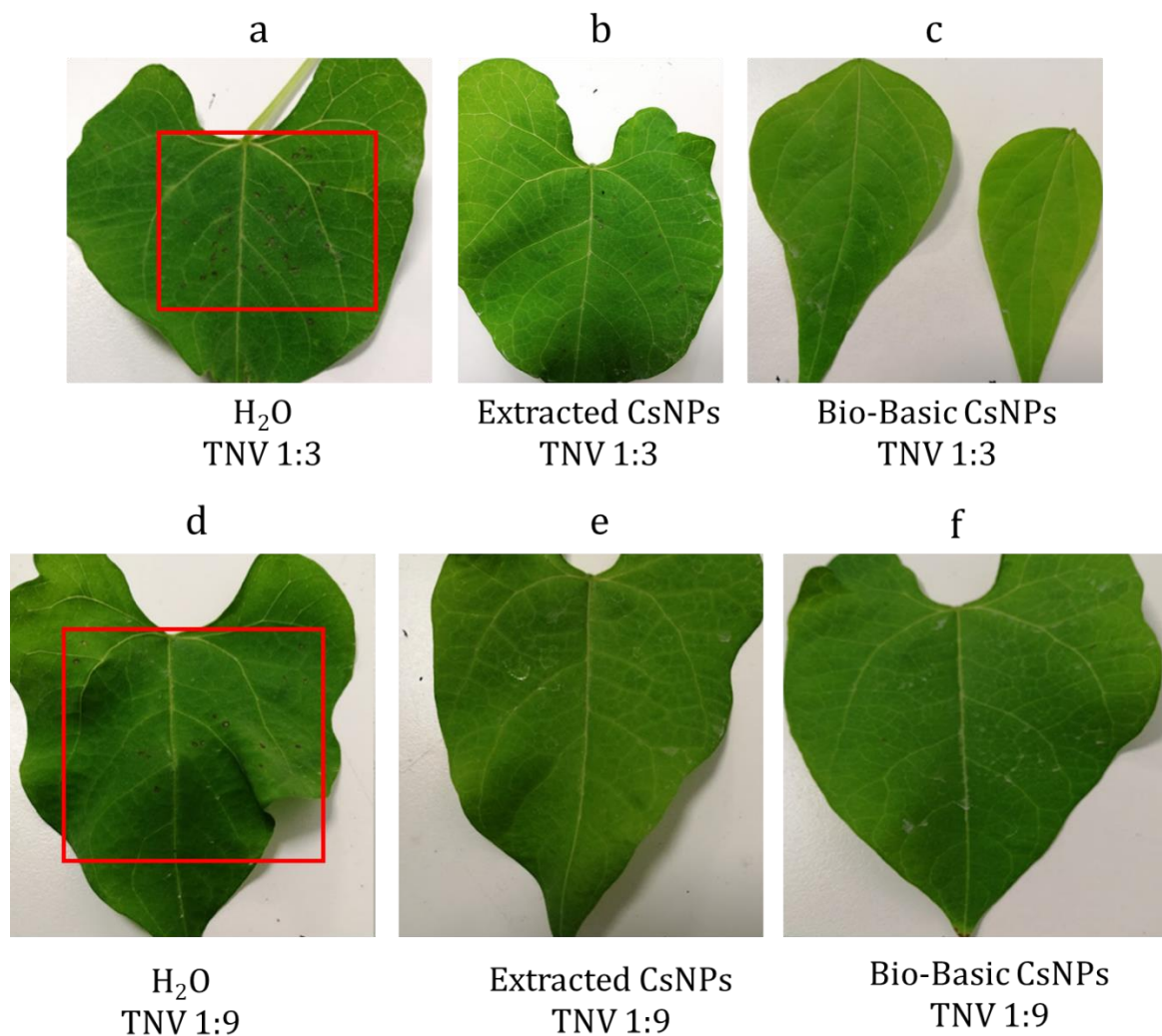


**Figure 5.6:** Photo of some representative leaves treated with CsNPs (extracted and Bio-Basic) after 3 days of inoculation. The necrotic spots induced from TNV on control samples are underlined with the red squares.

At first superficial analysis, it is clear that both types of CsNPs have a protective effect on the appearance of visible symptoms induced by TNV. The emergence of necrotic spots, which are appreciated on controls (a and d), is not evident, or is extremely reduced. So, we can assume that CsNPs are able to act as inductor of resistance.

As we expected, at a first visual analysis, the number of necrotic spots induced by the inoculum at concentration 1:9 (**Figure 5.6 d, e and f**) seems to be lower than those induced by 1:3 concentration (**Figure 5.6 a, b, c**), due to the reduced number of viral particles present in the most diluted inoculum.

More in-depth considerations on the outcome of these first exploratory tests, can be done by counting the number of lesions generated by the inoculation of the virus at the two concentrations, for each treated leaf.

The data obtained from the count of necrotic spots per leaf (in total 6 leaves were treated for each type of CsNPs in order to achieve a good data distribution) are summarized in the box diagrams reported in **Figure 5.7** and **5.8**.

For each sample, the "x" represents the average number of the necrotic spots appeared on one leaf after TNV inoculum, while the width represents the data distribution among the 6 leaves.

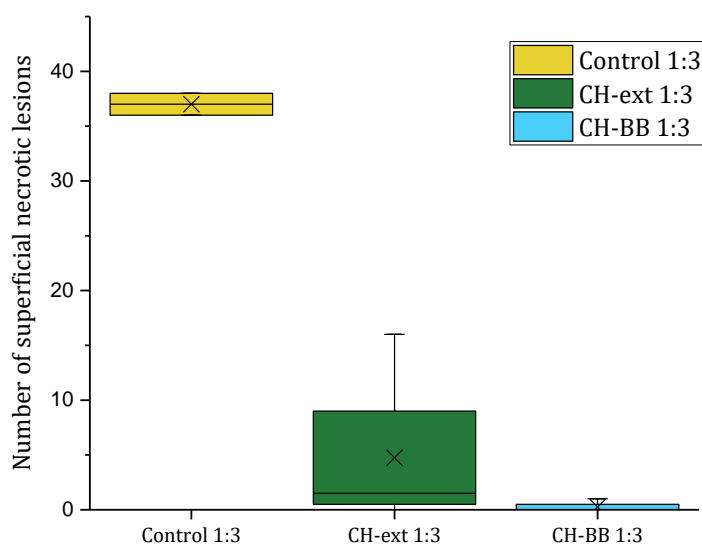


**Figure 5.7:** Box diagrams for leaves treated with water or extracted and Bio-Basic CsNPs and inoculated with TNV 1:3.

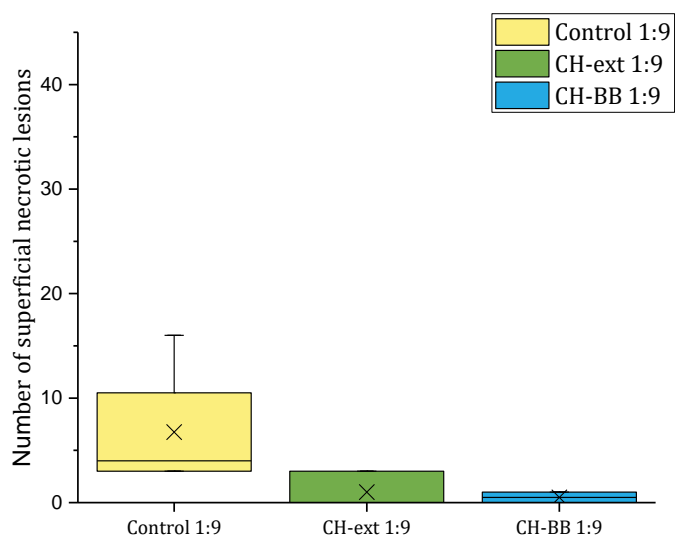


**Figure 5.8:** Box diagrams for leaves treated with water and extracted and Bio-Basic CsNPs and inoculated with TNV 1:9.

As anticipated in the visual analysis in **Figure 5.6**, a higher number of necrotic lesions appear in control leaves treated with 1:3 dilution (average value = 37) and in control leaves treated with 1:9 dilution (average value= 6.75). The significant difference between the two dilutions is due to the reduction of the number of viral particles in the second inoculum, with a lower concentration and higher dilution factor.

The most interesting result is that in both cases a reduction of more than 85% of symptoms induced by TNV is obtained when leaves are treated with extracted CsNPs, and more than 99% when they are treated with Bio-Basic CsNPs. The higher efficiency of Bio-basic CsNPs is probably due to the little higher DD value of biopolymer (see **chapter 2**) which promotes the dissolution and therefore the formation of nanoparticles.

The high distribution presents in some data (control 1:9 and CH-ext 1:9) is probably caused by a non-homogeneity in the set of 6 leaves chosen for the experiment. The smallest leaves, in fact, are generally more susceptible to the attack of the virus and, therefore, a greater number of lesions appear.

In conclusion, from an initial analysis of this exploratory experiment, we can say that the treatment of *P. Vulgaris* with CsNPs, either extracted or commercial Bio-Basic, seems to stimulate induced resistance mechanisms in plants, giving protection against TNV infection. This effect, is due to a trigger given by CsNPs that accelerate the resistance response, causing micro-lesions in the plant that mimic the action of HR-inducing virus infection by generating signals for SAR. As consequence, in the tissues treated with chitosan, the HR is limited to a few numbers of cells and results in practically invisible symptoms that, however, are capable to stimulate the acquired resistance mechanisms.

## 5.4 Conclusions

In summary, in this chapter is reported a preliminary study of the efficiency of chitosan nanoparticles as resistance inductors of *Tobacco Necrosis Virus* inoculated on *Phaseolus Vulgaris* leaves.

CsNPs were synthesized starting from extracted chitosan and commercial Bio-Basic chitosan, with an ionotropic gelation technique using TPP as a reducing agent. The best concentration of nanoparticles for our purpose was found to be 1 mg/mL. The obtained NPs, in fact, analysed with AFM, were well dispersed in water, with spheric morphology, and with a diameter between 1 and 100 nm.

From the analysis of the obtained results from in vivo experiments, we can conclude that CsNPs actually seem to induce resistance mechanisms in plants, stimulating their defence processes and putting them in a kind of alert state (priming) that makes them ready to face the viral action of the pathogen.

This results in a decrease in necrotic lesions of more than 85% when nanoparticles are prepared from extracted chitosan, and more than 99% when they are prepared from commercial chitosan Bio-Basic, which is characterized by better dissolution.

However, it must be considered that the results of experiments conducted in vivo and with food waste materials such as those described, are always influenced by different factors such as leaf morphology, the quality of the extraction source and biological variability.

In addition, further studies should be conducted regarding the expressed molecular defence mechanisms, such as the expression of PR genes and proteins involved. This work, however, goes beyond the scope of this thesis, the objective of which was to show a preliminary study aimed at evaluating a valid use of chitosan extracted from waste in the context of sustainable agriculture and in a circular economy perspective.

# Chapter 6

---

## 6. Concluding Remarks

In this thesis chitosan-based nano-systems were successfully prepared starting from crustaceans' shrimps' shells, through the chemical process with HCl and NaOH. A deeper characterization of the **Degree of Deacetylation (DD%)** of the extracted biopolymer, evaluated both with **FT-IR** spectroscopy and potentiometric titration, has confirmed a  $DD \sim 80\%$ , comparable to those of two commercial chitosan used as references.

Our attention has been focused on two particular fields of applications: water quality monitoring and agriculture protection fields.

Even if the study is centred on two applications of different types, in all cases the common denominator is chitosan, formulated in different ways, in order to merge the characteristics of biopolymer given by its structure, with the possibility to obtain it from food waste with an easy-preparation procedure, in a circular economy optic. In particular, the idea at the basis of this work is to recover materials from the environment to put it at the service of environmental protection, with economic, social, and ecological advantages.

In the first case, we proved that it is possible to obtain hybrid systems through the synergic combination of an active medium constituted by molecules extracted from food waste (chitosan dissolved in  $\text{CH}_3\text{COOH}$  or chitosan dissolved in citric acid + ascorbic acid mixture) with different carboxylated-AuNPs (citricated-AuNPs, 11-mercaptoundecanoic-AuNPs and 3-mercaptopropionic-AuNPs), for an efficient abatement of hexavalent chromium both from Milli-Q or real water. In particular, we have demonstrated that when chitosan is added to our nano-systems as active medium, it acts as universal scavenger by enhancing the adsorption capability of capped-AuNPs, thanks to its cationic nature that allows it to establish electrostatic interactions with oxoanionic Cr(VI) species. Moreover, the dissolution of the biopolymer in ascorbic acid: citric acid 1:3 mixture, enables the complete abatement of Cr(VI) until reach the **Low Limit Detection (LLD)** for residual pollutant species in solution. This achievement is the result of the synergic action of ascorbic and citric acids that reduce Cr(VI) to Cr(III), and the carboxylated capping agents of AuNPs, that are capable to complex Cr(III) species. Notably, the best results are achieved when 11-mercaptoundecanoic acid is used as stabilizing agent for AuNPs, allows us to obtain the best system in terms of efficiency and stability for this type of

applications. The role of each component of all the studied systems are deepened and confirmed through an electrochemical study.

Always in the field of water quality monitoring and remediation, chitosan has been used as starting material to obtain all-in-one hydrogels in form of bubbles through ionotropic gelation synthesis, capable to adsorb and photodegrade two other pollutants of industrial origin and opposite in charge: **Methylene Blue (MB** – positively charged) and **Methyl Orange (MO** – negatively charged). This study has underlined again as chitosan can act as a scavenger by adsorbing pollutant species efficiently, independently by their charge when the biopolymer is used alone to constitute the matrix of the hydrogel.

However, it has also been demonstrated that, for the studied systems, the ability to adsorb pollutants does not depend only on chitosan matrix, but can be rationally designed and controlled by a synergistic combination of individual, active components, such as polymer blends (PEDOT:PSS) or photocatalytic nanoparticles (AuNPs, AgNPs and TiO<sub>2</sub> NPs).

In particular, the incorporation of TiO<sub>2</sub> NPs and PEDOT:PSS ensures the enhancement of the adsorption capability through MB, that achieves percentages > 90% when the best adsorption system, CH@PEDOT:PSS 10%, is employed. Moreover, this system, together with CH@PEDOT:PSS 5%, are the only ones capable to reach a greater percentage of pollutant removal respect to pure chitosan matrix, even when the organic molecules is negatively charged, as MO, by demonstrating that, in these cases, not only electrostatic forces are involved in pollutants removal, but also non electrostatic  $\pi$ - $\pi$  interactions.

Furthermore, although the introduction of nanoparticles in the case of AuNPs and AgNPs lowers the adsorption efficiency, it opens the door to the complete removal of dyes through photocatalysis induced by solar radiation, especially in the case of CH@TiO<sub>2</sub> system, which is the only one capable to result in a full degradation of MO.

This work has demonstrated that food waste can be recovered and transformed into value-added materials, with good and proved mechanical properties and antimicrobial activity, for environmental remediation.

As regards the use of chitosan in agriculture protection field, we tested the efficiency of chitosan nanoparticles, also obtained through ionotropic gelation with TPP as reducing agent, as resistance inductors of *Tobacco Necrosis Virus* inoculated on *Phaseolus Vulgaris* leaves. The preliminary in vivo experiments have demonstrated that the nebulization of CsNPs at

concentrations 1 mg/mL on leaves of *P. Vulgaris* is capable to reduce the necrotic lesions due to TNV attack more than 80 %.

Ultimately, chitosan has been revealed as a polyhedric material, whose structure is responsible for most of its exciting properties.

In particular, the unexpected photocatalytic properties of the pure chitosan hydrogel and the possibility to stabilize in water challenging materials as perovskites, highlighted by this thesis, represent two strong elements of novelty which must certainly be deepened.

Moreover, the possibility to extract it from one of the most world abundant waste, as crustacean shells, makes it valuable example of starting polymer for the production of systems interesting from the point of view of network analysis.

This study, in fact, in addition to laying the foundations for environmental application, can be the starting point for an in-depth study of industrial symbiosis, where one or more solutions proposed in this thesis could be the trailblazers of an in-depth research on economic, environmental, logistic, regulatory aspects to be considered to generate interconnections between companies in the territory at regional and/or national level.

## References

1. Olivier Jan, Clément Tostivint, Anne Turbé, Clémentine O'Connor, Perrine Lavelle, Alessandro Flammini, Nadia El-Hage Scialabba, Jippe Hoogeveen, Mathilde Iweins, Francesco Tubiello, L. P. and C. B. *Food wastage footprint. Fao* (2013).
2. United Nations Environment Programme. *Food Waste Index Report 2021. Nairobi* (2021).
3. Stenmarck Å., Jensen C., Q. T. et al. *FUSIONS - Estimates of European food waste levels. Fusions* (2016).
4. United States Environmental Protection Agency. <https://www.epa.gov/sustainable-management-food/food-recovery-hierarchy> (2008).
5. European Commission & Report, T. *Preparatory Study on Food Waste Across Eu 27. October* vol. 33 (2010).
6. Weiss, J., Takhistov, P. & McClements, D. J. Functional materials in food nanotechnology. *J. Food Sci.* **71**, 107–116 (2006).
7. Patni, N.; Tripathi, N.; Bosmia, S. Casein Extraction from various milk samples and its role as a viable substitute for conventional plastics. *Int. J. Appl. Eng. Res.* **8**, 10–13 (2013).
8. FAO. *The state of World Fisheries and Aquaculture - towards blue transformation.* [https://www.fao.org/3/ca9229en/online/ca9229en.html#chapter-1\\_1](https://www.fao.org/3/ca9229en/online/ca9229en.html#chapter-1_1) (2022).
9. The Fish Site. Researchers find new method to convert shrimp processing waste to food. <https://thefishsite.com/articles/researchers-find-new-method-to-convert-shrimp-processing-waste-to-food>.
10. Yan, N. & Chen, X. Don't waste seafood waste. *Nature* vol. 524 157 (2015).
11. Thakur, V. K. & Voicu, S. I. Recent advances in cellulose and chitosan based membranes for water purification: A concise review. *Carbohydr. Polym.* **146**, 148–165 (2016).
12. Goci, M. C., Leudjo Taka, A., Martin, L. & Klink, M. J. Chitosan-Based Polymer Nanocomposites for Environmental Remediation of Mercury Pollution. *Polymers (Basel)*. **15**, 482 (2023).
13. Klongthong, W., Muangsin, V., Gowanit, C. & Muangsin, N. Chitosan Biomedical Applications for the Treatment of Viral Disease: A Data Mining Model Using Bibliometric Predictive Intelligence. *J. Chem.* **2020**, (2020).
14. Pandey, P., Kumar Verma, M. & De, N. Chitosan in Agricultural Context-A Review. *Bull. Env. Pharmacol. Life Sci* **7**, 87–96 (2018).
15. Albushabaa, S. & Haider, H. A quick overview of chitosan, its sources and applications-A review. (2022) doi:10.13140/RG.2.2.16590.54088.
16. Negi, H., Verma, P. & Singh, R. K. A comprehensive review on the applications of functionalized chitosan in petroleum industry. *Carbohydr. Polym.* **266**, 118125 (2021).
17. Wan Ngah, W. S., Teong, L. C. & Hanafiah, M. A. K. M. Adsorption of dyes and heavy metal ions by chitosan composites: A review. *Carbohydr. Polym.* **83**, 1446–1456 (2011).
18. Sakkayawong, N., Thiravetyan, P. & Nakbanpote, W. Adsorption mechanism of synthetic reactive dye wastewater by chitosan. *J. Colloid Interface Sci.* **286**, 36–42 (2005).
19. Hoang, N. H. et al. Chitosan Nanoparticles-Based Ionic Gelation Method: A Promising Candidate for Plant Disease Management. *Polymers (Basel)*. **14**, 1–28 (2022).
20. Kumaraswamy, R. V. et al. Salicylic acid functionalized chitosan nanoparticle: A sustainable biostimulant for plant. *Int. J. Biol. Macromol.* **123**, 59–69 (2019).
21. Rasul, R. M. et al. A review on chitosan and its development as pulmonary particulate anti-infective and anti-cancer drug carriers. *Carbohydr. Polym.* **250**, 116800 (2020).
22. Alqahtani, F. et al. Antibacterial activity of chitosan nanoparticles against pathogenic n. Gonorrhoea. *Int. J. Nanomedicine* **15**, 7877–7887 (2020).
23. Hua, C. et al. The effect of low and high molecular weight chitosan on the control of gray mold (*Botrytis cinerea*) on kiwifruit and host response. *Sci. Hortic. (Amsterdam)*. **246**, 700–709 (2019).

24. Ji, M. *et al.* Advances in chitosan-based wound dressings: Modifications, fabrications, applications and prospects. *Carbohydr. Polym.* **297**, 120058 (2022).
25. Flórez, M., Guerra-Rodríguez, E., Cazón, P. & Vázquez, M. Chitosan for food packaging: Recent advances in active and intelligent films. *Food Hydrocoll.* **124**, (2022).
26. Plucinski, A., Lyu, Z. & Schmidt, B. V. K. J. Polysaccharide nanoparticles: From fabrication to applications. *J. Mater. Chem. B* **9**, 7030–7062 (2021).
27. EPA. *EPA's Report on the environment.* (2008).
28. Vinuth, M., Naik, H. S. B., sekhar, K. C., Manjanna, J. & Vinoda, B. M. Environmental Remediation of Hexavalent Chromium in Aqueous Medium Using Fe(II)-Montmorillonite as Reductant. *Procedia Earth Planet. Sci.* **11**, 275–283 (2015).
29. Qasem, N. A. A., Mohammed, R. H. & Lawal, D. U. Removal of heavy metal ions from wastewater: a comprehensive and critical review. *npj Clean Water* **4**, (2021).
30. Galán, B., Castañeda, D. & Ortiz, I. Removal and recovery of Cr(VI) from polluted ground waters: A comparative study of ion-exchange technologies. *Water Res.* **39**, 4317–4324 (2005).
31. Willner, M. R. & Vikesland, P. J. Nanomaterial enabled sensors for environmental contaminants Prof Ueli Aebi, Prof Peter Gehr. *J. Nanobiotechnology* **16**, 1–16 (2018).
32. Kou, S. (Gabriel), Peters, L. M. & Mucalo, M. R. Chitosan: A review of sources and preparation methods. *Int. J. Biol. Macromol.* **169**, 85–94 (2021).
33. Liao, J. & Huang, H. Magnetic chitin hydrogels prepared from *Herichium erinaceus* residues with tunable characteristics: A novel biosorbent for Cu<sup>2+</sup> removal. *Carbohydr. Polym.* (2019) doi:10.1016/j.carbpol.2019.05.074.
34. Jones, M., Kujundzic, M., John, S. & Bismarck, A. Crab vs. Mushroom: A review of crustacean and fungal chitin in wound treatment. *Marine Drugs* (2020) doi:10.3390/md18010064.
35. Hamed, I., Ozogul, F. & Regenstein, J. M. Trends in Food Science & Technology Industrial applications of crustacean by-products ( chitin , chitosan , and chitoooligosaccharides ): A review. **48**, 40–50 (2016).
36. Aranaz, I., Alc, R. & Concepci, M. Chitosan : An Overview of Its Properties and Applications. (2021).
37. Rosenthal, R. *et al.* Biomaterials The effect of chitosan on transcellular and paracellular mechanisms in the intestinal epithelial barrier. **33**, (2012).
38. Maddaloni, M. & Vassalini, I. Green Routes for the Development of Chitin / Chitosan Sustainable Hydrogels. 325–344 (2020).
39. Ardean, C., Davidescu, C. M. & Neme, N. S. Factors Influencing the Antibacterial Activity of Chitosan and Chitosan Modified by Functionalization. (2021).
40. Kim, S.-K. Antioxidant, Antimicrobial Properties of Chitin, Chitosan, and Their Derivatives. in *Chitin and Chitosan derivatives - 1st edition* 12 (2013).
41. Thanou, T. K.; M. Chitin and Chitosan: Sources, Production and Medical Applications. in *Renewable Resources for Functional Polymers and Biomaterials* (ed. Williams, P.) (Royal Society of Chemistry, 2011).
42. Khan, Tanveer Ahmad;Peh, Kok Khiang;Ch'ng, H. S. Reporting degree of deacetylation values of chitosan: The influence of analytical methods. *J. Pharm. Pharm. Sci.* **5**, 205–212 (2002).
43. Hussain, R., Iman, M. & Maji, T. K. Determination of Degree of Deacetylation of Chitosan and Their effect on the Release Behavior of Essential Oil from Chitosan and Chitosan- Gelatin Complex Microcapsules. **2**, 4–12 (2013).
44. Younes, I. & Rinaudo, M. Chitin and Chitosan Preparation from Marine Sources. Structure, Properties and Applications. 1133–1174 (2015) doi:10.3390/md13031133.
45. Nilsen-nygaard, J., Strand, S. P., Vårum, K. M., Draget, K. I. & Nordgård, C. T. Chitosan: Gels and Interfacial Properties. 552–579 (2015) doi:10.3390/polym7030552.
46. Maddaloni, M., Alessandri, I. & Vassalini, I. Food-waste enables carboxylated gold nanoparticles to completely abate hexavalent chromium in drinking water. *Environ. Nanotechnology, Monit. Manag.* **18**, 100686 (2022).

47. Access, O. We are IntechOpen , the world ' s leading publisher of Open Access books Built by scientists , for scientists TOP 1 % Quantitative Analysis by IR : Determination of Chitin /.
48. N, V. The Use of Titration Technique and FTIR Bands to Determine the Deacetylation Degree of Chitosan Samples. *J. Text. Sci. Eng.* **07**, (2017).
49. Queiroz, M. F., Melo, K. R. T., Sabry, D. A., Sasaki, G. L. & Rocha, H. A. O. Does the use of chitosan contribute to oxalate kidney stone formation? *Mar. Drugs* **13**, 141–158 (2015).
50. VINO, A. B., RAMASAMY, P., SHANMUGAM, V., SHANMUGAM, A. & BIOLOGY, M. Extraction, characterization and in vitro antioxidative potential of chitosan and sulfated chitosan from Cuttlebone of Sepia aculeata Orbigny, 1848 Asian Pacific Journal of Tropical Biomedicine journal homepage:www.elsevier.com/locate/apjtb \*Corresponding. *Asian Pac. J. Trop. Biomed.* 334–341 (2012).
51. Song, C., Yu, H., Zhang, M., Yang, Y. & Zhang, G. Physicochemical properties and antioxidant activity of chitosan from the blowfly *Chrysomya megacephala* larvae. *Int. J. Biol. Macromol.* **60**, 347–354 (2013).
52. Brugnerotto, J. *et al.* An infrared investigation in relation with chitin and chitosan characterization. *Polymer (Guildf)*. **42**, 3569–3580 (2001).
53. Maddaloni, M., Alessandri, I. & Vassalini, I. Food-waste enables carboxylated gold nanoparticles to completely abate hexavalent chromium in drinking water. *Environ. Nanotechnology, Monit. Manag.* **18**, 100686 (2022).
54. Gijpalaj, J. & Alessandri, I. Easy recovery, mechanical stability, enhanced adsorption capacity and recyclability of alginate-based TiO<sub>2</sub> macrobead photocatalysts for water treatment. *J. Environ. Chem. Eng.* **5**, 1763–1770 (2017).
55. Pollicino, L. C. *et al.* Multi-aquifer susceptibility analyses for supporting groundwater management in urban areas. *J. Contam. Hydrol.* **238**, 103774 (2021).
56. Oze, C., Bird, D. K. & Fendorf, S. Genesis of hexavalent chromium from natural sources in soil and groundwater. *Proc. Natl. Acad. Sci. U. S. A.* **104**, 6544–6549 (2007).
57. R. Jobby, P. Jha, A. K. Yadav, and N. D. Biosorption and biotransformation of hexavalent chromium [Cr(VI)]: a comprehensive review. *Chemosphere* **207**, 225–266 (2018).
58. Liu, H. & Yu, X. Hexavalent chromium in drinking water: Chemistry, challenges and future outlook on Sn(II)- and photocatalyst-based treatment. *Front. Environ. Sci. Eng.* **14**, 1–9 (2020).
59. Ešťoková, A., Palašćáková, L., Singovszká, E. & Holub, M. Analysis of the chromium concentrations in cement materials. *Procedia Eng.* **42**, 123–130 (2012).
60. Vogel, C. *et al.* Chromium (VI) in phosphorus fertilizers determined with the diffusive gradients in thin-films (DGT) technique. *Environ. Sci. Pollut. Res.* **27**, 24320–24328 (2020).
61. Yao, Q., Wang, Y., Chen, H., Huang, H. & Liu, B. Mechanism of High Chrome Uptake of Tanning Pickled Pelt by Carboxyl-Terminated Hyper-Branched Polymer Combination Chrome Tanning. *ChemistrySelect* **4**, 670–680 (2019).
62. Alvarez, C. C., Bravo Gómez, M. E. & Hernández Zavala, A. Hexavalent chromium: Regulation and health effects. *J. Trace Elem. Med. Biol.* **65**, (2021).
63. Dubey, S., Gopal, K. G. & Bersillon, J. *O n l i n e C o.* (2009).
64. Huang, G., Zou, L., Su, Y., Lv, T. & Wang, L. Adsorption of uranium(VI) from aqueous solutions using cross-linked magnetic chitosan beads. *J. Radioanal. Nucl. Chem.* **307**, 1135–1140 (2016).
65. Ye, J. *et al.* Tumor Grade and Overall Survival Prediction of Gliomas Using Radiomics. *Sci. Program.* **2021**, (2021).
66. Bhowal, A. & Datta, S. Studies on transport mechanism of Cr(VI) extraction from an acidic solution using liquid surfactant membranes. *J. Memb. Sci.* **188**, 1–8 (2001).
67. Kalidhasan, S., Sricharan, S., Ganesh, M. & Rajesh, N. Liquid - Liquid extraction of chromium(VI) with tricaprilmethylammonium chloride using isoamylalcohol as the diluent and its application to industrial effluents. *J. Chem. Eng. Data* **55**, 5627–5633 (2010).
68. Erçağ, E., Kanmaz, N., Buğdaycı, M. & Hızal, J. Cr(VI) adsorption on binary and ternary composites of raw cocoa shell with magnetic nanoparticle and Prussian blue. *Environ. Nanotechnology, Monit. Manag.* **17**,

(2022).

69. Vassalini, I., Litvinava, M. & Alessandri, I. All food waste-based membranes for Chromium(VI) removal. *Environ. Sustain.* **4**, 429–435 (2021).
70. Knecht, M. R. & Sethi, M. Bio-inspired colorimetric detection of Hg<sup>2+</sup> and Pb<sup>2+</sup> heavy metal ions using Au nanoparticles. *Anal. Bioanal. Chem.* **394**, 33–46 (2009).
71. Yao, Y. *et al.* Synchronous detection of heavy metal ions in aqueous solution by gold nanoparticle surface-enhanced laser-induced breakdown spectroscopy. *J. Anal. At. Spectrom.* (2021) doi:10.1039/d1ja00310k.
72. Pandikumar, A. & Ramaraj, R. Photocatalytic reduction of hexavalent chromium at gold nanoparticles modified titania nanotubes. *Mater. Chem. Phys.* **141**, 629–635 (2013).
73. Bendicho, C., Bendicho-Lavilla, C. & Lavilla, I. Nanoparticle-assisted chemical speciation of trace elements. *TrAC - Trends Anal. Chem.* **77**, 109–121 (2016).
74. Kantar, C., Ari, C. & Keskin, S. Comparison of different chelating agents to enhance reductive Cr(VI) removal by pyrite treatment procedure. *Water Res.* **76**, 66–75 (2015).
75. Dong, J., Carpinone, P. L., Pyrgiotakis, G., Demokritou, P. & Moudgil, B. M. Synthesis of precision gold nanoparticles using Turkevich method. *KONA Powder Part. J.* **37**, 224–232 (2020).
76. Liu, L., Leng, Y. & Lin, H. Photometric and visual detection of Cr(VI) using gold nanoparticles modified with 1,5-diphenylcarbazide. *Microchim. Acta* **183**, 1367–1373 (2016).
77. Njus, D., Kelley, P. M., Tu, Y. J. & Schlegel, H. B. Ascorbic acid: The chemistry underlying its antioxidant properties. *Free Radic. Biol. Med.* **159**, 37–43 (2020).
78. Welling, S. H. *et al.* The role of citric acid in oral peptide and protein formulations: Relationship between calcium chelation and proteolysis inhibition. *Eur. J. Pharm. Biopharm.* **86**, 544–551 (2014).
79. Di Palma, L. & Mecozzi, R. Heavy metals mobilization from harbour sediments using EDTA and citric acid as chelating agents. *J. Hazard. Mater.* **147**, 768–775 (2007).
80. Erçağ, E., Kanmaz, N., Buğdaycı, M. & Hızal, J. Cr(VI) adsorption on binary and ternary composites of raw cocoa shell with magnetic nanoparticle and Prussian blue. *Environ. Nanotechnology, Monit. Manag.* **17**, 100625 (2022).
81. Ntuli, T. D. *et al.* Removal of hexavalent chromium via an adsorption coupled reduction mechanism using olive oil derived carbon nano-onions. *Environ. Nanotechnology, Monit. Manag.* **16**, 100477 (2021).
82. Koetting, M. C., Peters, J. T., Steichen, S. D. & Peppas, N. A. Stimulus-responsive hydrogels: Theory, modern advances, and applications. *Mater. Sci. Eng. R Reports* **93**, 1–49 (2015).
83. Ullah, F., Othman, M. B. H., Javed, F., Ahmad, Z. & Akil, H. M. Classification, processing and application of hydrogels: A review. *Mater. Sci. Eng. C* **57**, 414–433 (2015).
84. Quesada-Pérez, M., Maroto-Centeno, J. A., Forcada, J. & Hidalgo-Alvarez, R. Gel swelling theories: The classical formalism and recent approaches. *Soft Matter* **7**, 10536–10547 (2011).
85. Ganji, F., Vasheghani-Farrahani, S. & Vasheghani-Farahani, E. Theoretical Description of Hydrogel Swelling: A Review. *Iran. Polym. J. (English Ed.)* **19**, 375–398 (2010).
86. Garg, S. & Garg, A. Hydrogel : classification , properties , preparation and technical features. *Asian J. Biomater. Res.* **2**, 163–170 (2016).
87. Maddaloni, M., Vassalini, I. & Alessandri, I. Green Routes for the Development of Chitin/Chitosan Sustainable Hydrogels. *Sustain. Chem.* **1**, 325–344 (2020).
88. Peppas, N. A., Bures, P., Leobandung, W. & Ichikawa, H. Hydrogels in pharmaceutical formulations. *Eur. J. Pharm. Biopharm.* **50**, 27–46 (2000).
89. Gil, E. S. & Hudson, S. M. Stimuli-responsive polymers and their bioconjugates. *Prog. Polym. Sci.* **29**, 1173–1222 (2004).
90. N. Kashyap, N. Kumar, M. R. K. Hydrogels for pharmaceutical and biomedical applications. *Crit. Rev. Ther. Drug Carr. Syst.* **22**, 107–150 (2005).
91. Nguyen, K. T. & West, J. L. Photopolymerizable hydrogels for tissue engineering applications. *Biomaterials* **23**, 4307–4314 (2002).

92. Aly, A. S. Self-dissolving chitosan, I: Preparation, characterization and evaluation for drug delivery system. *Angew. Makromol. Chem* **259**, 13–18 (1998).
93. Maitra, J.; Shukla, V. K. Cross-linking in Hydrogels—A Review. *Am. J. Polym. Sci.* **4**, 25–31 (2014).
94. Catoira, M. C., Fusaro, L., Di Francesco, D., Ramella, M. & Boccafoschi, F. Overview of natural hydrogels for regenerative medicine applications. *J. Mater. Sci. Mater. Med.* **30**, (2019).
95. Dash, M., Chiellini, F., Ottenbrite, R. M. & Chiellini, E. Chitosan - A versatile semi-synthetic polymer in biomedical applications. *Prog. Polym. Sci.* **36**, 981–1014 (2011).
96. Hamed, H., Moradi, S., Hudson, S. M., Tonelli, A. E. & King, M. W. Chitosan based bioadhesives for biomedical applications: A review. *Carbohydr. Polym.* **282**, 119100 (2022).
97. Bakshi, P. S., Selvakumar, D., Kadirvelu, K. & Kumar, N. S. Chitosan as an environment friendly biomaterial – a review on recent modifications and applications. *Int. J. Biol. Macromol.* **150**, 1072–1083 (2020).
98. Akakuru, O.U.; Isiuku, B. O. Chitosan Hydrogels and their Glutaraldehyde-Crosslinked Counterparts as Potential Drug Release and Tissue Engineering Systems—Synthesis, Characterization, Swelling Kinetics and Mechanism. *J. Phys. Chem. Biophys.* **7**, (2017).
99. Peralta Ramos, M. L. *et al.* Chitin hydrogel reinforced with TiO<sub>2</sub> nanoparticles as an arsenic sorbent. *Chem. Eng. J.* **285**, 581–587 (2016).
100. Shen, X., Shamshina, J. L., Berton, P., Gurau, G. & Rogers, R. D. Hydrogels based on cellulose and chitin: Fabrication, properties, and applications. *Green Chem.* **18**, 53–75 (2015).
101. Huang, Y., Onyeri, S., Siewe, M., Moshfeghian, A. & Madihally, S. V. In vitro characterization of chitosan-gelatin scaffolds for tissue engineering. *Biomaterials* **26**, 7616–7627 (2005).
102. Tamura, H.; Furuike, T.; Nair, S.V.; Jayakumar, R. Biomedical applications of chitin hydrogel membranes and scaffolds. *Carbohydr. Polym.* **84**, 820–824 (2011).
103. Hamed, H., Moradi, S., Hudson, S. M. & Tonelli, A. E. Chitosan based hydrogels and their applications for drug delivery in wound dressings: A review. *Carbohydr. Polym.* **199**, 445–460 (2018).
104. Bernkop-Schnürch, A. & Dünnhaupt, S. Chitosan-based drug delivery systems. *Eur. J. Pharm. Biopharm.* **81**, 463–469 (2012).
105. Parhi, R. Drug delivery applications of chitin and chitosan: a review. *Environ. Chem. Lett.* **18**, 577–594 (2020).
106. Hejazi, R. & Amiji, M. Chitosan-based gastrointestinal delivery systems. *J. Control. Release* **89**, 151–165 (2003).
107. Zhang, Z. *et al.* Al<sup>3+</sup> coordinated chitosan hydrogel with ultrahigh water absorbency and environmental response. *Mater. Des.* **214**, 110390 (2022).
108. Pedroso-Santana, S. & Fleitas-Salazar, N. Ionotropic gelation method in the synthesis of nanoparticles/microparticles for biomedical purposes. *Polym. Int.* **69**, 443–447 (2020).
109. Li, L., Fang, Y., Vreeker, R., Appelqvist, I. & Mendes, E. Reexamining the egg-box model in calcium - Alginate gels with X-ray diffraction. *Biomacromolecules* **8**, 464–468 (2007).
110. Grenha, A., Seijo, B. & Remuñán-López, C. Microencapsulated chitosan nanoparticles for lung protein delivery. *Eur. J. Pharm. Sci.* **25**, 427–437 (2005).
111. Park, J. S. *et al.* N-acetyl histidine-conjugated glycol chitosan self-assembled nanoparticles for intracytoplasmic delivery of drugs: Endocytosis, exocytosis and drug release. *J. Control. Release* **115**, 37–45 (2006).
112. Vila, A. *et al.* Low molecular weight chitosan nanoparticles as new carriers for nasal vaccine delivery in mice. *Eur. J. Pharm. Biopharm.* **57**, 123–131 (2004).
113. Quiñones, J. P., Peniche, H. & Peniche, C. Chitosan based self-assembled nanoparticles in drug delivery. *Polymers (Basel)*. **10**, 1–32 (2018).
114. Huang, Y. & Lapitsky, Y. Monovalent salt enhances colloidal stability during the formation of chitosan/tripolyphosphate microgels. *Langmuir* **27**, 10392–10399 (2011).
115. Al-Tohamy, R. *et al.* A critical review on the treatment of dye-containing wastewater: Ecotoxicological and

- health concerns of textile dyes and possible remediation approaches for environmental safety. *Ecotoxicol. Environ. Saf.* **231**, 113160 (2022).
116. Samsami, S., Mohamadi, M., Sarrafzadeh, M. H., Rene, E. R. & Firoozbahr, M. Recent advances in the treatment of dye-containing wastewater from textile industries: Overview and perspectives. *Process Saf. Environ. Prot.* **143**, 138–163 (2020).
  117. Yaseen, D. A. & Scholz, M. *Textile dye wastewater characteristics and constituents of synthetic effluents: a critical review. International Journal of Environmental Science and Technology* vol. 16 (Springer Berlin Heidelberg, 2019).
  118. Vassalini, I., Ribauda, G., Gianoncelli, A., Casula, M. F. & Alessandri, I. Plasmonic hydrogels for capture, detection and removal of organic pollutants. *Environ. Sci. Nano* **7**, 3888–3900 (2020).
  119. Vassalini, I. *et al.* Cyclodextrins enable indirect ultrasensitive Raman detection of polychlorinated biphenyls captured by plasmonic bubbles. *Chem. Phys. Lett.* **775**, (2021).
  120. Confederat, L. G., Tuchilus, C. G., Dragan, M., Sha'at, M. & Dragostin, O. M. Preparation and Antimicrobial Activity of Chitosan and Its Derivatives: A Concise Review. *Molecules* **26**, (2021).
  121. Wang, Q. Z. *et al.* Protonation constants of chitosan with different molecular weight and degree of deacetylation. *Carbohydr. Polym.* **65**, 194–201 (2006).
  122. Strand, S. P., Tømmeraas, T., Vårum, K. M. & Østgaard, K. Electrophoretic light scattering studies of chitosans with different degrees of N-acetylation. *Biomacromolecules* **2**, 1310–1314 (2001).
  123. Huseynova, G., Hyun Kim, Y., Lee, J. H. & Lee, J. Rising advancements in the application of PEDOT:PSS as a prosperous transparent and flexible electrode material for solution-processed organic electronics. *J. Inf. Disp.* **21**, 71–91 (2020).
  124. Eom, S. H. *et al.* Polymer solar cells based on inkjet-printed PEDOT:PSS layer. *Org. Electron.* **10**, 536–542 (2009).
  125. Ibanez, J. G. *et al.* Conducting Polymers in the Fields of Energy, Environmental Remediation, and Chemical-Chiral Sensors. *Chem. Rev.* **118**, 4731–4816 (2018).
  126. Louwet, F. *et al.* PEDOT/PSS: Synthesis, characterization, properties and applications. *Synth. Met.* **135–136**, 115–117 (2003).
  127. Fan, Z. & Ouyang, J. Thermoelectric Properties of PEDOT:PSS. *Adv. Electron. Mater.* **5**, 1–23 (2019).
  128. UN Environment Programme. *Too Little, Too Slow Climate adaptation failure puts world at risk.* (2022).
  129. Shi, H., Magaye, R., Castranova, V. & Zhao, J. Titanium dioxide nanoparticles: A review of current toxicological data. *Part. Fibre Toxicol.* **10**, (2013).
  130. Shukla RK, Sharma V, Pandey AK, Singh S, Sultana S, D. A. ROS-mediated genotoxicity induced by titanium dioxide nanoparticles in human epidermal cells. *Toxicol Vitro.* **25**, 231–241 (2011).
  131. Ni M, Leung MKH, Leung DY, S. K. Review and recent developments in photocatalytic water-splitting using TiO<sub>2</sub> for hydrogen production. *Renew. Sustain. Energy Rev.* **11**, 401–425 (2007).
  132. Azeez, F. *et al.* The effect of surface charge on photocatalytic degradation of methylene blue dye using chargeable titania nanoparticles. *Sci. Rep.* **8**, 1–9 (2018).
  133. Warheit DB, Webb TR, Reed KL, Frerichs S, S. C. Pulmonary toxicity study in rats with three forms of ultrafine-TiO<sub>2</sub> particles: differential responses related to surface properties. *Toxicology* **230**, 90–104 (2007).
  134. Sayes, C. M. *et al.* Correlating nanoscale titania structure with toxicity: A cytotoxicity and inflammatory response study with human dermal fibroblasts and human lung epithelial cells. *Toxicol. Sci.* **92**, 174–185 (2006).
  135. Salehi, M., Hashemipour, H. & Mirzaee, M. Experimental Study of Influencing Factors and Kinetics in Catalytic Removal of Methylene Blue with TiO<sub>2</sub> Nanopowder. *Am. J. Environ. Eng.* **2**, 1–7 (2012).
  136. Lakshmi, S., Renganathan, R. & Fujita, S. Study on TiO<sub>2</sub>-mediated photocatalytic degradation of methylene blue. *J. Photochem. Photobiol. A Chem.* **88**, 163–167 (1995).
  137. Romário J. da Silva, Lizeth Carolina Mojica-Sánchez, Filipe D.S. Gorza, Graciela C. Pedro, Bruna G. Maciel, Gabriela P. Ratkovski, Hérica D. da Rocha, Kamila T.O. do Nascimento, Juan C. Medina-Llamas, Alicia E.

- Chávez-Guajardo, José J. Alcaraz-Espinoza, C. P. de M. Kinetics and thermodynamic studies of Methyl Orange removal by polyvinylidene fluoride-PEDOT mats. *J. Environ. Sci. (China)* **100**, 62–73 (2021).
138. Zhang, L., Jamal, R., Zhao, Q., Wang, M. & Abdiryim, T. Preparation of PEDOT/GO, PEDOT/MnO<sub>2</sub>, and PEDOT/GO/MnO<sub>2</sub> nanocomposites and their application in catalytic degradation of methylene blue. *Nanoscale Res. Lett.* **10**, 1–9 (2015).
  139. Falsini, N. *et al.* Analysis of the Urbach tail in cesium lead halide perovskites. *J. Appl. Phys.* **131**, (2022).
  140. López, C. A. *et al.* Crystal Structure Features of CsPbBr<sub>3</sub> Perovskite Prepared by Mechanochemical Synthesis. *ACS Omega* **5**, 5931–5938 (2020).
  141. Ullah, S. *et al.* All-inorganic CsPbBr<sub>3</sub> perovskite: A promising choice for photovoltaics. *Mater. Adv.* **2**, 646–683 (2021).
  142. Tian, J. *et al.* Gain-switching in CsPbBr<sub>3</sub> microwire lasers. *Commun. Phys.* **5**, 1–8 (2022).
  143. Wang, H. *et al.* Efficient CsPbBr<sub>3</sub> Nanoplatelet-Based Blue Light-Emitting Diodes Enabled by Engineered Surface Ligands. *ACS Energy Lett.* **7**, 1137–1145 (2022).
  144. Cheng, L. P. *et al.* Efficient CsPbBr<sub>3</sub> Perovskite Light-Emitting Diodes Enabled by Synergetic Morphology Control. *Adv. Opt. Mater.* **7**, 1–9 (2019).
  145. Kumar, N., Rani, J. & Kurchania, R. Advancement in CsPbBr<sub>3</sub> inorganic perovskite solar cells: Fabrication, efficiency and stability. *Sol. Energy* **221**, 197–205 (2021).
  146. Hoffman, J. B., Zaiats, G., Wappes, I. & Kamat, P. V. CsPbBr<sub>3</sub> Solar Cells: Controlled Film Growth through Layer-by-Layer Quantum Dot Deposition. *Chem. Mater.* **29**, 9767–9774 (2017).
  147. Zeng, J. *et al.* Interfacial-Tunneling-Effect-Enhanced CsPbBr<sub>3</sub> Photodetectors Featuring High Detectivity and Stability. *Adv. Funct. Mater.* **29**, (2019).
  148. Li, Y. *et al.* High-performance perovskite photodetectors based on solution-processed all-inorganic CsPbBr<sub>3</sub> thin films. *J. Mater. Chem. C* **5**, 8355–8360 (2017).
  149. Clinckemalie, L. *et al.* Challenges and Opportunities for CsPbBr<sub>3</sub> Perovskites in Low- and High-Energy Radiation Detection. *ACS Energy Lett.* **6**, 1290–1314 (2021).
  150. Tesh, S. J. & Scott, T. B. Nano-composites for water remediation: A review. *Adv. Mater.* **26**, 6056–6068 (2014).
  151. Xu, Y. *et al.* Robust and multifunctional natural polyphenolic composites for water remediation. *Mater. Horizons* **9**, 2496–2517 (2022).
  152. Yu, S. *et al.* MXenes as emerging nanomaterials in water purification and environmental remediation. *Sci. Total Environ.* **811**, 152280 (2022).
  153. Hoang, A. T. *et al.* Energy-related approach for reduction of CO<sub>2</sub> emissions: A critical strategy on the port-to-ship pathway. *J. Clean. Prod.* **355**, (2022).
  154. Liu, Z., Deng, Z., Davis, S. J., Giron, C. & Ciais, P. Monitoring global carbon emissions in 2021. *Nat. Rev. Earth Environ.* **3**, 217–219 (2022).
  155. FAO. International year of plant health 2020. <https://www.fao.org/plant-health-2020/about/en/> (2020).
  156. FAO. The State of Food and Agriculture 2019: Moving forward on food loss and waste reduction. [https://reliefweb.int/report/world/state-food-and-agriculture-2019-moving-forward-food-loss-and-waste-reduction?gclid=CjwKCAiAlp2fBhBPEiwA2Q10D950xuUWDFDB-vrXtVdOSDvvHoYG3OwWjBkLG\\_Mrs\\_3xzhnEdFQPThOCLcwQAvD\\_BwE](https://reliefweb.int/report/world/state-food-and-agriculture-2019-moving-forward-food-loss-and-waste-reduction?gclid=CjwKCAiAlp2fBhBPEiwA2Q10D950xuUWDFDB-vrXtVdOSDvvHoYG3OwWjBkLG_Mrs_3xzhnEdFQPThOCLcwQAvD_BwE).
  157. Gazzarelli, C. *et al.* Making Agriculture More Sustainable: An Environmentally Friendly Approach to the Synthesis of Lignin@Cu Pesticides. *ACS Sustain. Chem. Eng.* **8**, 14886–14895 (2020).
  158. Chhipa, H. Nanofertilizers and nanopesticides for agriculture. *Environ. Chem. Lett.* **15**, 15–22 (2017).
  159. Zamir, D. Improving plant breeding with exotic genetic libraries. *Nat. Rev. Genet.* **2**, 983–989 (2001).
  160. Conley DJ, Paerl HW, Howarth RW, Boesch DF, S. S. & Al, H. K. *et al.* Controlling eutrophication: nitrogen and phosphorus. *Science (80- )*. **323**, 1014–1015 (2009).
  161. Chhipa H, J. P. Nanofertilisers, nanopesticides and nanosensors in agriculture. *Nanosci. Food Agric.* **1** **20**, 247–282 (2016).

162. Taha, R. A., Hassan, M. M., Ibrahim, E. A., Abou Baker, N. H. & Shaaban, E. A. Carbon nanotubes impact on date palm in vitro cultures. *Plant Cell. Tissue Organ Cult.* **127**, 525–534 (2016).
163. Taran, N. Y. *et al.* The effect of colloidal solution of molybdenum nanoparticles on the microbial composition in rhizosphere of *Cicer arietinum* L. *Nanoscale Res. Lett.* **9**, 1–8 (2014).
164. Pradhan, S. *et al.* Photochemical modulation of biosafe manganese nanoparticles on *vigna radiata*: A detailed molecular, biochemical, and biophysical study. *Environ. Sci. Technol.* **47**, 13122–13131 (2013).
165. Dhoke, S. K., Mahajan, P. & Khanna, A. S. Effect of nano-ZnO particle suspension on growth of mung (*Vigna radiata*) and gram (*Cicer arietinum*) seedlings using plant agar method. *J. Nanotechnol.* **2011**, (2011).
166. Nekrasova, G. F., Ushakova, O. S., Ermakov, A. E., Uimin, M. A. & Byzov, I. V. Effects of copper(II) ions and copper oxide nanoparticles on *Elodea densa* Planch. *Russ. J. Ecol.* **42**, 458–463 (2011).
167. Esteban-Tejeda, L., Malpartida, F., Esteban-Cubillo, A., Pecharromn, C. & Moya, J. S. Antibacterial and antifungal activity of a soda-lime glass containing copper nanoparticles. *Nanotechnology* **20**, (2009).
168. Giannousi, K., Sarafidis, G., Mourdikoudis, S., Pantazaki, A. & Dendrinou-Samara, C. Selective synthesis of Cu<sub>2</sub>O and Cu/Cu<sub>2</sub>O NPs: Antifungal activity to yeast *saccharomyces cerevisiae* and DNA interaction. *Inorg. Chem.* **53**, 9657–9666 (2014).
169. Slavin, Y. N., Asnis, J., Häfeli, U. O. & Bach, H. Metal nanoparticles: Understanding the mechanisms behind antibacterial activity. *J. Nanobiotechnology* **15**, 1–20 (2017).
170. Arena, M. *et al.* Peer review of the pesticide risk assessment of the active substance copper compounds copper(I), copper(II) variants namely copper hydroxide, copper oxychloride, tribasic copper sulfate, copper(I) oxide, Bordeaux mixture. *EFSA J.* **16**, 1–25 (2018).
171. S.N. Chirkov, A.V. Il'ina, N.A. Surgucheca, E.V. Letunova, Y. A. V. & Tatarinova, N. Y. Effect of chitosan on systemic viral infection and some defense responses in potato plants. *Russ. J. Plant Physiol* **48**, 890–896 (2001).
172. H. Pospieszny, J. G. A. Effect of chitosan on the hypersensitive response reaction of bean to Alfalfa Mosaic Virus. *Plant Sci.* **62**, 29–31 (1989).
173. H. Pospieszny, S.N. Chirkov, J. G. Induction of antiviral resistance in plants by chitosan. *Plant Sci.* **79**, 63–38 (1991).
174. Se-Kwon Kim. *Antioxidant, Antimicrobial Properties of Chitin, Chitosan, and Their Derivatives. Chitin and Chitosan derivatives - 1st edition* (2013).
175. Xing, K., Zhu, X., Peng, X. & Qin, S. Chitosan antimicrobial and eliciting properties for pest control in agriculture: a review. *Agron. Sustain. Dev.* **35**, 569–588 (2015).
176. Faoro, F. & Gozzo, F. Is modulating virus virulence by induced systemic resistance realistic? *Plant Sci.* **234**, 1–13 (2015).
177. Amorim, M. S., Sales, M. G. F. & Frasco, M. F. Recent advances in virus imprinted polymers. *Biosens. Bioelectron. X* **10**, (2022).
178. Bulgari, D., Landi, N., Ragucci, S., Faoro, F. & Di Maro, A. Antiviral activity of PD-L1 and PD-L4, type 1 ribosome inactivating proteins from leaves of *Phytolacca dioica* L. In the pathosystem *Phaseolus vulgaris*-Tobacco Necrosis Virus (TNV). *Toxins (Basel)*. **12**, (2020).
179. JAMES H. STRAUSS, E. G. S. *Viruses and Human Disease (Second Edition)*. (2008).
180. Teakle, D. S. Transmission of tobacco necrosis virus by a fungus, *Oplidium brassicae*. *Virology* **18**, 224–231 (1962).

## ***Acknowledgements***

I wish to thank:

Prof. Ivano Alessandri and Dr. Irene Vassalini for the opportunity, the teachings, the passion shared during this journey and for your trust in me in these three years. It was a pleasure share with you this experience.

Regione Lombardia, ENEA and Ms. Sara Cortesi for supporting this research in the framework of the program “Smart agriculture for the sustainability of the agro-food system”.

Prof. Laura E. Depero for the opportunity to carry out this Ph.D project, and all the members of the Chem4Tech group, for the scientific and not-scientific discussions and for making me grow as young research scientist.